

# Performance Analysis and Coverage Optimization Methods for a Digital Radio System in the VHF Bands

Von der Fakultät für Elektrotechnik und Informatik  
der Gottfried Wilhelm Leibniz Universität Hannover  
zur Erlangung des akademischen Grades

Doktor-Ingenieurin

genehmigte

## Dissertation

von

Dipl.-Ing. Friederike Maier  
geboren am 24.12.1980 in Tübingen

2013

1. Referent : Prof. Dr.-Ing. H. P. Kuchenbecker  
2. Referent : Prof. Dr.-Ing. I. Rolfes  
Vorsitz : Prof. Dr.-Ing. M. Fidler  
Tag der Promotion : 24.10.2013

# Acknowledgements

This thesis would not have been possible without the support of all those people who have accompanied me during the past years of my PhD. studies.

I would especially like to thank my colleagues from the IKT for the good working atmosphere and collaboration. Prof. Peissig for his great support finishing this thesis, Prof. Kuchenbecker for reviewing the thesis, Prof. Rolfes from Ruhr University Bochum for the second review and Prof. Fidler for chairing.

I want to thank the members of the DRM Consortium and the German DRM platform for the great collaboration and a lot of fruitful discussions. Special thanks to Detlef Pagel from NLM for his great support and collaboration in conducting all the trials, Albert Waal and all RFmondial for their support and good cooperation and Nils Eulig from NDR for the critical revision of this work.

Furthermore I would like to thank my family for giving me all the support and especially my partner Raffaello for his patience while finishing this work.





# Abstract

DRM+ (Digital Radio Mondiale, Mode E) is an extension of the DRM standard for long, medium and shortwave for the use in the VHF band up to 230 MHz. It has been approved in the open ETSI-DRM standard and added to the ITU recommended digital radio standards above 30 MHz in 2011. With a bandwidth of 96 kHz, the OFDM based DRM+ system fits into a 100 kHz-FM frequency grid and thus can be operated in parallel to FM radio. Several field trials for the evaluation of the system performance, that have been conducted within this work, contributed to the ITU standardization process.

DRM+ formerly was standardized up to 174 MHz, excluding the VHF-Band III. As a switch-over from analogue to digital will require some time of parallel analogue and digital broadcasting, which is hardly possible in the crowded FM Band, evaluations about the use of DRM+ in Band III were started. Band III, which allocates the frequencies from 174 to 230 MHz, offers lots of free spectrum intended for digital audio broadcast systems. DRM+ can coexist there with the digital system DAB(+) (Digital Audio Broadcast), offering local and community radios a cheap and flexible possibility to digitize their signals. Due to the multiplex structure of DAB(+), this is hardly possible with this system. Some of the evaluations that resulted in an extension of the frequencies mentioned in the DRM-standard are part of this work.

As especially local radios are often licensed for low power and using low antenna facilities, techniques to enhance the reception quality are of interest to increase the coverage area. One possibility to achieve this is the use of transmitter diversity techniques, using more than one antenna to transmit the signal. To investigate the benefit for the system performance, evaluations and a field trial with Transmitter Delay Diversity have been conducted.

As a digital OFDM radio system, DRM+ is capable to build a Single Frequency Network (SFN) with several distant transmitters operating on the same frequency. Due to its small bandwidth care has to be taken in the overlapping area to avoid 'flat fading'. For the DRM+ system, the parameters for setting up a SFN have been evaluated and a field trial was conducted.

At the receiver side, receiver diversity techniques can provide a significant enhancement of the reception quality. Different receiver diversity techniques and methods to combine the signals have been evaluated according to their gain and complexity and a field trial has been conducted.

**Key Words:** Digital Broadcasting, Digital Radio Mondiale, DRM+, OFDM, Transmit Diversity, Receiver Diversity, Single Frequency Network



# Kurzfassung

DRM+ (Digital Radio Mondiale Mode E) ist eine Erweiterung des ursprünglich für die Lang-, Mittel- und Kurzwellenbereich entwickelten DRM-Standards für das obere VHF-Band. Es ist Teil des offenen ETSI-DRM Standards und seit 2011 einer der von der ITU empfohlenen Digitalradio-Standards für Frequenzen über 30 MHz. Mit einer Bandbreite von 96 kHz, passt das OFDM-basierte DRM+ System in das 100 kHz-FM Frequenzraster und kann parallel zum analogen FM Radio betrieben werden. Mehrere Feldversuche wurden im Rahmen dieser Arbeit durchgeführt, deren Ergebnisse in die ITU Standardisierung eingeflossen sind.

DRM+ wurde ursprünglich nur bis zu einer Frequenz von 174 MHz standardisiert, also ohne das VHF-Band III. Da bei der Digitalisierung des Hörfunks ein zeitweiser paralleler Betrieb von analogem und digitalem Radio stattfinden wird und dies im überfüllten FM Band aufgrund fehlender freier Frequenzen nicht möglich ist, wurden Untersuchungen über die Nutzung von DRM+ im Band III gestartet. Dieses, von 174 bis 230 MHz reichende Band, ist für Digitalradio vorgesehen und verfügt über ungenutzte Frequenzbereiche. DRM+ kann dort mit dem breitbandigeren Digitalradio DAB(+) (Digital Audio Broadcast) koexistieren. Dies würde lokalen und Community Radios eine günstige und flexible Möglichkeit zur Digitalisierung bieten was mit DAB aufgrund seiner Multiplex-Struktur schwer möglich ist. Untersuchungen und Messungen hierzu, die zu einer Erweiterung des Standards zu höheren Frequenzen beigetragen haben, sind in dieser Arbeit beschrieben.

Da Lokal- und Community Radios oft für geringe Sendeleistung und niedrige Antennenanlagen lizenziert werden, sind Techniken zur Verbesserung der Empfangsqualität und der Reichweite von großem Interesse. Eine Möglichkeit hierzu ist die Verwendung von Sender-Diversitäts-Techniken. Dabei wird das Signal von mehreren Antennen ausgestrahlt um Auslöschungen des Signals in bestimmten Bereichen zu vermeiden. Ein 'Transmitter Delay Diversity' Setup wurde im Rahmen dieser Arbeit untersucht und in einem Feldversuch evaluiert.

Als digitales OFDM System kann DRM+ in einem Gleichwellennetz betrieben werden. Aufgrund der geringen Bandbreite muss im Überlappungsbereich darauf geachtet werden, dass es nicht zu Signalauslöschungen durch destruktive Überlagerung der Signale mehrerer Sender kommt. Dieses wurde im Rahmen dieser Arbeit untersucht und es wurde ein Feldversuch mit zwei synchronisierten Sendern durchgeführt.

Auf der Empfangsseite können Empfänger-Diversitäts-Techniken die Empfangsqualität signifikant verbessern. Verschiedene dieser Techniken wurden hinsichtlich ihrer Komplex-

ität und der Auswirkung auf die Verbesserung der Empfangsqualität untersucht.

**Schlagworte:** Digital Broadcasting, Digital Radio Mondiale, DRM+, OFDM, Sender-Diversität, Empfänger-Diversität, Gleichwellennetz

# Contents

<b>Abstract</b>	<b>I</b>
<b>Kurzfassung</b>	<b>III</b>
<b>List of Abbreviations and Symbols</b>	<b>IX</b>
<b>1 Introduction</b>	<b>1</b>
<b>2 The DRM+ System</b>	<b>5</b>
<b>3 The Transmission Channel</b>	<b>13</b>
3.1 Wave Propagation . . . . .	13
3.2 Propagation models . . . . .	15
3.2.1 Free Space Loss . . . . .	15
3.2.2 Theoretical and Empirical models . . . . .	16
3.2.3 Site-specific Models . . . . .	17
3.3 Statistical Models . . . . .	18
3.3.1 The Time-Variant Channel . . . . .	19
3.3.2 Channel Simulation . . . . .	23
3.3.3 Channel Models . . . . .	24
<b>4 Performance of the DRM+ System in the VHF Band II</b>	<b>27</b>
4.1 DRM+ Trial in Hannover . . . . .	27
4.1.1 Measurements in Urban Environment . . . . .	28
4.1.2 Measurement of the Coverage Limit . . . . .	32
4.2 Additional Measurements in Different Environments . . . . .	36
4.3 Protection Ratios for Analogue Systems . . . . .	39
4.4 Combined Transmission of DRM+ and FM . . . . .	42
<b>5 The DRM+ System in the VHF Band III</b>	<b>47</b>
5.1 Impact of the Mobile Channel . . . . .	47
5.1.1 Inter-Carrier-Interference . . . . .	47
5.1.2 The Pilot Grid . . . . .	51
5.1.3 Flat Fading at Low Speed . . . . .	52
5.2 Measurements in the VHF Band III . . . . .	53
5.2.1 Measurements in Urban Environment . . . . .	54
5.2.2 Measurements of the Coverage Limit . . . . .	56

5.3	Conclusions on DRM+ in the VHF Band III . . . . .	60
<b>6</b>	<b>Transmitter Diversity Techniques</b>	<b>61</b>
6.1	Transmitter Delay Diversity . . . . .	61
6.2	Dependency of the System Performance on the Correlation between the Propagation Paths . . . . .	64
6.3	Correlation between the Transmission Paths . . . . .	67
6.3.1	2D Model . . . . .	67
6.3.2	Raytracing Calculations . . . . .	68
6.4	Field Trial . . . . .	70
6.4.1	Transmitter Hardware Setup . . . . .	71
6.4.2	Measurement Locations . . . . .	72
6.4.3	Measurement Equipment and Parameters . . . . .	73
6.4.4	Measurement Results . . . . .	74
6.5	Conclusions on Transmitter Delay Diversity with DRM+ . . . . .	77
<b>7</b>	<b>Single Frequency Networks</b>	<b>79</b>
7.1	Propagation Conditions in a SFN . . . . .	79
7.2	A Single Frequency Network Field Trial . . . . .	83
7.2.1	Hardware Setup . . . . .	84
7.2.2	Field Strength Prediction and Measurement Locations Overview . .	84
7.2.3	Measurement of the Coverage Area . . . . .	85
7.2.4	High Velocity Measurements . . . . .	86
7.2.5	Low Velocity Urban Measurements . . . . .	88
7.2.6	Measurements in Mixed Surrounding . . . . .	89
7.3	Conclusions on a DRM+ Single Frequency Network . . . . .	90
<b>8</b>	<b>Receiver Diversity Techniques</b>	<b>91</b>
8.1	Combining Methods . . . . .	91
8.2	Antenna Diversity Methods . . . . .	95
8.2.1	Space Diversity . . . . .	95
8.2.2	Polarization Diversity . . . . .	99
8.3	Measurements . . . . .	100
8.4	Conclusions on the use of Receiver Diversity Techniques for DRM+ . . . .	106
<b>9</b>	<b>Summary</b>	<b>107</b>
<b>A</b>	<b>Channel Profiles for the Evaluation of the DRM+ System</b>	<b>109</b>
<b>B</b>	<b>Differential Operations</b>	<b>113</b>
	<b>List of Figures</b>	<b>114</b>
	<b>List of Tables</b>	<b>119</b>







# List of Abbreviations and Symbols

## Abbreviations

AFS	Alternative Frequency Signalling
AGC	Automatic Gain Control
BER	Bit Error Rate
CCIR	Consultative Committee on International Radio
CDD	Cyclic Delay Diversity
CEPT	Conférence Européenne des Administrations des Postes et des Télécommunications
COFDM	Coded Orthogonal Frequency-Division Multiplex
DAB	Digital Audio Broadcast
DD	Delay Diversity
DDC	Digital-Down-Converter
DRM	Digital Radio Mondiale
DVB	Digital Video Broadcast
EGC	Equal Gain Combining
EIRP	Equivalent Isotropically Radiated Power
EPG	Electronic Program Guide
ERP	Effective Radiated Power
ETSI	European Telecommunications Standards Institute
FAC	Fast Access Channel
FEC	Forward Error Correction

FPGA	Field Programmable Gate Array
GI	Guard Interval
GPS	Global Positioning System
HE-AAC	High Efficiency - Advanced Audio Coding
HF	High frequency
IBOC	In-Band On-Channel
ICI	Inter-Carrier-Interference
ISI	Inter-Symbol-Interference
ITM	Irregular Terrain Model
ITU	International Telecommunication Union
LF	Low frequency
LOS	Line-of-sight
LW	Long wave
MER	Modulation Error Ratio
MF	Medium frequency
MLC	Multi Level Coding
MMSE	Minimize Mean Square Error
MRC	Maximum Ratio Combining
MW	Medium wave
OFDM	Orthogonal Frequency-Division Multiplex
PRBS	Pseudo Random Bit Sequence
PSD	Power spectral density
QAM	Quadrature Amplitude Modulation
RSCI	Receiver Status and Control Interface
RSTA	Receiver Status Information
SC	Selection Combining

---

SDC	Service Description Channel
SFN	Single Frequency Network
SNR	Signal to Noise Ratio
SW	Short wave
SWC	Switched Combining
TDL	Tapped-Delay-Line
TMC	Traffic Message Channel
UHF	Ultra High Frequency (0,3 – 3 GHz)
VHF	Very High Frequency (30 – 300 MHz)
VSWR	Voltage Standing Wave Ratio

### Symbols

$\Gamma$	Reflection factor
$\lambda$	Wavelength
$\mu_0$	Permeability of free space
$\nabla \cdot$	Divergence
$\nabla \times$	Curl
$\omega_n$	Frequency of the $n$ -th subcarrier
$\rho$	Charge density
$\tau_n$	Delay of the $n$ th path
$\varepsilon_0$	Permittivity of free space
$A_n$	Tap gains of the uniformly spaced TDL
$d_n(i)$	Symbol
$f_0$	Subcarrier distance
$g_n(t)$	Complex valued channel gain of the $n$ -th multipath component
$G_r$	Gain of the receiver antenna

$G_t$	Gain of the transmitter antenna
$H(f), H(f; t)$	Channel transfer function
$h(t)$	Channel impulse response
$N$	Number of OFDM subcarriers
$P(f)$	Power spectral density
$P_t$	Transmitted power
$r(t)$	Received signal
$r_{LP}$	Received equivalent lowpass signal
$s(t)$	Transmitted signal
$s_{LP}$	Transmitted equivalent lowpass signal
$s_{OFDM}(t)$	OFDM baseband signal at the transmitter
$T_s$	Symbol duration
<b>B</b>	Magnetic induction
<b>D</b>	Electric induction
<b>E</b>	Electric field
<b>H</b>	Magnetic field
<b>J</b>	Current density
<b>k</b>	Wavenumber
<b>S</b>	Poynting vector

# 1 Introduction

The digitalization of sound broadcasting is planned or already going on in Germany and many other countries. Here the main drivers are an increased spectrum efficiency, better audio quality and additional data services.

The first evaluations on Digital Audio Broadcasting (DAB) have been conducted in the early 1980s at the Institut für Rundfunktechnik (IRT), the research centre of the Austrian, Swiss and German public broadcasters. Part of the development of DAB which later became an European Union research project (EUREKA 147) was the MPEG-1 Audio Layer II ('MP2') codec. With this compression technique it was possible to use the spectrum more efficiently than with analogue FM radio with a comparable sound quality. DAB is among the first standards based on the Orthogonal Frequency Division Multiplex (OFDM) transmission scheme which has become the most popular modulation technique for broadcast and communication systems today.

DAB was developed mainly by the public broadcasters and is very suitable for their needs, to transmit several programs economically with one transmitter in a multiplex. However for small-scale local and community radios this inflexible structure can lead to the problem that a local multiplex cannot be filled if e.g. only one local broadcaster is existing in a region. If not setting up a whole multiplex for one radio program, which would waste a lot of bandwidth, the only possibility is to move to the next bigger multiplex that normally covers an area far larger than the area needed to reach local listeners. This poses economic problems both in terms of transmitting in larger areas than needed and in terms of copyright levies that are based on the number of potential listeners in an area and not on the subset thereof that constitutes the target audience.

In other countries the radio stations would never 'give away' their signal to a transmitter operator. Instead these transmitters are operated directly by the radios. For radio companies with too little programs to fill a multiplex the DAB/DAB+ system is therefore difficult to use. This is the reason why countries like e.g. Brazil are not considering the multiplex system DAB/DAB+ for the digitalisation of their analogue FM radio stations.

To overcome this problem, DRM+ or DRM Mode E, was developed as an extension of the long, medium and short-wave Digital Radio Mondiale (DRM) standard for the upper VHF bands. With a bandwidth of 96 kHz, the OFDM based DRM+ system fits into the European FM frequency grid of 100 kHz and offers the chance to a successive digitalization of the FM broadcasting band. Especially for local and community radio stations, the system can be a way to digitize their signals, as in contrast to the DAB multiplex system, it offers a flexible frequency planning with an individual coverage area.

Additionally it can be used in the VHF Bands I and III (channels 5 and 6 in the Americas) which have been made available by the digital dividend after the digitization of terrestrial television broadcasting.

Another digital radio system was developed by the US company Ibiquity under the name HD Radio or In-Band On-Channel (IBOC). As this is a proprietary system with a total bandwidth of 400 kHz, which does not fit into the European channel grid, it was not considered in this thesis.

When starting to work with DRM at the Institute of Communication Technology (IKT) of Leibniz University of Hannover, the standard parameters of the DRM+ system had already been defined but field trials were missing to analyse the performance in a real world environment. As there was the chance to get a test licence for broadcasting DRM+ in the FM broadcasting band in Hannover, extensive field tests were conducted. Also other countries showed interest in trials with DRM+. There was the chance to attend and conduct some of these trials in Sri Lanka, India and Brazil. The results of these trials served as contributions to Working Party 6A on terrestrial broadcasting delivery of the International Telecommunication Union's (ITU) for the standardization of DRM+ within the ITU. By the end of 2011 Recommendation ITU-R BS.1114-7 'Systems for terrestrial digital sound broadcasting to vehicular, portable and fixed receivers in the frequency range 30-3 000 MHz' and Recommendation ITU-R BS.1660-5 'Technical basis for planning of terrestrial digital sound broadcasting in the VHF band' were published with DRM+ included.

While the digitalization of terrestrial television was accomplished within a short period, the radio sector needs a transition period with analogue and digital transmissions in parallel. In Germany and other countries the VHF Band II (87,5-108 MHz) is fully occupied by FM-radio which will not be switched off in the next years. At the same time, in band III, which allocates the frequencies from 174 to 230 MHz, there is a lot of free spectrum intended for digital audio broadcasting, therefore evaluations about the use of DRM+ in this available frequency space were started. Initially DRM+ was only standardized up to the FM band (VHF Band II). These evaluations and measurement results were also contributed by the German regulatory agency 'Bundesnetzagentur' to the ITU WP6A. The ITU documents mentioned above now also include the VHF Band III as possible frequency range for DRM+.

Especially local radios are often licensed with low power and using low antenna facilities. Therefore techniques to enhance the reception quality can be interesting to increase the coverage area.

One possibility is the use of transmitter diversity techniques, using more than one antenna to transmit the signal. Different diversity techniques are already used to enhance the performance in many OFDM based systems as IEEE 802.11, DAB or DVB-T. The DRM+ channel coding also offers the possibility to take advantage of the channel diversity. Especially with slow receiver velocities, destructive interference can produce channel attenuation over the whole signal bandwidth for a time period which exceeds the abil-

---

ity of the systems error correction to recover the data. To enhance system performance, evaluations and a field trial with transmitter delay diversity was conducted.

As a digital OFDM radio system, DRM+ is capable of transmitting in a Single Frequency Network (SFN) with several transmitters running on the same frequency. This can also be seen as a transmitter diversity system with very distant antennas. Due to a guard interval added before every OFDM symbol, differences in time of arrival from the different transmitters at the receiver site are not resulting in Inter-Symbol-Interference (ISI) if they are within the guard interval duration. A SFN offers the possibility of covering a big area with several transmitters on only one frequency which saves bandwidth and simplifies frequency planning significantly. It also enhances the reception quality in areas with obstacles like buildings, hills or mountains. Other uses for SFN are gap filling transmitters and coverage extenders. This technique is already used within other digital broadcasting systems as DAB/DAB+ or DVB-T. For the DRM+ system, the parameters for setting up a SFN have been evaluated. A field trial was conducted to confirm that the setup is working and different parameters were examined.

Besides the usage of diversity techniques at the transmitter site, receiver diversity techniques can provide a significant enhancement of the reception quality, too. Different receiver diversity techniques and methods to combine the signals have been evaluated regarding their gain and complexity and a field trial shows the outdoor functionality.

As all these techniques depend on the properties of the propagation channel, the main focus of these evaluations has therefore been set on the propagation channel at the relevant frequencies. Channel simulations should show the theoretical characteristics of the channel variations with the different diversity systems. Measurements then have been conducted to confirm those results.

## **Organisation of the thesis**

This thesis starts with a description of the DRM+ system with a closer look at the OFDM parameters that are relevant regarding propagation. Chapter 3 describes the transmission channel and the different models that are used to analyse the performance of a system with the expected properties in a real-world scenario. Chapter 4 analyses the performance of the DRM+ system in the VHF Band II, including the requirements for compatibility and coexistence with analogue FM radio. Chapter 5 analyses the opportunities and limits of DRM+ at higher frequencies in the VHF Band III. Chapter 6 to 8 discuss the possibilities of optimizing the performance by different diversity methods. Starting with transmitter diversity techniques, followed by Single Frequency Networks and on the receiver side, analysing the possibilities of different receiver diversity techniques. The thesis is summarized in Chapter 9.





## 2 The DRM+ System

The Digital Radio Mondiale system was designed to offer a digital replacement for analogue radio broadcasting in the AM (DRM30) and FM/VHF bands (DRM+) with a better audio quality and higher spectrum efficiency. It can be operated within the same channelling and spectrum allocations as employed by analogue radio [1]. An overview of the frequency-bands for DRM compared to analogue radio and DAB is shown in Figure 2.1.

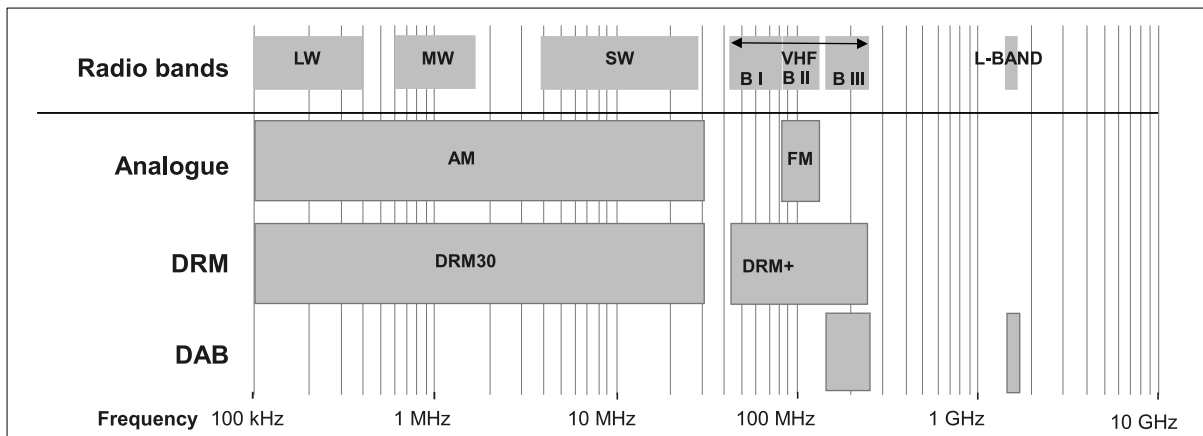


**Figure 2.1:** Frequency bands overview, analogue radio compared to DRM and DAB

The DRM standard describes a number of different operating modes, which can be split into two groups as follows:

- DRM30 is specifically designed to utilise the AM broadcast bands (long wave (LW), medium wave (MW) and short wave (SW)) below 30 MHz
- DRM+ utilises the spectrum in the VHF Band from 30 MHz to 230 MHz

The development of the DRM standard started in 1997 with the foundation of the DRM consortium in Guangzhou, China in 1997 [2]. Initially with the objective of 'digitising' the AM broadcast bands up to 30 MHz as the poor audio quality of the AM broadcast due to the bad channel conditions. With a digital system like DRM comprising appropriate audio codecs, channel coding and modulation the audio quality can be enhanced a lot. Additionally data services and even small scale video streams are applicable. The DRM system specification for broadcasting below 30 MHz was first published by the European Telecommunications Standards Institute (ETSI) in 2001.

The decision to extend the system to the VHF Band was taken in 2005. In August 2009, DRM+ (Mode E) has become an official broadcasting standard with the publication of the technical specification by the ETSI. As the propagation conditions in the VHF are

quite different from the LW, MW and SW bands this is effectively a new release with more bandwidth and different system parameters.

DRM+ was then successfully tested and standardized also in the VHF Band III. This gives the DRM system the widest frequency usage as can be seen in Figure 2.1. It can be used in the VHF Band I, II and III. It is possible that DRM+ can co-exist with DAB in the VHF Band III. It also could be used in the present FM broadcasting band and even in the former analogue television radio frequency range from 47 MHz to 88 MHz (Band I).

DRM+ has a narrow bandwidth and is designed to fit in the FM broadcast band plan with a channel span of 100 kHz. The small spectrum requirements support its use in crowded bands. DRM+ provides bit rates from 37 kbps to 186 kbps and, like DRM, permits up to four services. It is therefore a flexible solution allowing single or small numbers of audio services to be broadcasted together.

This Chapter provides an overview of the DRM+ system. Starting with source and channel coding and a description of the data services that can be included in the stream. This is followed by an overview of the transmission multiplex, the multicarrier modulation and receiver architectures.

### **Transmission Data**

The audio source coding for DRM+ is currently done with MPEG-4 HE-AAC (High Efficiency - Advanced Audio Coding). HE-AAC is an audio coder suited for voice and music with an optional extension for reconstruction of high frequencies (spectral bandwidth replication). Tests by the European Broadcasting Union indicated that HE-AAC at 48 kbps still ranked as 'excellent' quality [3]. At very low bit rates as 24 kbps, it still provides 'good' quality.

Additionally data services as text-messages, Electronic Program Guide (EPG) or traffic information (Traffic Message Channel - TMC) can be included in the signal. More information can be included with the 'Journaline' text information service which includes web feeds in the stream or slide shows with a sequence of images. An emergency warning/alert feature is also implemented.

### **The OFDM Multiplex**

The OFDM multiplex, created in the transmitter consists of three logical channels as shown in Figure 2.2. The encoded audio and broadcast data services form the Main Service Channel (MSC). The Fast Access Channel (FAC) contains a set of core parameters required by the receiver to quickly check for available services within a multiplex to allow demodulation of the DRM signal. The Service Description Channel (SDC) carries advanced information like audio and data coding parameters, service labels, current time and date and AFS (Alternative Frequency Signalling) tables, providing information on other frequencies and radio standards containing the same program.

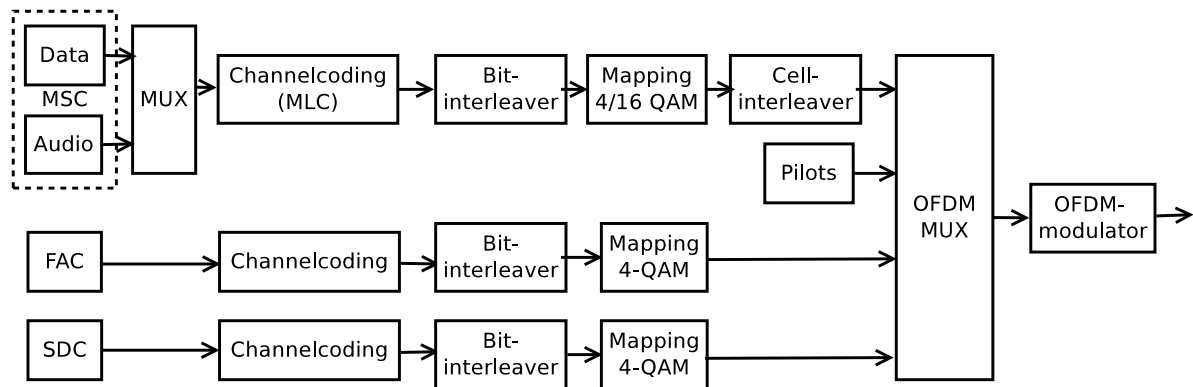


**Figure 2.2:** The OFDM multiplex created in the DRM+ transmitter

The channel encoding process of the MSC is based on a Multi Level Coding (MLC) scheme. The aim of MLC is to reach the best transmission performance by the joint optimization of coding and modulation. This denotes that more error prone bit positions in the QAM mapping get a higher protection. The different levels of protection are obtained by using different component codes which are realized with punctured convolutional codes, derived from the same mother code [4].

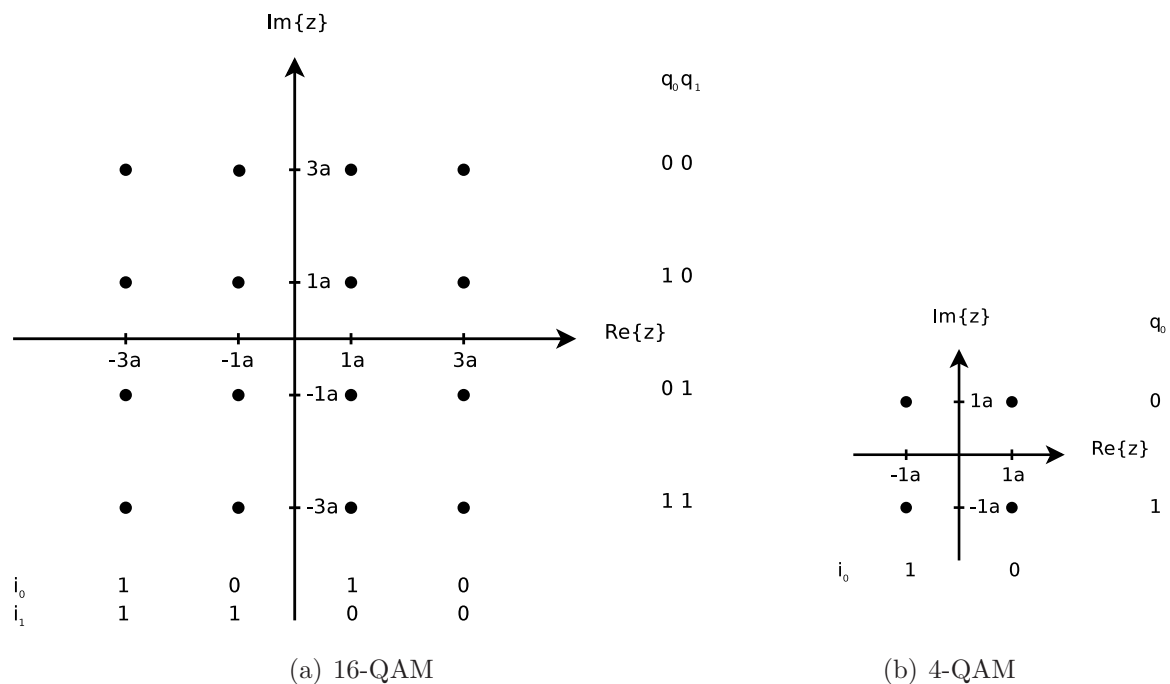


**Figure 2.3:** QAM mapping with corresponding bit pattern

After the channel coding, bit-interleaving is applied over one frame (100 ms) independently for the FAC, SDC and MSC in order to improve the robustness of the bit stream against burst errors. In DRM Mode E a mapping to 4- and 16-QAM can be applied. The corresponding mapping schemes are shown in Figure 2.3. In the MSC stream additionally cell-interleaving over 6 frames (600 ms) is applied. The possible use of different code rates

and QAM modes results in data rates from 37 to 186 kbps. A signal with a low data rate is more robust and therefore needs a lower signal level at the receiver for proper reception. Table 2.1 shows the available protection levels, code rates and resulting bit rates in an overview.

**Table 2.1:** DRM+ protection level and bit rates for 4-QAM modulation

Protection level	Code rate	Bit rate [kbit/s]
MSC: 4-QAM		
0	0.25	37.3
1	0.33	49.8
2	0.4	59.7
3	0.5	74.6
MSC: 16-QAM		
0	0.33	99.5
1	0.41	122.6
2	0.5	149.3
3	0.62	186.6

The SDC (Service Description Channel), which contains signalling data, is modulated with 4-QAM and can be configured to the code rates 0.25 and 0.5. The FAC (Fast Access Channel) uses a fix code rate of  $R = 0.25$ .

The MSC, FAC and SDC data streams are then combined to a multiplex. A pilot generator injects non-data carriers of prescribed amplitude and phase which permits a receiver to derive channel equalisation information, thereby allowing coherent demodulation of the signal. The multiplex is then modulated with Coded Orthogonal Frequency-Division Multiplex (COFDM) or Orthogonal Frequency-Division Multiplex (OFDM). The word 'coded' here refers to the use of Forward Error Correction (FEC) [5] which is used in almost every OFDM system. OFDM is used in many wireless systems like DVB , Wifi or DAB as it enables a robust transmission over mobile channels and is adaptable to many different situations. This is achieved by using a number of closely spaced orthogonal sub-carriers to carry the data. The next Section gives some more details on OFDM.

### The Multicarrier OFDM System

For digital communications OFDM has become a popular scheme in the last years. In OFDM a number of orthogonal subcarriers are used to carry the data. Each subcarrier is modulated independently with a conventional modulation scheme. The distribution of the symbols on different subcarriers extends the symbol duration by the number of subcarriers. This makes the use of a guard interval between symbols affordable to avoid Inter-Symbol-Interference (ISI). ISI originates from multipath propagation in the transmission channel (see Chapter 3) producing an echo signal in the receiver. The guard interval with duration

$T_g$  is added as cyclic prefix to every symbol. Figure 2.4 shows the ability of a guard interval to eliminate Inter-Symbol-Interference. As long as the echo duration  $\tau$  is smaller than  $T_g$ , ISI can be eliminated. At the receiver the guard interval is also used for the time synchronisation.

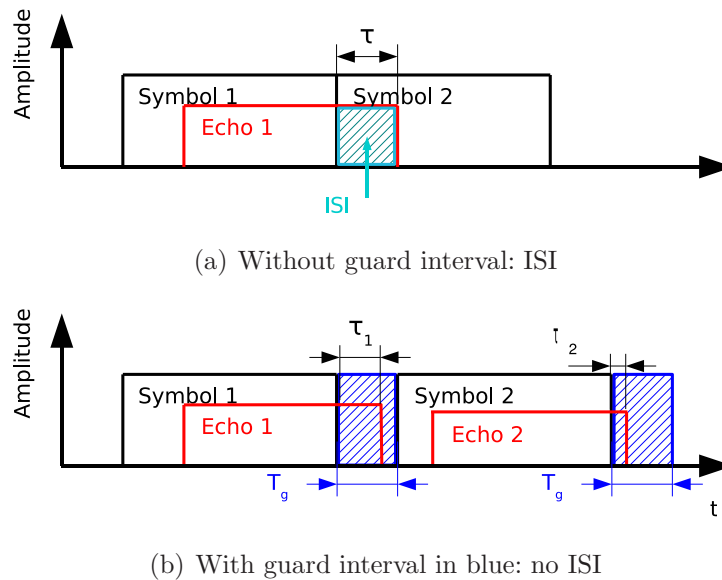


**Figure 2.4:** Received OFDM symbols with an echo produced by multipath propagation

At the transmitter  $N$  parallel symbols  $d_0(i), \dots, d_{N-1}(i)$  are generated from an incoming serial symbol stream. The duration of each symbol  $T_s$  becomes  $N$ -times the duration of the serial symbols. Then the parallel symbols are modulated to the subcarriers at frequencies  $f_0, \dots, f_{N-1}$ . If the subcarrier distance comply with  $1/T_s$  and a rectangle transmission pulse is used, the multicarrier signal satisfies the first Nyquist criterion and becomes orthogonal in the frequency domain [6]. The orthogonality ensures that the carriers do not influence each other at their respective center frequency. It also allows for efficient modulator and demodulator implementation using the FFT algorithm on the receiver side, and inverse FFT at the transmitter side.

With this rectangle transmission pulse with a duration  $T_s$  the multicarrier signal within one symbol duration results in [6]:

$$s_{OFDM}(t) = \sum_{n=0}^{N-1} d_n(i) e^{j2\pi f_n t} \quad \text{for} \quad iT_s \leq t \leq (i+1)T_s. \quad (2.1)$$

Because of the rectangular pulse shape, at every subcarrier frequency  $f_n = n/T_s$ , the spectral shape is given by a sinc function [7]. Figure 2.5 shows the spectrum of an OFDM signal with 4 subcarriers plotted against the subcarrier distance  $f_0$ .

Adding the guard interval has the effect, that the transmit pulses are not orthogonal to each others. However, at the receiver the guard interval is removed and the orthogonality is restored.

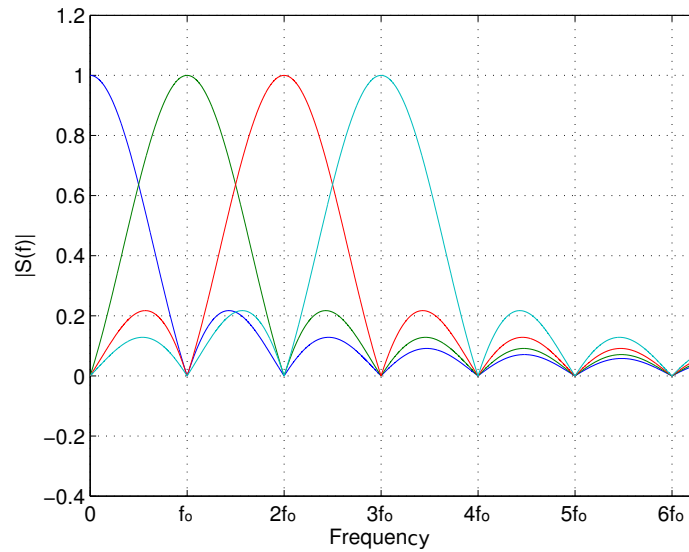


**Figure 2.5:** Base band OFDM spektrum

### The DRM+ System Parameters

The OFDM parameters of DRM+ are adapted to the propagation conditions in the VHF Band. The subcarrier spacing limits the mobile characteristics of an OFDM system. Mobile reception in combination with multipath propagation causes Doppler shifts of the carriers. The larger the subcarrier spacing, the more robust a system is against Doppler.

The symbol duration in the DRM+ system is 2.25 ms, the guard interval (GI) adds another 0.25 ms which is adapted to a propagation delay corresponding to a distance of 75 km. E.g. in a Single Frequency Network the signals of the transmitters contributing to the reception should not have a greater difference of their distance than 75 km.

**Table 2.2:** DRM+ system parameters

Modulation	COFDM
Data rate	37 - 186 kbps
Subcarrier modulation	4-/16-QAM
Signalbandwith	96 kHz
Subcarrierspread	444.444 Hz
Number of subcarriers	213
Symbol duration	2.25 ms
Guard interval duration	0.25 ms
Frame length	100 ms
Number of programs	1-4

For the protection of the data against flat fading a bit interleaver is applied over one transmission frame (100 ms) and cell interleaving over 6 transmission frames (600 ms). With this the clustered erroneous bits produced by fading are distributed over the transmission frames and the error correction in the receiver (Viterbi decoder) can perform.

However, in difficult environments e.g. very slowly moving receivers, adding additional diversity to the channel e.g. by receiver or transmitter diversity techniques or by setting up a Single Frequency Network can enhance the system performance, see Chapter 6, 7 or 8. The DRM+ system parameters are summarized in Table 2.2.

## Receiver Architecture

Figure 2.6 shows a simplified receiver architecture of a DRM+ receiver. The RF-frontend transforms the signal into the baseband or an intermediate frequency where it is filtered and sampled by an analogue-to-digital converter (ADC). In case of oversampling, the signal has to be interpolated or resampled to the necessary sampling rate. For DRM+ the minimal usable sampling rate is 96 kHz. Automatic gain control is performed in the frontend to adapt the signal to the ADC range.

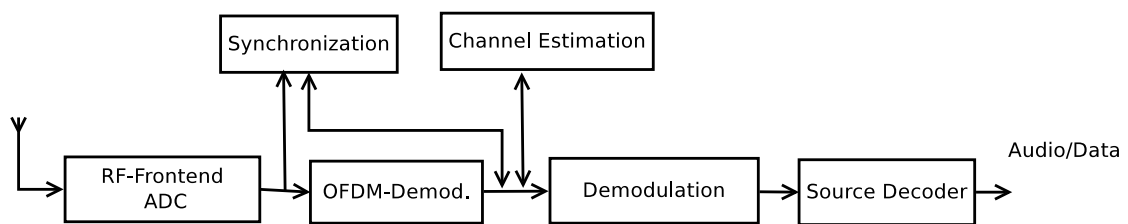


**Figure 2.6:** Receiver architecture

The received signal is disturbed by the transmission channel (see Chapter 3) and additional noise. A time and frequency synchronization is necessary to detect the beginning of a symbol/frame and to correct frequency deviations.

To equalize the channel effects, channel correction is performed. The necessary channel estimation is done by interpolating the known channel characteristics at the pilot cell locations over all carriers. The interpolation itself can be done with a Wiener estimator to minimize the mean square error (MMSE). At this stage the channel properties can significantly affect the reception. If the channel changes too fast, for example if the receiver is located in a fast moving vehicle, the distance between the pilot cells in time direction can be too large and proper interpolation cannot be done. This can be described as a sampling of the channel at the pilot cell locations. If the channel changes too fast, the sampling theorem cannot be fulfilled. This topic is discussed in detail in Section 5.1.

After the demodulation a Viterbi decoder is used for decoding the convolutional encoded stream. Depending on the code rate, the distribution of the errors and the Viterbi length a dedicated amount of errors can be repaired. After the source decoder, the audio/data services should be available.

Different receiver profiles as a 'Standard Radio Receiver' or a 'Rich Media Radio Receiver' are specified in [8]. With proper transmitter setup a seamless switching between DRM+, analogue FM and different digital radio standards as DAB/DAB+ is possible.

The measurement receiver, used in the trials can record different reception parameters necessary to evaluate the measurements. For example the estimated Signal-to-Noise Ratio (SNR) and the audio errors, the GPS data are part of the implemented Receiver Status and Control Interface. The details of the receiver parameters are given in [9].



## 3 The Transmission Channel

The transmission channel in the VHF Band from 30 - 300 MHz is characterized by diffraction, reflection and scattering. With this, reception often becomes possible, even if the direct path between transmitter and receiver is obstructed. Unlike high frequencies (HF), the ionosphere does not usually reflect VHF radio and thus transmissions are restricted to the local area and don't interfere with transmissions thousands of kilometres away. This makes the VHF band very suitable for broadcasting systems.

This Chapter will describe the transmission channel. The physical fundamentals of wave propagation can be derived by the famous Maxwell's equations, that have been published by the Scottish physicist James Clerk Maxwell between 1861 and 1862 and summarized 1865 in his scientific paper 'A dynamical theory of the electromagnetic field' [10]. However, they are quite complex and not easy to use for practical purposes, therefore different models have been developed, taking into account different aspects of the channel. Different models have been deployed for this thesis and will be introduced in this Chapter. An overview about the physical fundamentals and different propagation models are given, followed by coverage prediction methods and statistical channel models that are used for simulation purposes.

### 3.1 Wave Propagation

The propagation of electromagnetic waves can be derived by Maxwell's equations. These equations describe how electric and magnetic fields are generated and altered by each other and by charges and currents in time and space within a medium. Maxwell's four equations in differential form are [11]:

$$\nabla \cdot \mathbf{D} = \rho \quad (3.1)$$

$$\nabla \cdot \mathbf{B} = 0 \quad (3.2)$$

$$\nabla \times \mathbf{E} = -\frac{\partial \mathbf{B}}{\partial t} \quad (3.3)$$

$$\nabla \times \mathbf{H} = \mathbf{J} + \frac{\partial \mathbf{D}}{\partial t} \quad (3.4)$$

With the the electric induction  $\mathbf{D}$ , the magnetic induction  $\mathbf{B}$ , the vector electric field  $\mathbf{E}$ , the vector magnetic field  $\mathbf{H}$ , the current density  $\mathbf{J}$  and the charge density  $\rho$ .

Interaction with material with the permittivity  $\varepsilon$ , the permeability  $\mu$  is given as  $\mathbf{D} = \varepsilon\mathbf{E}$  and  $\mathbf{B} = \mu\mathbf{H}$ . In free space  $\varepsilon$  and  $\mu$  are equal to  $\varepsilon_0$ , the permittivity of free space and  $\mu_0$ , the permeability of free space.

The differential operators used here are the divergence  $\nabla \cdot$  and the curl  $\nabla \times$ . The definitions of these operators are given in Annex B.

For the assumption of propagation in a vacuum with no charges ( $\rho = 0$ ) and no currents ( $\mathbf{J} = 0$ ), Maxwell's equations reduce to:

$$\nabla \cdot \mathbf{D} = 0 \quad (3.5)$$

$$\nabla \cdot \mathbf{B} = 0 \quad (3.6)$$

$$\nabla \times \mathbf{E} = -\frac{\partial \mathbf{B}}{\partial t} \quad (3.7)$$

$$\nabla \times \mathbf{H} = \frac{\partial \mathbf{D}}{\partial t} \quad (3.8)$$

Taking the curl of equation 3.7 and 3.8 returns:

$$\nabla \times \nabla \times \mathbf{E} = -\frac{\partial}{\partial t} \nabla \times \mathbf{B} = -\mu_0 \varepsilon_0 \frac{\partial^2 \mathbf{E}}{\partial t^2} \quad (3.9)$$

$$\nabla \times \nabla \times \mathbf{H} = \frac{\partial}{\partial t} \nabla \times \mathbf{D} = \varepsilon_0 \frac{\partial}{\partial t} \nabla \times \mathbf{E} = -\mu_0 \varepsilon_0 \frac{\partial^2 \mathbf{H}}{\partial t^2} \quad (3.10)$$

By using the vector identity  $\nabla \times (\nabla \times \mathbf{V}) = \nabla(\nabla \cdot \mathbf{V}) - \nabla^2 \mathbf{V}$  and with the speed of light in free space  $c_0 = \frac{1}{\sqrt{\mu_0 \varepsilon_0}} = 2.99792458 \cdot 10^8$  m/s this turns into the well known wave equation:

$$\frac{\partial^2 \mathbf{E}}{\partial t^2} - c_0^2 \cdot \nabla^2 \mathbf{E} = 0 \quad (3.11)$$

$$\frac{\partial^2 \mathbf{H}}{\partial t^2} - c_0^2 \cdot \nabla^2 \mathbf{H} = 0 \quad (3.12)$$

Many solutions to Maxwell's equations exist and can be represented as a sum of plane waves, which represent the simplest possible time varying solution [12]. A plane wave travelling in direction  $\mathbf{z}$  only consists of an electrical component  $E_x$  and a magnetic component  $H_y$ . Both components are orthogonal to the propagation direction and are only a function of  $z$  and  $t$ .

$$E_x(z, t) = E_0 e^{j(\omega t - kz)} \quad (3.13)$$

$$H_y(z, t) = H_0 e^{j(\omega t - kz)} \quad (3.14)$$

The wavenumber  $k = \frac{2\pi}{\lambda}$  represents the rate of change of the phase and is pointing in the direction of propagation.

The Poynting vector represents the energy flux density in the direction of propagation and is defined as:

$$\mathbf{S} = \mathbf{E} \times \mathbf{H} \quad (3.15)$$

The alignment of the electric field vector of a plane wave defines the polarization of the wave. If the electric field vector has a single direction it is called linearly polarized. If there are two orthogonal components with exactly the same amplitude which are ninety degree out of phase it is called circular polarization. The direction, the electric field rotates is dependent on which component is ninety degree ahead of the other. If the two components do not have the same amplitude it is called elliptical polarization.

## 3.2 Propagation models

For the practical usage in planning broadcasting systems different propagation models have been developed. The path-loss prediction models can be roughly divided into four types. Empirical models, theoretical models, site-specific models and a mixture of those. A comprehensive review of the propagation prediction models for terrestrial wireless communication systems is given in [13]. The following Section will shortly introduce the models that have been applied in this thesis.

### 3.2.1 Free Space Loss

The benchmark by which the loss in a transmission link can be measured is the loss that would be expected in free space, in a region which is free of all objects that might absorb or reflect energy of the electromagnetic wave.

For the purpose of coverage prediction, the distance between the transmission antenna and the receiving antenna normally exceeds the antenna length and also the wavelength by several multiples. In this case, the Poynting vector seems to radiate from a single point and considering just the far-field of an antenna is suitable. For this the Fraunhofer or far-field approximation can be used to simplify the solution of the magnetic vector potential. The Fraunhofer approximation can be divided in a term that describes the spherical propagation and a term that describes the three-dimensional profile.

The three-dimensional profile is dependent on the form of the antenna pattern. Due to the spherical propagation, the received power decays with one over the square of the path length  $d$  between the receiver and transmitter. The power at the receiver  $P_r$  can then be written as [14]:

$$P_r = P_t \left( \frac{\lambda}{4\pi d} \right)^2 G_t G_r \quad (3.16)$$

$P_t$  is the transmitted power,  $\lambda$  is the wavelength,  $G_t$  is the gain of the transmitter antenna in the direction of the receiver antenna and  $G_r$  the gain of the receiver antenna in the direction of the transmitter antenna.

The product  $P_t \cdot G_t$  is called the equivalent isotropically radiated power (EIRP). This describes the amount of power that an isotropic antenna would emit to produce the peak power density observed in the direction of maximum antenna gain. More often the ERP (effective radiated power) is used. Here the gain is set in relation to a  $\lambda/2$ -dipole.

As the free space model is too inaccurate for most of the situations, different models taking into account for example reflections of the signal, have been derived over the years.

### 3.2.2 Theoretical and Empirical models

Theoretical models are derived, assuming some ideal conditions of known physical parameters. For example, the over-rooftop diffraction model is derived using physical optics assuming uniform heights and spacing of buildings. They are developed based on large collections of data for a specific scenario.

Important parameters for the empirical models are the location and time variability. As the area-coverage prediction methods are intended to provide the statistics of reception conditions over a given area, rather than at any particular point, the location and time variability gives information about the percentage of locations and time in which a certain field strength is available. For planning purposes reception modes are given for the different systems, defining the location and time variability necessary for good reception in a certain situation. For example a location probability of 95 % is assumed to obtain good portable reception according to the ITU Recommendation ITU-R BS.1660-5, which provides a guideline on planning of terrestrial digital sound broadcasting in the VHF band [15].

When one terminal of a radio path is stationary, and the other terminal is being moved, path loss will vary continuously with location, according to the totality of influences affecting it. These influences can be classified into three main categories [16]:

- **Multipath variations:** Signal variations will occur over scales of the order of a wavelength due to phasor addition of multipath effects, e.g. reflections from the ground or buildings. The statistics of these variations are found to follow a Rayleigh distribution (see subsection 3.3).
- **Local ground cover variations:** Signal variations will occur due to obstruction by ground cover in the local vicinity, e.g. buildings or trees over scales of the order of the sizes of such objects. The scale of these variations will normally be significantly larger than that for multipath variations.
- **Path variations:** Signal variations will also occur due to changes in the geometry of the entire propagation path e.g. the presence of hills. For all except very short paths, the scale of these variations will be significantly larger than that for local ground cover variations.

Two models, often used for the VHF band are the Longley-Rice or Irregular Terrain Model and the ITU-Recommendation P.1546-4. A brief introduction of both models follows.

### Longley-Rice or Irregular Terrain Model

The Irregular Terrain Model (ITM) is also known as the Longley-Rice model named for Anita Longley and Phil Rice whose publication [17] describes the method. The model was developed by the Institute for Telecommunication Sciences, Boulder, Colorado and made available to the public.

The ITM radio propagation model for frequencies between 20 MHz and 20 GHz is based on electromagnetic theory and on statistical analyses of both terrain features and radio measurements. It predicts the median attenuation of a radio signal as a function of distance and the variability of the signal in time and in space. The ITM takes into account the path variations, but no local ground cover variations (buildings, woods, etc.). These have to be considered separately as well as the multipath variations.

### ITU-R P.1546-4

This ITU Recommendation describes a method for point-to-area radio propagation predictions for terrestrial services in the frequency range 30 MHz to 3000 MHz. It is intended for use on tropospheric radio circuits over land paths, sea paths and/or mixed land-sea paths between 1-1000 km length for effective transmitting antenna heights less than 3000 m. The method is based on interpolation/extrapolation from empirically derived fieldstrength curves as functions of distance, antenna height, frequency and percentage of time. The calculation procedure also includes corrections to the results obtained from this interpolation/extrapolation to account for terrain clearance and terminal clutter obstructions [16].

### 3.2.3 Site-specific Models

Site-specific models often also called deterministic models are based on numerical methods such as ray-tracing and the finite-difference time-domain (FDTD) method [13]. The input parameters can be very detailed and accurate but are only valid for a specific situation and can become computationally intensive for complex environments.

The basic procedure of a ray-tracing method is the Shooting-and-Bouncing Ray (SBR) algorithm. First, a ray is launched from the transmitting antenna. Then this ray is traced to see if it hits any object or is received directly by the receiving antenna. When an object is hit, reflection, transmission, diffraction, or scattering will occur, depending on the geometry and the electric properties of the object. When a ray reaches the receiving antenna, the electric field associated with this ray is calculated [13].

The number of rays considered and the distance from the transmitter to the receiver location determines the available spatial resolution and, hence, the accuracy of the model [18]. Different methods and algorithms like the image method or the Angular Z-Buffer are being developed to accelerate the ray-tracing algorithms. An overview can be found in [13] and [18].

### 3.3 Statistical Models

As a result of multipath propagation caused by reflections and scattering as shown in Figure 3.1, small scale fading occurs in the range of a wavelength. This fading can badly affect the reception especially in mobile systems, when the receiver or transmitter is moving through this fading pattern. The fading duration depends on the wavelength and the speed of the mobile unit. The time delay between the arriving rays results in frequency dependant fading, which also has to be taken into account.

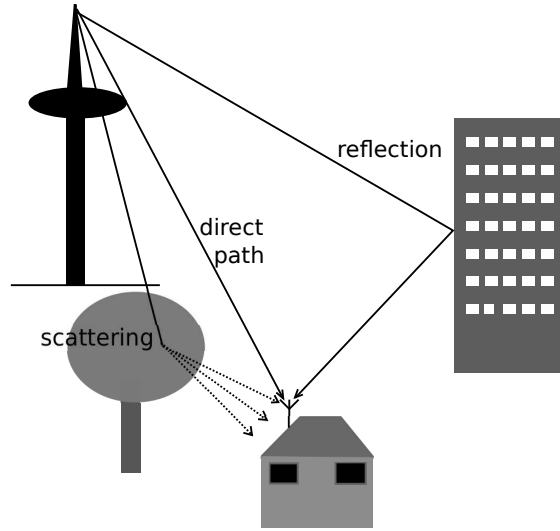


**Figure 3.1:** Multipath propagation

This small-scale channel modelling is usually investigated using statistical methods [13].

Mathematically this time variant transmission channel can be described as a random process. With the transmitted signal  $s(t)$  as a process whose spectral components cover a band of frequencies which is small compared to any frequency in the band may be expressed as [19]:

$$s(t) = \text{Re}\{s_{LP}(t)e^{j2\pi f_c t}\} \quad (3.17)$$

where  $s_{LP}(t)$  is the equivalent lowpass signal of  $s(t)$ .

The received signal  $r(t)$  after the transmission over a time invariant multipath channel with infinite paths can be expressed as:

$$\begin{aligned} r(t) &= \sum_{n=-\infty}^{\infty} g_n s(t - \tau_n) \\ &= \sum_{n=-\infty}^{\infty} g_n \text{Re}\{s_{LP}(t - \tau_n)e^{j2\pi f_c(t - \tau_n)}\} \\ &= \text{Re}\left\{\left(\sum_{n=-\infty}^{\infty} g_n e^{-j2\pi f_c \tau_n} s_{LP}(t - \tau_n)\right) e^{j2\pi f_c t}\right\} \end{aligned} \quad (3.18)$$

Where  $g_n$  is the complex valued channel gain of the  $n$ -th multipath component and  $\tau_n$  the delay of the  $n$ -th path.

A comparison with (3.17) shows that the sum

$$r_{LP}(t) = \sum_{n=-\infty}^{\infty} g_n e^{-j2\pi f_c \tau_n} s_{LP}(t - \tau_n) \quad (3.19)$$

represents the lowpass equivalent of  $r(t)$ . The term  $2\pi f_c \tau_n$  is the phase rotation of each path caused by  $\tau_n$ . The lowpass equivalent transmit and receive signal  $s_{LP}(t)$  and  $r_{LP}(t)$  are related by:

$$r_{LP}(t) = h(t) * s_{LP}(t) \quad (3.20)$$

The impulse response  $h(t)$  of the channel then can be expressed as [7]:

$$\begin{aligned} h(t) &= \sum_{n=-\infty}^{\infty} g_n e^{-j2\pi f_c \tau_n} \delta(t - \tau_n) \\ &= \sum_{n=-\infty}^{\infty} G_n \delta(t - \tau_n) \end{aligned} \quad (3.21)$$

With  $G_n = g_n e^{-j2\pi f_c \tau_n}$ .

The impulse response is a useful characterization of the system, since the output of the system can be computed through convolution of the input with the impulse response. The channel transfer function in the frequency domain can be derived with the Fourier transformation  $\xrightarrow{\mathcal{F}}$  of the impulse response. With the Fourier transforms  $f(t - a) \xrightarrow{\mathcal{F}} F(\omega)e^{-j\omega a}$  and  $\delta(t) \xrightarrow{\mathcal{F}} 1$  the channel transfer function becomes:

$$H(f) = \sum_{n=-\infty}^{\infty} G_n e^{-j2\pi f \tau_n} \quad (3.22)$$

### 3.3.1 The Time-Variant Channel

In real life the channel mostly is not static. Moving receivers or reflections at moving objects can lead to time-variant channel properties. This results in a time-dependent distribution of the channel gain  $G_n(t)$  and the delay  $\tau_n(t)$ . The transfer function also becomes time-dependent:

$$H(f; t) = \sum_{n=-\infty}^{\infty} G_n(t) e^{-j2\pi f \tau_n(t)} \quad (3.23)$$

The stochastic fading of the received signal can be handled by describing  $G_n(t)$  as a random process in  $t$ . Different probability distributions are used to characterize the statistics

of the fading channel. When a large number of scatterers are in the channel that contribute to the signal at the receiver, the application of the central limit theorem leads to a Gaussian process model for the channel impulse response. If the process is zero-mean, then the envelope of the channel impulse response  $|G_n(t)|$  has a Rayleigh probability distribution and the phase is uniformly distributed [20]. This corresponds to reception just over reflections and scattering with no direct line-of-sight component. With a line-of-sight path between transmitter and receiver the function  $|G_n(t)|$  is following a Rice distribution.

### The Doppler Effect

One effect of the time-variant channel is the Doppler effect. With a receiver moving towards or away from the transmitter as seen in Figure 3.2 the signal is affected by the Doppler effect.

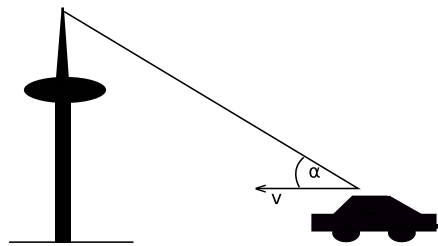


**Figure 3.2:** The Doppler effect with a moving receiver

If the mobile receiver is moving towards the source of the wave, the apparent frequency is increased whereas it decreases for motions away from the source. This occurs because the mobile crosses the wave fronts of the incoming wave at a different rate from when it is stationary [12]. Having a sine wave with frequency  $f_0$  the Doppler frequency  $f_d$  is given by:

$$f_d = \frac{v}{c_0} \cdot f_0 \cdot \cos \alpha \quad (3.24)$$

With the speed of light  $c_0$ , the velocity of the moving receiver  $v$  and the angle between the direction of motion and the direction of the incoming wave.

In case of multipath propagation waves are arriving from different directions resulting in different Doppler frequencies, which leads to a spread of the received signal, called Doppler spread. For the shape of the Doppler spectrum a statistical model of the arrival angle of the multipath components is used. In the most commonly used model in a Rayleigh fading channel, the arriving waves at the mobile are assumed to be equally likely to come from any horizontal angle with the same power. The resulting power spectral density  $S(f)$  is called the classical or Jakes Doppler spectrum and is given as [12]:

$$S(f) = \frac{A}{\sqrt{1 - (\frac{f}{f_d})^2}} \quad \text{for} \quad |f| \leq f_d \quad (3.25)$$



With  $A = \sigma_r / \pi f_d$  and the complex signal power  $\sigma_r$ . Figure 3.3 shows the Jakes Doppler spectrum.

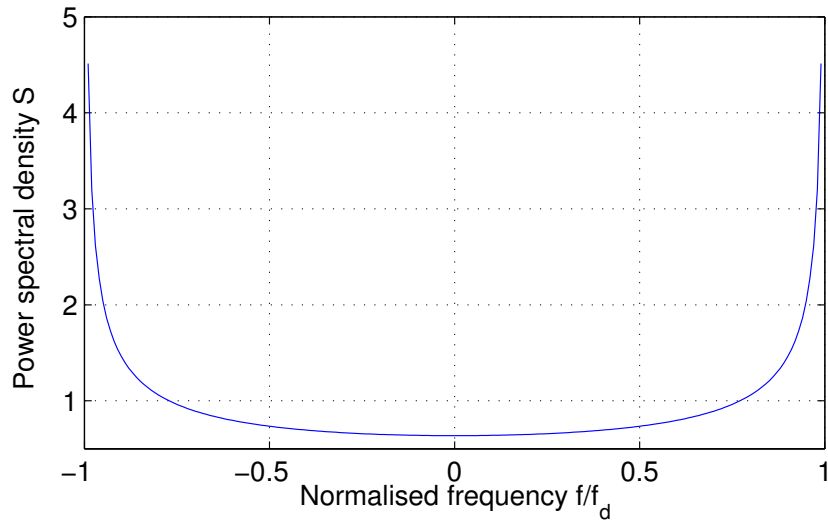


**Figure 3.3:** Jakes Doppler spectrum

If there is an additional direct component in the received signal, this has to be added to the Jakes spectrum as:

$$S(f) = \frac{A}{\sqrt{1 - (\frac{f}{f_d})^2}} + B \cdot \delta(f - f_d) \quad \text{for} \quad |f| \leq f_d \quad (3.26)$$

This distribution is called Rice-spectrum, with the Rice-factor  $RF = B / (\pi f_d A)$  describing the power ratio between the direct and the stochastic component.

Further spectra that are used in Annex A are the *GAUSS1* and *GAUSS2* spectra used for propagation paths with long delays. They are defined with the help of the Gaussian function  $G(f, A, f_1, f_2)$ :

$$G(f, A, f_1, f_2) = A e^{-\frac{(f-f_1)^2}{2f_2^2}} \quad (3.27)$$

The Gauss Doppler spectra are defined as [4]:

$$S(f) = G(f, A, \pm 0.7f_d, 0.1f_d) \quad \text{for} \quad |f| \leq f_d \quad (3.28)$$

Where the plus stands for *GAUSS1* and the minus for *GAUSS2*.

Every path component, in addition to the time variant specific delay, is characterized by a Doppler spectrum.

### Coherence Time

Another way to describe the effect of the Doppler spread is in the time domain. This leads to the coherence time of the channel.

The normalised autocorrelation function  $\rho(\tau)$  of a Rayleigh faded channel at a constant velocity, resulting in a maximum Doppler shift  $f_d$  is given as a Bessel function of the first kind and zero order [14]:

$$\rho(\tau) = J_0(2\pi f_d \tau) \quad (3.29)$$

The autocorrelation function expresses the correlation between a signal at a given time and its value at a specific time delay  $\tau$ . It leads to the coherence time  $T_c$  as the time over which the channel can be assumed constant. Often the following relation between the coherence time  $T_c$  as and the Doppler frequency  $f_d$  is used [21]:

$$T_c = \sqrt{\frac{9}{16\pi f_d^2}} = \frac{0.423}{f_d} \quad (3.30)$$

This results in two important constraints. On the one hand, if the coherence time is less than the symbol duration, reception can become problematic. On the other hand if the coherence time is very long, which can be the case if the receiver is moving very slowly at a place with destructive fading, no error correction or interleaving code can recover the signal.

### Coherence Bandwidth

Another impact of multipath propagation is frequency selectivity which can be described with the coherence bandwidth.

The coherence bandwidth  $B_c$  gives information about the channel transfer function in the frequency domain. It is inversely proportional to the delay spread  $\Delta\tau$ , which describes the average delay.

For the calculation of  $\Delta\tau$ , the power transmitted by the different path components with delay  $\tau_n$  and their respective Doppler spectra  $S(\tau_n, f)$  first has to be calculated as [22]:

$$P(\tau_n) = P_0 \int_{-f_d}^{f_d} S^2(\tau_n, f) df \quad (3.31)$$

where  $P_0$  is a normalising power. For discrete values of the power delay spectrum  $\Delta\tau$  is given as the second moment:

$$\Delta\tau = \sqrt{\frac{1}{P_m} \sum_{n=1}^N \tau_n^2 P(\tau_n) - \left(\frac{1}{P_m} \sum_{n=1}^N \tau_n P(\tau_n)\right)^2} \quad , \quad (3.32)$$

with the number of tabs  $n$  and the sum of the transmitted power  $P_m = \sum_{n=1}^N P(\tau_n)$ .  $B_c$  is then calculated as:

$$B_c = \frac{1}{\Delta\tau} \quad (3.33)$$

The following channel properties can be derived from the ratio between the signal bandwidth and the coherence bandwidth of the channel:

- **Frequency selective channel:** The coherence bandwidth is smaller than the signal bandwidth. Different spectral components of the signal are being affected distinctly by the channel. Some spectral components can be attenuated significantly, others can be amplified by additive interferences.
- **Frequency flat channel:** The coherence bandwidth is larger than the signal bandwidth. With disadvantageous phase constellations the whole signal can be attenuated. This is often called 'flat fading'.

### 3.3.2 Channel Simulation

To evaluate the performance of a system in a mobile channel, a model is needed that takes into account the relevant statistical properties of the channel. Mainly two methods are in use. The Monte-Carlo-Method, which is described for example in [23] and the tapped-delay-line model. In this work the tapped-delay-line model (TDL) was used and will be shortly introduced.

The TDL model can be interpreted as a superposition of a certain number  $N$  of discrete fading paths corresponding to propagation delay values  $\tau_n, n = 1, 2, \dots, N$ . Each resolvable multipath component can be modelled with its own appropriate Doppler power spectrum, the medium power level and delay  $\tau_n$ .

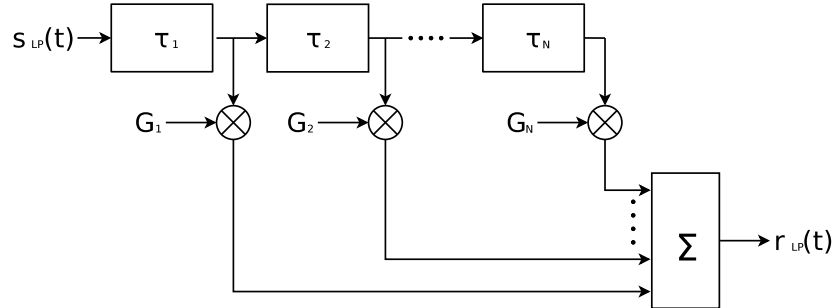


**Figure 3.4:** Tapped-delay-line model with variable delays

The lowpass-equivalent impulse response was given in Equation 3.21 as:

$$h(t) = \sum_{n=1}^N G_n(t) \delta(t - \tau_n). \quad (3.34)$$

The lowpass-equivalent output is:

$$r_{LP}(t) = \sum_{n=1}^N G_n(t) s_{LP}(t - \tau_n), \quad (3.35)$$

which can be represented as a tapped-delay-line, as shown in Figure 3.4.

To increase the efficiency of the simulation, which especially suffers, when the differential delays are small compared to the simulation sampling time  $T_s$ , a band-limiting filter is added to obtain a uniformly spaced tapped-delay-line. This can be done by adding an ideal rectangular filter with bandwidth equal to that of the signal  $B$ . The tap gains  $A_n$  can then be expressed as [23]:

$$A_n = \sum_{k=1}^K G_k(t) \text{sinc}(B(\tau_k - nT)), \quad -N_1 \leq n \leq N_2 \quad (3.36)$$

with  $T = B^{-1}$ .  $K$  is the total number of paths in the multipath fading channel.  $N_1$  and  $N_2$  are chosen so that  $A_n$  is small when  $n$  is less than  $-N_1$  or greater than  $N_2$ .

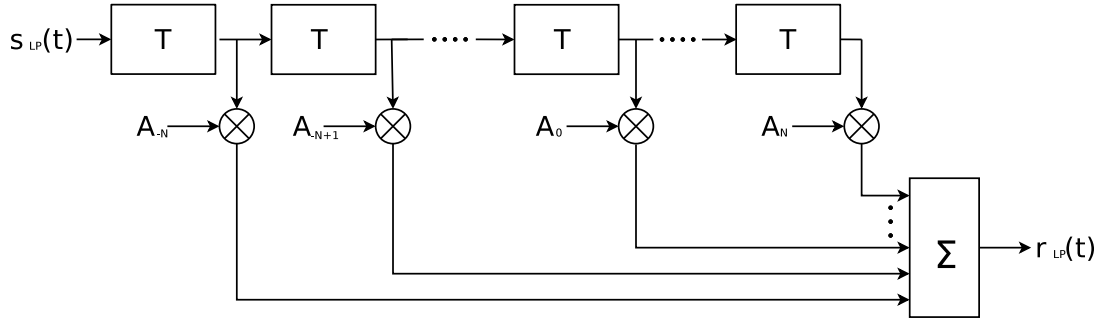


**Figure 3.5:** Uniformly spaced TDL model

The output then becomes a superposition of the weighted and uniformly delayed input signal as can be seen in Figure 3.5:

$$r_{LP}(t) = \sum_{n=-N_1}^{N_2} A_n s_{LP}(t - nT) \quad (3.37)$$

As the *sinc* function is declining very fast, small values of  $N$  are sufficient and simulation costs can be reduced significantly.

The tap gain processes  $G_n$  are generated as follows: A set of  $n$  AWGN processes is generated and filtered by the desired Doppler spectrum. The multipath characteristic then is applied by scaling the noise process by the expected value of the Rayleigh or Rice distribution. Then they are transformed by Equation 3.36 to obtain the bandlimited tap gains.

### 3.3.3 Channel Models

For the evaluation of the DRM+ system performance several channel models have been defined in the DRM ETSI-standard. They are derived from different existing models and measurements.

The European working group COST 207 has defined several power-delay profiles for the characterization of frequency selective channels in different scenarios as urban, rural or hilly terrain in [22]. These evaluations were mainly for the development of mobile communication systems as GSM and UMTS for frequencies above 800 MHz. Figure 3.6 shows the power delay profile and the appropriate Doppler spectra of the COST-'Typical Urban' channel model.

Path No.	Delay [ $\mu$ s]	Power [dB]	Doppler-type
1	0	-4	JAKES
2	0,2	-3	JAKES
3	0,4	0	JAKES
4	0,6	-2	GAUSS1
5	0,8	-3	GAUSS1
6	1,2	-5	GAUSS1
7	1,4	-7	GAUSS1
8	1,8	-5	GAUSS1
9	2,4	-6	GAUSS2
10	3,0	-9	GAUSS2
11	3,2	-11	GAUSS2
12	5,0	-10	GAUSS2

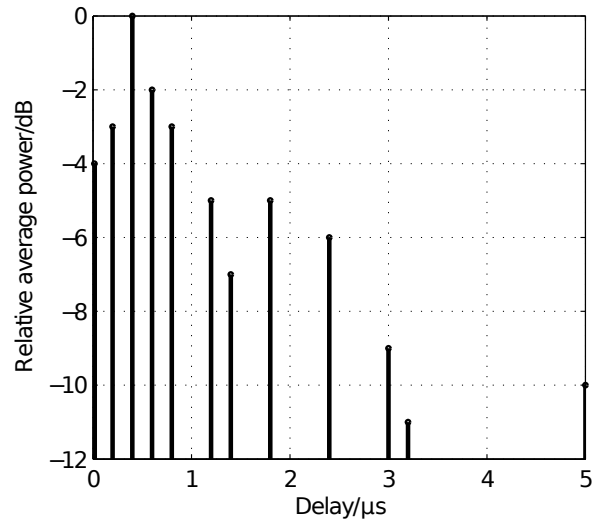


**Figure 3.6:** COST 207 channel model 'Typical Urban'

For the development of DAB and DVB-T a lot of measurements have been conducted in the upper VHF band (Band III) and in the UHF band in Europe. According to [24] these are widely corresponding to the COST models. Evaluations and channel measurements below 120 MHz in the VHF Band II have been conducted in the US for the development of the IBOC/HD-Radio system. The results of these measurements are also quite equivalent to the COST models and have been chosen for the DRM+ system evaluation of the 'urban', 'rural' and 'terrain obstructed' scenarios.

The 'hilly terrain' model was created from measurements in hilly regions in Germany. For the evaluation of Single Frequency Networks (SFN) a model with large delays as resulting from hexagonal distributed transmitters in an SFN was added.

Annex A shows the channel profiles used for the simulations.



## 4 Performance of the DRM+ System in the VHF Band II

In order to analyse the system performance of DRM+ several field trials have been conducted at different locations and environments around the world. The main measurements have been conducted in Hannover between 2009 and 2011 within a project financed by the local media authority 'Niedersächsische Landesmedienanstalt' (NLM) concerning the evaluation of digital sound broadcast for local radios. More information about this project is given in [25].

Additionally the DRM consortium was conducting trials in different parts of the world. There have been the opportunity to take part in trials in Sri Lanka, India and Brazil. The results of these trials in Hannover [26] and Sri Lanka [27] were submitted to the ITU-R study-group WP6A on 'Terrestrial broadcasting delivery' for the ITU standardization process of DRM+. They were also used to define a framework for calculating the relevant DRM+ planning parameters, which have been added to the ITU Recommendation ITU-R BS.1660-5 on 'Technical basis for planning of terrestrial digital sound broadcasting in the VHF band' [15]. For the evaluation of the planning parameters additional measurements of the protection ratios between DRM+ and analogue FM radio were conducted and are presented at the end of this Chapter.

### 4.1 DRM+ Trial in Hannover

In Hannover the main transmitter was located on the campus of the Leibniz University. The transmitting antenna was mounted on the roof of the University building (Appelstr. 9A, 30167 Hannover, GPS: lat: 52.388, long: 9.712) at a height of 70 m above ground. Transmitting power was licensed for up to 30 W ERP at a frequency of 95.2 MHz.

The tests were conducted with a very robust 4-QAM modulation and a 16-QAM modulation with high data rates. The details can be found in Table 4.1.

**Table 4.1:** Modulation settings used in the field trial

Modulation	Protection level	Code rate	Bit rate [kbit/s]
4-QAM	1	0.33	49.8
16-QAM	2	0.5	149.3

The SDC was set to the robust code rate of 0.25. For these settings simulation results

of the SNR values required for reception are available in the DRM ETSI standard [4] in Annex A.

The following equipment was used for the measurements:

- Fraunhofer Contentserver
- RFmondial Modulator LV6
- Nautel Exciter/Amplifier NVE
- Transmit antenna: Kathrein K 52 40 1, 4-element Yagi directional antenna (direction: 120 °), measurements were conducted with horizontal (antenna array) and vertical polarization
- Receive antenna: Kathrein K 51 16 4 / BN 510 351, magnetic monopole, an antenna-factor of = 10 dB was measured, the antenna was mounted on the roof of a van at a height of 2 m
- RF-Frontend: Rhode & Schwarz measuring receiver (ESVB), 10.7 MHz IF
- Field strength measurements: ESVB, with an IF bandwidth of 300 kHz
- A/D converter Perseus
- For later tests a frontend from RFmondial (RF-SE1 RFbox) was used as RF-frontend, A/D converter and for the field strength measurements
- RFmondial software receiver

The transmission consisted in both modes of an AAC encoded stereo audio stream and a synchronous pseudo random bit sequence (prbs), which was used for the calculation of the Bit Error Rate (BER) (see [9] for details).

The following parameters were recorded and analysed during the measurements:

- Field strength (measured with Rhode & Schwarz ESVB measuring receiver, BW: 300 kHz, RMS, triggered via GPIB every 16th frame (1.6 sec), in later measurements measured with calibrated RFmondial RF-SE1 RFbox)
- GPS coordinates
- Bit Error Rate
- Signal-to-Noise Ratio (calculated in the receiver via the time correlation/synchronisation, see [28])
- Receiver status information (the status of audio decoding shows if one or more audio frames are corrupted within one DRM multiplex frame, see [9] for details)

#### 4.1.1 Measurements in Urban Environment

The first measurements were conducted with horizontal antenna polarization at the transmitter site. As the receiving antenna was vertically mounted on the roof of a car, the

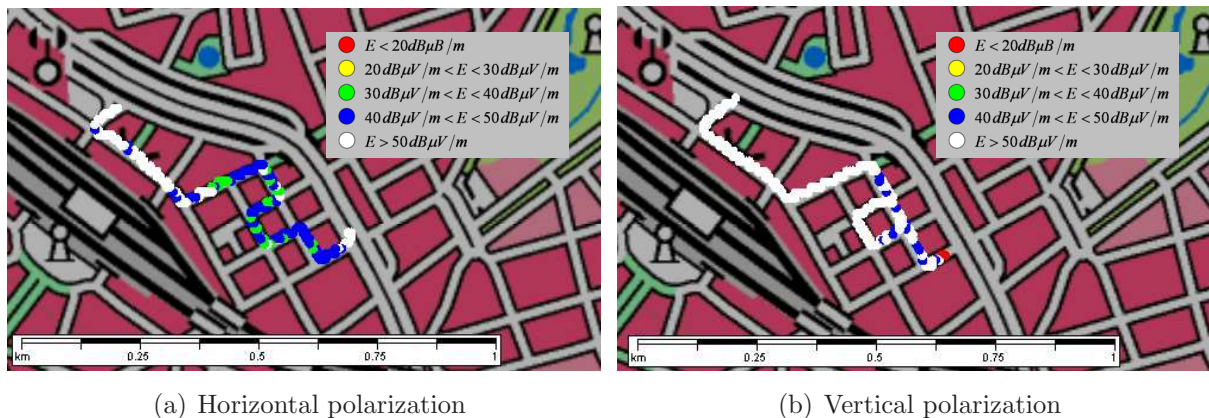


TX-antenna was rotated to vertical polarization for additional tests and the measurement results were compared. As the different antenna patterns in vertical and horizontal polarization have to be taken into account, the locations were chosen close to the main beam of the TX-antenna. With constant ERP in both polarization directions at this locations the effect of the different polarizations can be evaluated.

The measurements of the horizontal polarized transmission were conducted in January 2010. There was some snow and a lot of ice on the ground. The vertically polarized measurements were conducted in March 2010. There was sometimes sun, mostly overcast and little snow on the ground.

The investigated area behind the main station of Hannover (Raschplatz) has a kind of dense urban environment with high buildings and small streets can be found. The average distance to the transmitter is about 2.5 km. Measurements were conducted with 16-QAM (code rate 0.5).

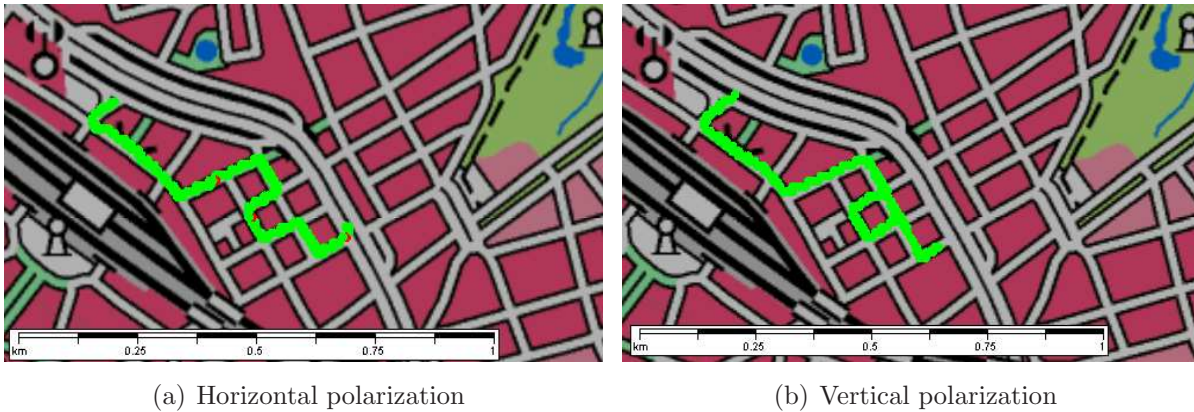
Figure 4.1 shows the field strength distribution for the horizontal and vertical polarized transmissions. For the horizontal transmission the variability of the field strength is between 30 and above 50 dB $\mu$ V/m, for the vertical transmission it was mostly above 50 dB $\mu$ V/m.



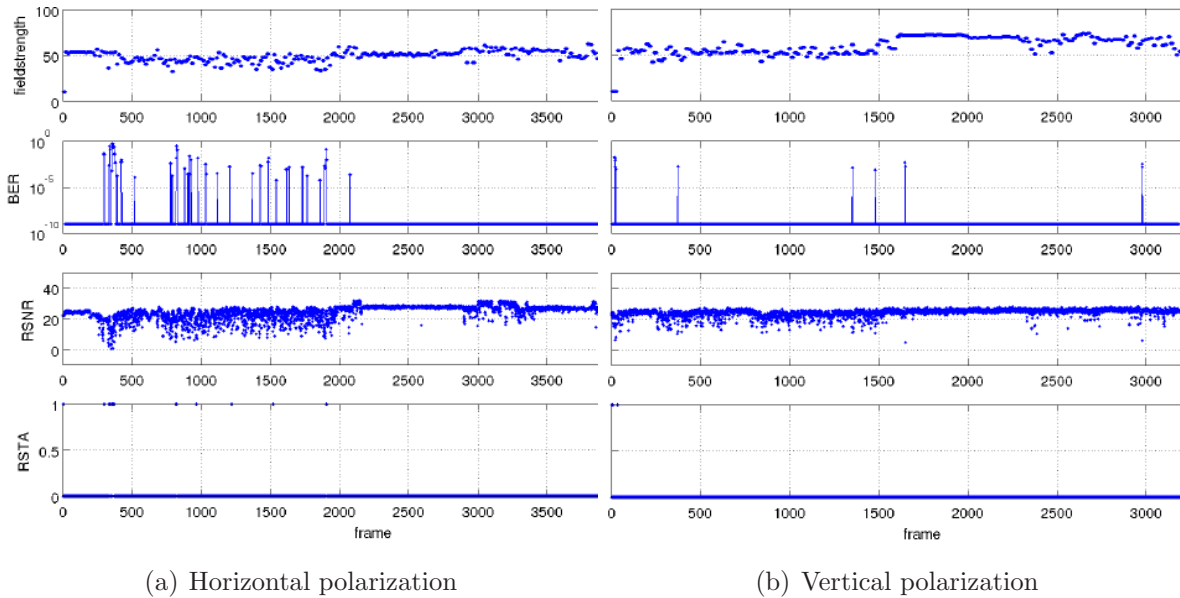
**Figure 4.1:** Field strength in urban environment (Raschplatz) (map source: Bundesamt für Kartographie und Geodäsie)

Figure 4.2 shows a plot of the receiver status information (RSTA), which describes whether all audio frames were ok (green) or one or more audio-frames were corrupted (red). As there was enough field strength, reception was possible mostly without errors in both polarizations.

In Figure 4.3 a comparison of the field strength, the SNR, the BER and the status of the audio decoder RSTA (0: all audio frames ok, 1 one or more audio frames corrupted) for the horizontal and the vertical polarized transmission is plotted against the OFDM frames. One frame corresponds to a duration of 100 ms. Here the differences of the field strength in horizontal and vertical polarization are more obvious than in the maps. In horizontal transmission the field strength is mostly around 50 dB $\mu$ V/m, for vertical transmission it



**Figure 4.2:** Measurement of the audio data in the urban environment (Raschplatz), green: audio OK, red: one or more audio errors (map source: Bundesamt für Kartographie und Geodäsie)



**Figure 4.3:** Measurement results in urban environment (Raschplatz)

is up to 70 dB $\mu$ V/m. With horizontal polarization the Bit Error Rate is higher at some places and there are some corrupted audio frames, whereas with vertical polarization it is almost error free due to the higher field strength. The calculated SNR varies much more in horizontal polarization, the maximum value of around 28 dB is caused by the calculation process.

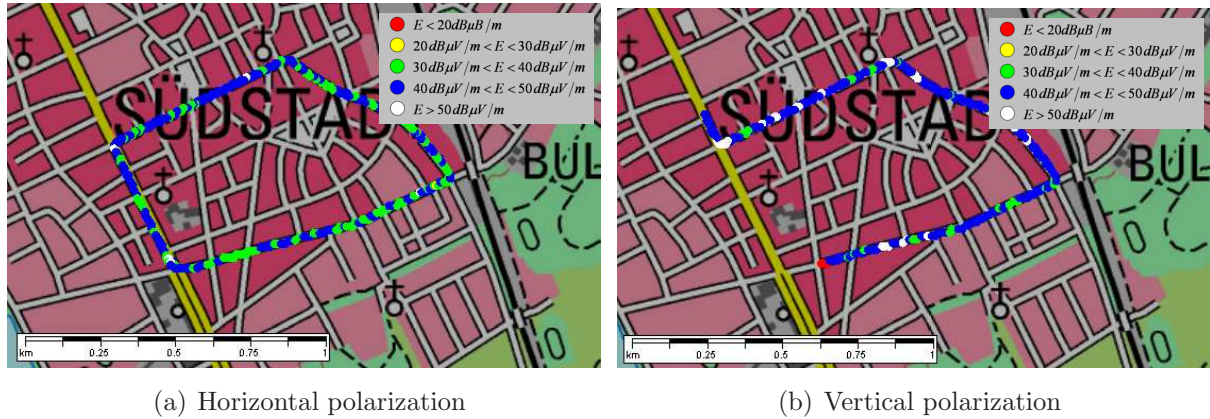
Further measurements were conducted in 'Suedstadt' in the southern part of Hannover, an urban residential district with most buildings having a height between ten and twenty meters. The average distance to the transmitter was 4 km.

Figure 4.4 shows the field strength distribution for the horizontal and vertical polarized transmission. For the horizontal transmission the variability of the field strength is between



30 and 50 dB $\mu$ V/m, for the vertical transmission it was mostly between 40 and 50 dB $\mu$ V/m and above.

The field strength difference between horizontal and vertical polarization fits quite well to the 10 dB polarization discrimination between vertical and horizontal polarization given by the ITU in [29].



**Figure 4.4:** Field strength in 'Suedstadt' (map source: Bundesamt für Kartographie und Geodäsie)

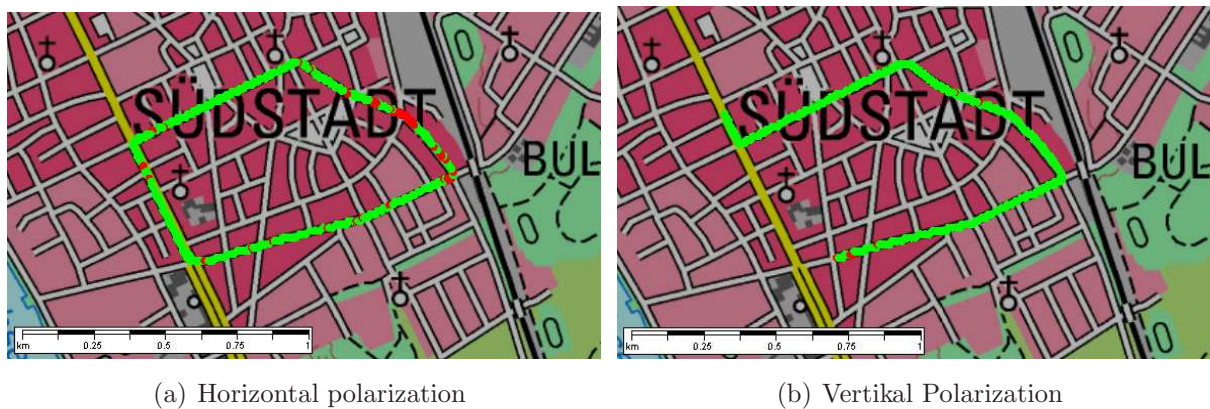


**Figure 4.5:** Measurement of the audio data in 'Suedstadt', green: audio OK, red: one or more audio errors (map source: Bundesamt für Kartographie und Geodäsie)

Figure 4.5 shows a plot of the receiver status information (RSTA). As the field strength is lower at this location some errors occur with horizontal polarization as well as with vertical polarization. In Figure 4.6 this can be seen in more detail. The vertical polarized transmission shows higher field strength and SNR, less bit errors and less audio errors.

With field strengths above approximately 45 dB $\mu$ V/m reception is possible without errors in the urban environment. The corresponding calculated SNR is approx. 18 dB. This is slightly higher than the 15.4 dB SNR given in Annex A in [4] as simulation result for an urban channel at a receiver velocity of 60 km/h. However, the simulated system performance is assuming perfect channel estimation, ideal synchronisation and the absence

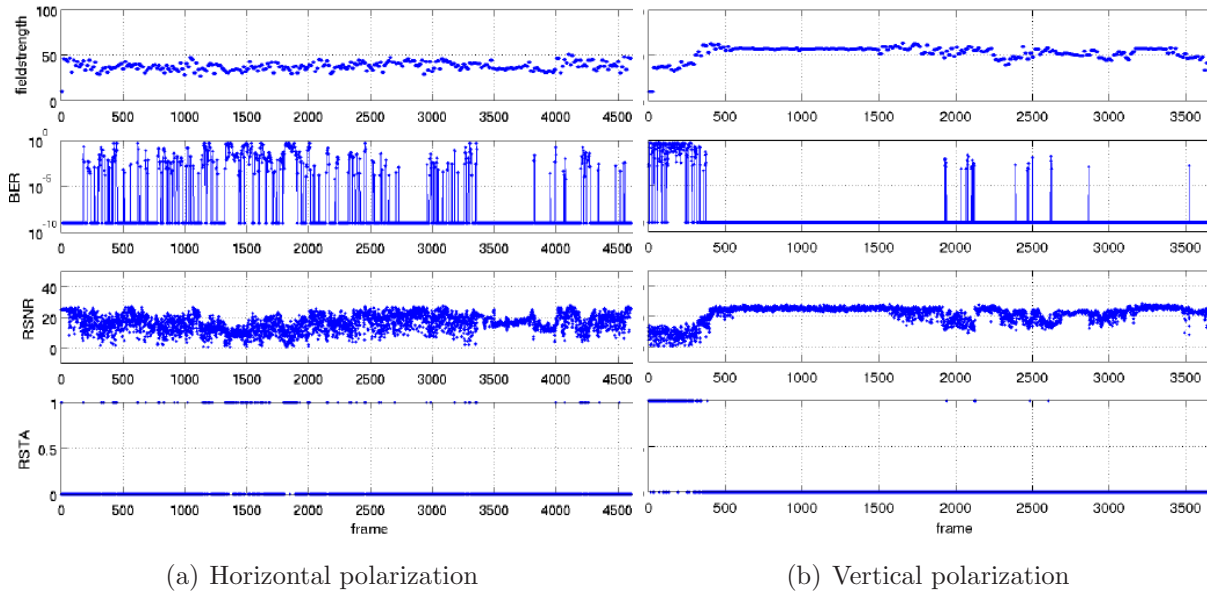


**Figure 4.6:** Measurement results in the Suedstadt

of phase noise and quantization effects. In the tests the velocity was much lower than 60 km/h, which can produce reception problems such as severe fading, which makes the results more pessimistic compared to the simulation. More evaluations and approaches to solve this problem are given in Chapter 6.

### 4.1.2 Measurement of the Coverage Limit

As the reception antenna was fixed to a vertical polarized position due to mechanical reasons, the vertical polarized transmission was chosen for further tests. Measurements of the coverage limit were conducted in the main beam of the transmitting antenna with 16- and 4-QAM modulation. The route was chosen to be on the B65, a rural road in the main beam of the transmitting antenna. The measurement was continued until audio quality became bad at most of the locations.

#### Measurements with 4-QAM

The first measurements were conducted with 4-QAM modulation. Figure 4.7 shows the field strength measured on the route. On the map in Figure 4.8 the audio status measured on the route is plotted. It can be seen that with greater distance to the transmitter, passing the villages, the audio-status became erroneous, whereas passing the countryside with almost no obstacles (the countryside in the surroundings of Hannover is quite flat) reception quality was still good.

Figure 4.9 shows the reception parameters plotted against the time in the direction away from the transmitter. On the radial route reception was possible with 4-QAM modulation down to a field strength of about 30 dB $\mu$ V/m with an SNR of approx. 10 dB. Additionally



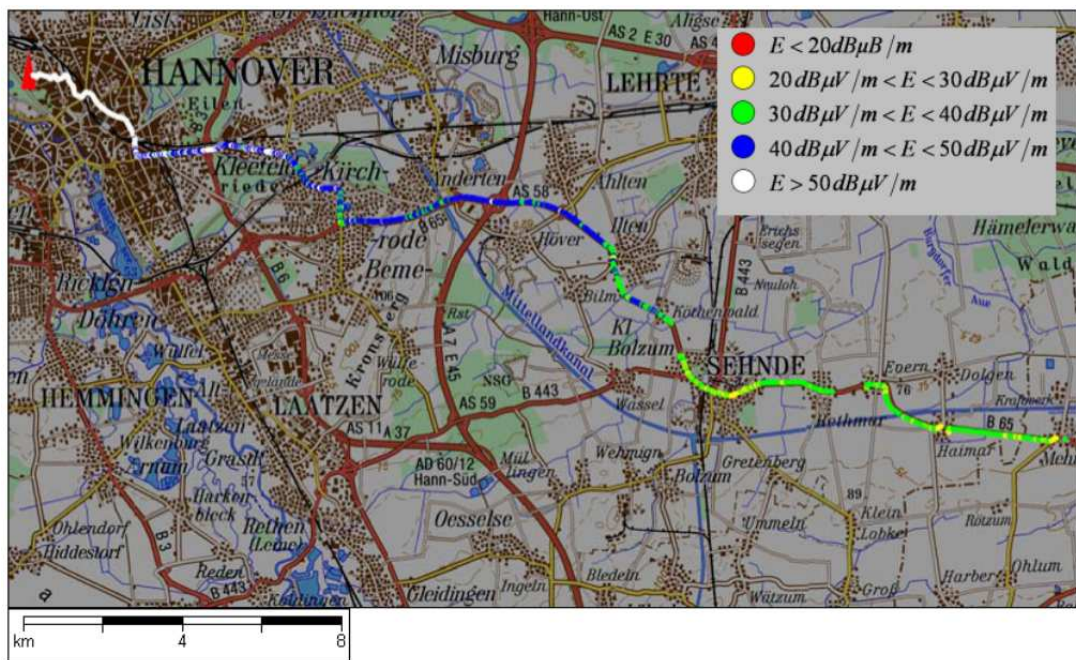


**Figure 4.7:** Field strength measurement of the coverage limit, 4 QAM mode (code rate: 0.33), start of the measurement at the transmitter on the left side of the map, stop at right border (map source: Bundesamt für Kartographie und Geodäsie)



**Figure 4.8:** Measurement of the coverage limit in 4 QAM mode (code rate: 0.33), green: audio frames ok, red: one or more audio frames corrupted (map source: Bundesamt für Kartographie und Geodäsie)

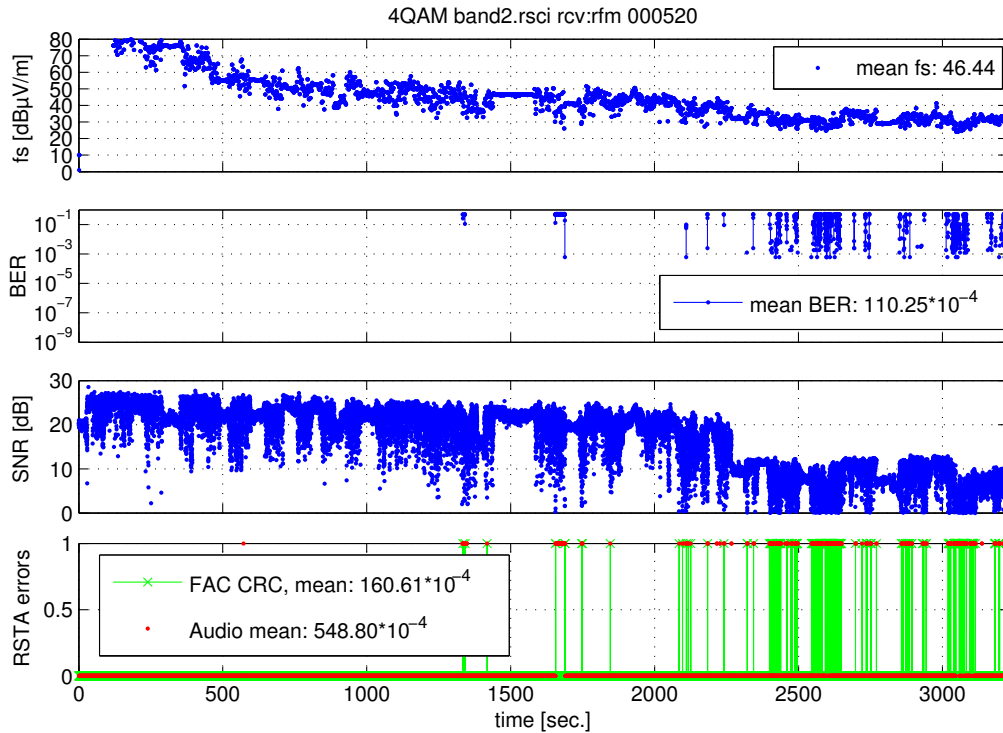


**Figure 4.9:** Reception parameter on the B65 with 30 W ERP and 4 QAM mode (code rate: 0.33)

to the audio errors in red, the FAC CRC errors from the Fast Access Channel are plotted in green.

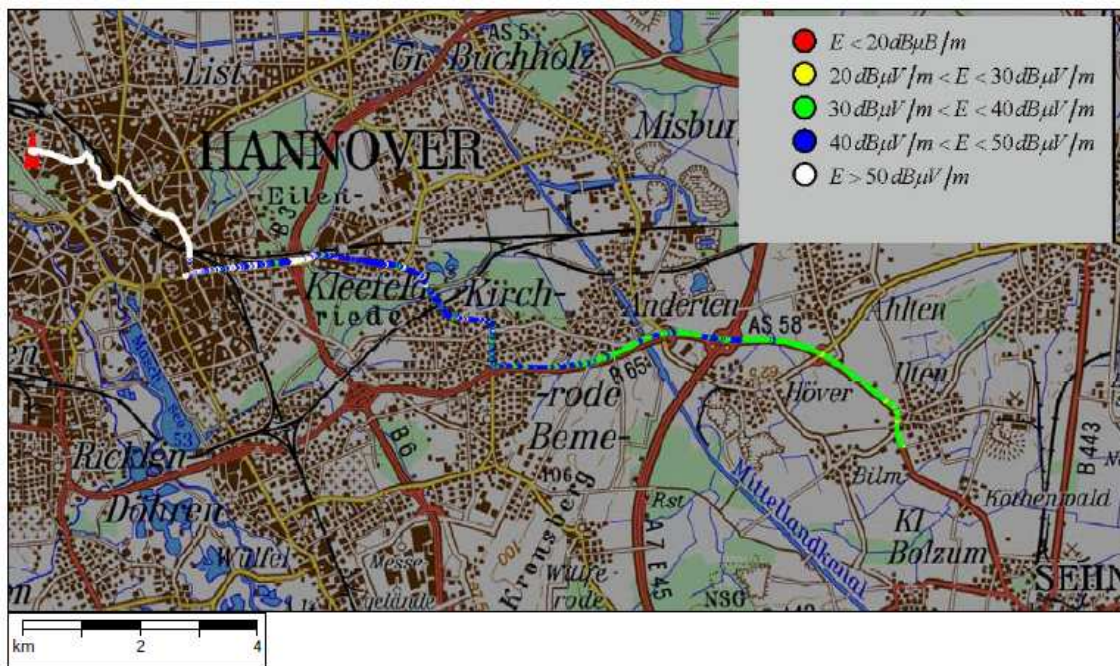
The measurement was stopped at a distance of around 30 km from the transmitter (at the right border of the maps in Figure 4.8 and 4.9), where audio quality became bad at most of the locations.

### Measurements with 16-QAM

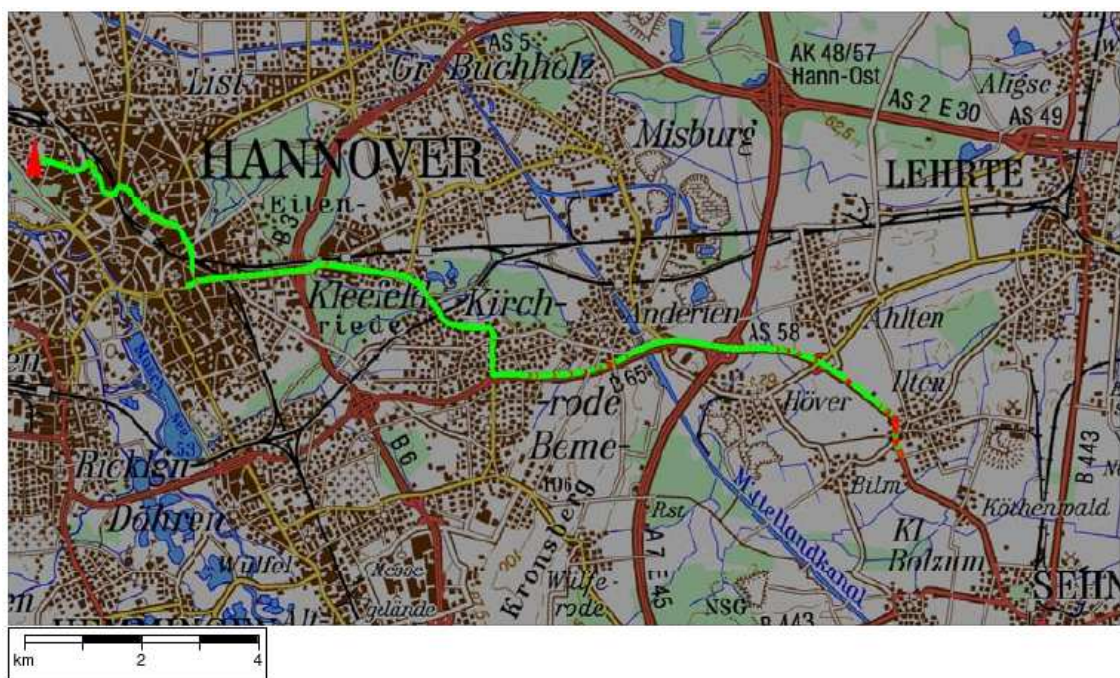
On the way back the 16-QAM mode was measured. Figure 4.10 shows the received field strength. A reason, why there is less field strength measured on the way back, is probably an asymmetrical behaviour of the receiving antenna mounted on the car, as 4-QAM and 16-QAM should not make a difference with respect to field strength. There were also measurements in 16-QAM mode driving in the direction away from the transmitter. In this case the field strength values were the same at the corresponding locations as in 4-QAM mode in the previous tests.

Figure 4.11 shows a plot of the received audio frames. With green points no audio errors were present, with red points one or more audio frames were corrupted. The measurement was started at a distance of around 15 km away from the transmitter, driving into the direction of the transmitter.





**Figure 4.10:** Field strength measurement of the coverage limit, 16 QAM mode (code rate: 0.5) (map source: Bundesamt für Kartographie und Geodäsie)



**Figure 4.11:** Measurement of the coverage limit, 16 QAM mode (code rate: 0.5), green: audio frames ok, red: one or more audio frames corrupted (map source: Bundesamt für Kartographie und Geodäsie)

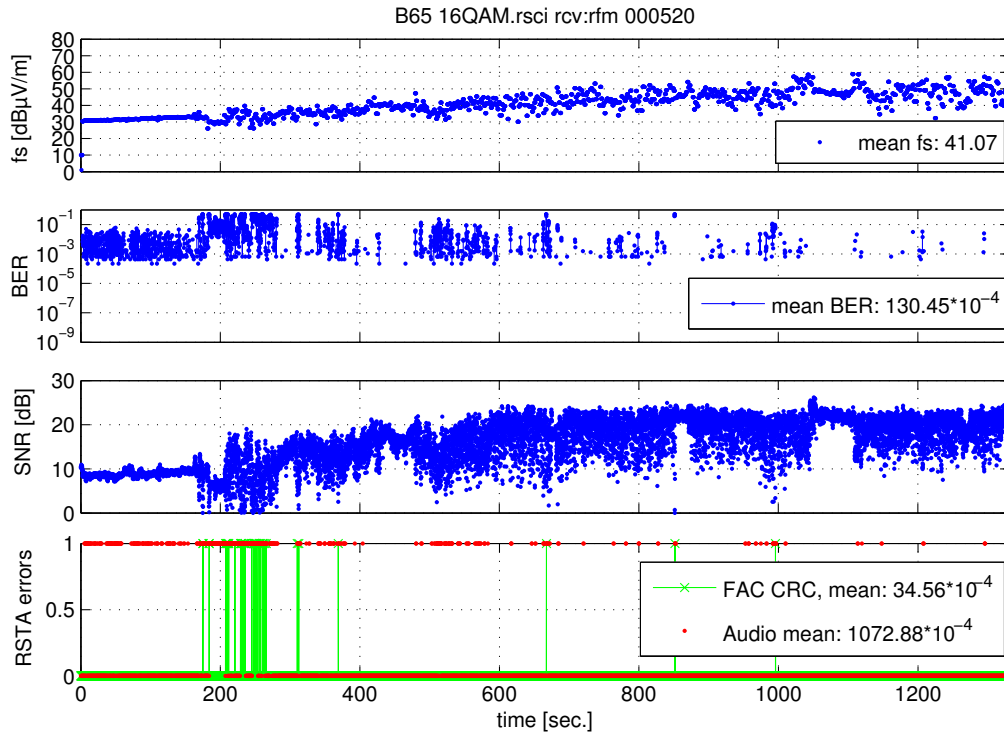


**Figure 4.12:** Reception parameter on the B65 with 30 W ERP and 16 QAM mode (code rate: 0.5)

In Figure 4.12 the field strength is plotted in comparison to the Signal-to-Noise Ratio (SNR), the Bit Error Rate (BER) and the audio and FAC status (RSTA) against the time. The reception was good, if the field strength is approximately 46 dB $\mu$ V/m or higher a calculated SNR of approximately 18 dB is present. As expected, the 16-QAM modulation with higher data rate needs some more signal level than the 4-QAM modulation.

## 4.2 Additional Measurements in Different Environments

Additional measurements have been conducted in Hannover, India, Sri Lanka and Brazil, in 4-QAM mode. They have been evaluated with respect to the environment and the minimum field strength and SNR necessary for a reception with  $BER < 10^{-4}$ . A further remark was set to the location probability of the reception. The location probability describes the probability that the signal measured at multiple locations has to be higher than a certain value. It is defined in coverage prediction models and used also for different reception scenarios. E.g. for fixed reception a location probability of 70 % is assumed in [15] to obtain a good reception situation. For portable reception it is 95 %.



Figure 4.13 shows as an example the evaluation of one measurement route rural environment between the villages Harenberg and Lathwehren near Hannover. On the left, the BER is plotted against the calculated SNR, on the right side the BER is plotted against the field strength. The red plot is the mean BER for a specific SNR or field strength taking into account all the measurements values, corresponding to 100% location probability. The green plot is taking into account only the best 95% of the measurement results. The worst 5% are ignored as it is done when planning for portable outdoor reception with a location probability of 95%. The increase of the red curve after constant declining is caused by a small amount of values. As a result an individual deviation can produce significant variations.

The example results in a minimum SNR of 8 dB necessary for a location probability of 95% and 12 dB for 100% probability as marked on the left side Figure 4.13. In terms of field strength, a minimum of 30 dB $\mu$ V/m is necessary for 95% location probability and 36 dB $\mu$ V/m for 100% as shown on the right side of Figure 4.13.

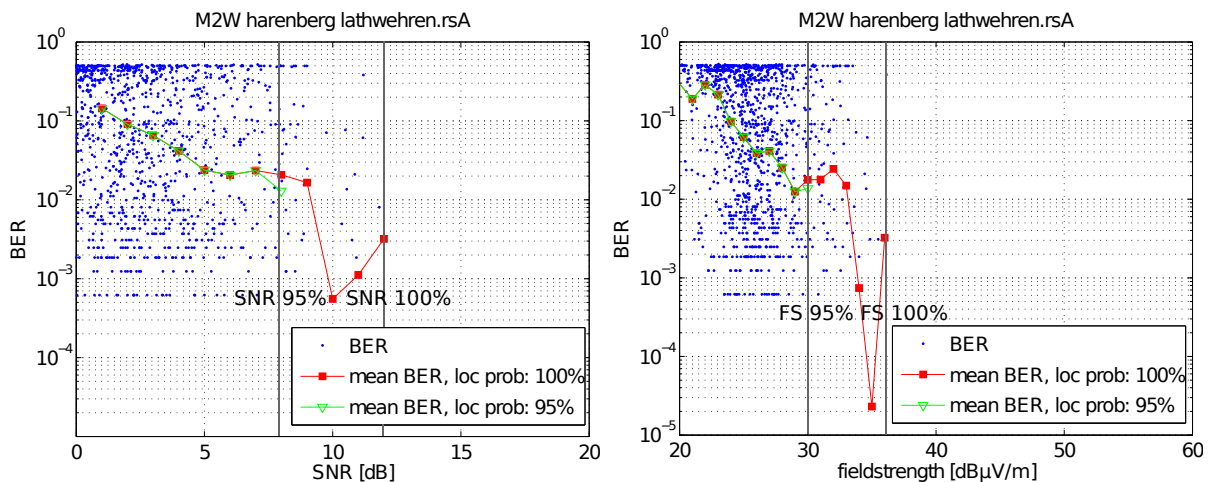


**Figure 4.13:** Evaluation of the necessary SNR and field strength in rural area

Several measurement routes have been evaluated in the same way. Table 4.2 shows the mean SNR and field strength values of the resulting minimum SNR and field strength values necessary for reception in an overview. At some routes no field strength was recorded. That is why the number of measurement routes for the SNR is higher than the on for field strength. For comparison the table also provides the simulated SNR values (for 100% loc. prob.) given in the ETSI DRM standard [4]. The measured SNR values are higher than in the simulation results. As stated before, the simulated system performance is anticipating perfect channel estimation, ideal synchronisation and the absence of phase noise and quantization effects. The implementation loss factor is assumed to be 3 dB in [15].

Additionally to the measured field strength values, the values from the ITU DRM+ Planning Parameters [15] are given. The derivation of this values is also given in [30]. The portable outdoor (PO) reception assumes 95% location probability in a suburban area with a portable receiver at no less than 1.5 m above ground level. Mobile reception (MO)

**Table 4.2:** Evaluation of the reception in different surroundings

Surrounding	Urban	Suburban	Rural
<b>Evaluation of the minimum necessary SNR [dB]</b>			
No. of meas. routes	11	4	5
Meas. 100% loc. prob.	15.5	14.5	13.3
Meas. 95% loc. prob.	11.8	13	8.6
ETSI simulations	7.3	-	5.6
<b>Evaluation of the minimum necessary field strength [dB<math>\mu</math>V/m]</b>			
No. of meas. routes	4	4	5
Meas. 100% loc. prob.	39.5	39.25	36.2
Meas. 95% loc. prob.	35.75	35.75	31.2
DRM+ planning parameters	-	40.74 (PO)	42.27 (MO)
Analogue FM radio (stereo)	66 (h=10 m) 76 (h=1.5 m)	-	54 (h=10 m) 64 (h=1.5 m)

is defined as reception in a rural area with hilly terrain by a receiver in motion also at high speed with a matched antenna situated at no less than 1.5 m above ground level. As the measurements in rural area were mostly conducted around Hannover, where it is hard to find any hills, this can be the reason of the different trends of the measured field strength and the values given in the Planning Parameters.

For comparison, also the minimal usable field strength for analogue FM radio is given in Table 4.2. The values from Recommendation ITU-R BS.412-9, 'Planning Standards for terrestrial FM sound broadcasting at VHF' are assuming an antenna height of 10 m. Considering a height of 1.5 m a height loss correction factor of 10 dB has to be added. The resulting values are given in the last row in Table 4.2. Compared to those values the minimum field strength necessary for DRM+, both the measured values and those from the planning parameters are significantly lower.

The measurements compared to the simulation results are showing that the measured SNR values are higher than the simulated ones. This could be caused by the SNR estimation process in the receiver. Additionally the limited number of measurements and as a result differences of the channel statistics between the real channel and the simulated channel can cause this differences. In contrast to the SNR, the measured field strength is lower than the field strength given in the DRM+ planning parameters. This is especially interesting as the calculation of the field strength in the planning parameters depends on the calculated SNR values from the ETSI simulations.

### 4.3 Protection Ratios for Analogue Systems

Besides the minimal usable field strength for planning of a broadcasting system the interoperability with other systems in the same frequency band is important. For this purpose measurements of the protection ratios have been conducted. The protection ratios with other digital systems, especially DAB in the VHF Band III have been measured by the University of Applied Sciences Kaiserslautern and the Media Authority Rheinland-Pfalz. They are given in [31].

In the VHF Band II the systems that can be interfered with are analogue FM radio and directly above Band II the aeronautical services. As a transition to digital broadcasting will rather be conducted as a slow switchover with analogue and digital systems running in parallel for some time, the protection ratios between these different services are of interest. In case digital and analogue radio will be used in parallel, protection ratios have to be defined for the planning of the services. Within the compilation of the DRM+ Planning Parameters, measurements have been conducted to analyse the behaviour of different FM receivers if a DRM+ transmitter shows up in the FM-Band. Figure 4.14 shows an example of a spectrum with an DRM+ signal next to a FM signal. Here the frequency offset between the analogue and digital signal is 150 kHz and the power level of the FM signal is 23 dB higher than the DRM+ signal.

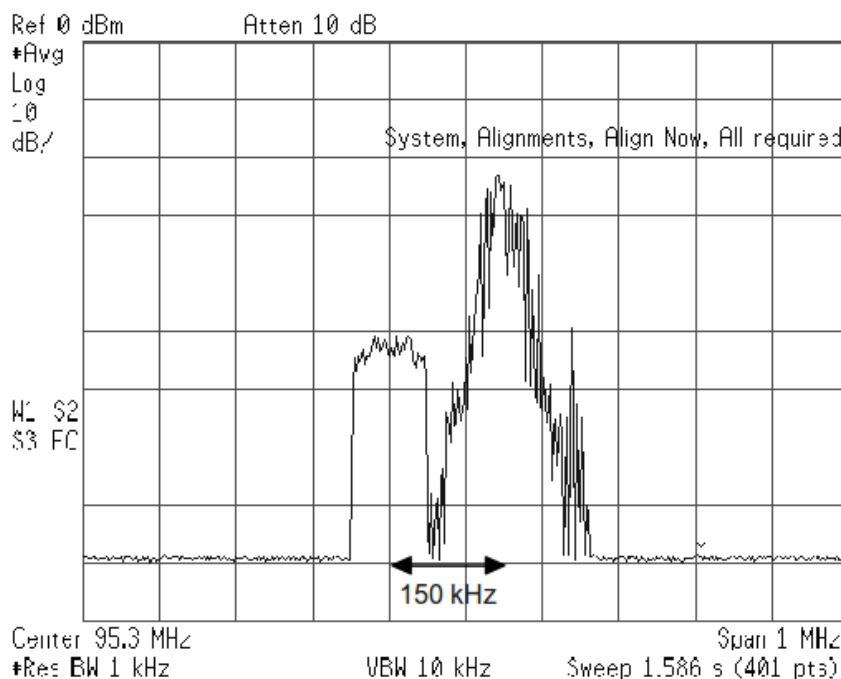


**Figure 4.14:** Spectrum of a DRM+ and a FM transmitter with  $\Delta f = 150$  kHz and  $\Delta P = 23$  dB

For the determination of the protection ratios of FM radio adjacent to another FM ra-

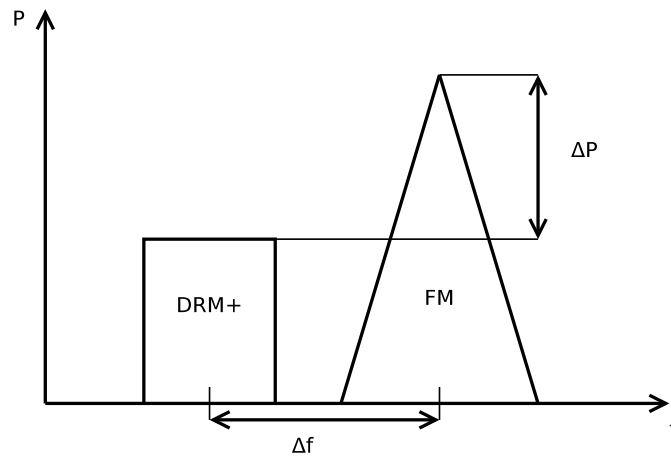


**Figure 4.15:** Signal setup for the evaluation of the protection ratios

dio signal, an ITU recommendation (ITU-R BS.641 on 'Determination of radio-frequency protection ratios for frequency-modulated sound broadcasting' see [32]) defines the procedure. For our measurements this procedure was adapted. Instead of the interfering FM signal, a DRM+ signal was used.

The procedure can be summarized as follows: without an interfering signal, the FM receiver has to show an audio SNR of more than 56 dB. For this test a 500 Hz test signal was generated and modulated in stereo FM. Connected by cables and scalable attenuators, the demodulated analogue FM audio signal of the different FM receivers were evaluated with a Rohde & Schwarz UPD Audio Analyser. To get rid of the 19 kHz pilot, a 15 kHz low pass was inserted. Then a weighted CCIR filter was switched on in the audio analyser. The FM test signal was switched off and the DRM+ interference signal switched on at different frequency offsets to the FM. The DRM+ signal level was then increased until the audio SNR has decreased to 50 dB. The input level to the FM receivers was set to -52 dBm by scalable attenuators. After the DRM+ transmitter an additional bandpass filter was inserted.

Figure 4.15 shows the setup of an analogue FM spectrum besides a digital DRM+ signal.  $\Delta f$  is the center frequency distance between the two signals and  $\Delta P$  the difference of power levels in dB.

Figure 4.16 shows the protection ratios (PR) measured over the frequency offset between the FM and DRM+ transmitters for the different FM receivers that were evaluated. As a reference the protection ratios FM-FM from ITU-R BS.641 are plotted in green and the values that were finally included into the DRM+ Planning Parameters and ITU-Recommendation 1660 in dark red. The values for multiples of 100 kHz of  $\Delta f$  are also given in Table 4.3.

The results show significant differences between the receivers. With the Uniwave receiver in FM mode a PR of -30 dB can be achieved at a frequency offset of around 300 kHz. This means that a FM transmitter still can be received without the influence of a neighbouring

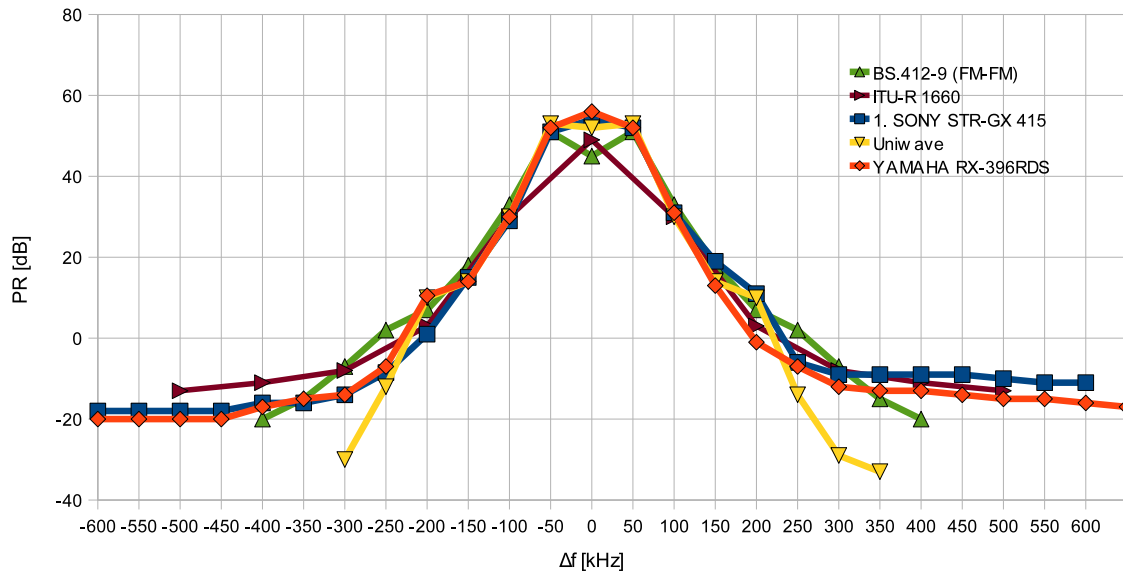


Figure 4.16: Protection ratios, FM interfered by DRM+

Table 4.3: Protection ratios for FM disturbed with by DRM+ measured with different receivers at various frequency offsets

$\Delta f$	FM-FM	Sony STR	Uniwave	Yamaha	ITU-R 1660
-600		-18		-20	
-500		-18		-20	-13
-400	-20	-16		-17	-11
-300	-7	-14	-30	-14	-8
-200	7	1	10	10.5	3
-100	33	29	30	30	30
0	45	54	52	56	49
100	33	31	30	31	30
200	7	11	10	-1	3
300	-7	-9	-29	-12	-8
400	-20	-9		-13	-11
500		-10		-15	-13
600		-11		-16	

DRM+ transmitter with 20 dB more power at a distance of 300 kHz. With the other receivers it was only approx. 15 dB at the same frequency offset or even higher offsets.

Further protection ratio measurements have been conducted by BBC research [33], T-Systems [34] and the University of Applied Sciences Kaiserslautern [35]. All of them concluded that DRM+ as an OFDM system has more interfering potential on FM than another FM transmitter. Therefore the protection ratios included in the ITU-Recommendation 1660 exceed the ones needed for the planning of FM systems only. The values can be compared in Table 4.3. The FM-FM values are listed in the second column, the FM-DRM+ values in the last column.

Protection ratio measurements with aeronautical services, that are located directly above the FM band II have been conducted by the Bundesnetzagentur together with the University of Applied Sciences Kaiserslautern. They conclude in [36]: 'The measurements have shown that in principle DRM+ has nearly equal or even less interference potential to adjacent band services than a standard FM broadcast signal, provided that additional filtering at the DRM+ transmitter output is deployed to reduce sideband emissions outside the wanted channel.'

## 4.4 Combined Transmission of DRM+ and FM

A proposal of a combined mode of DRM+ and FM was added to the ETSI DRM standard [4] as Annex S. If FM and DRM+ are directly located side by side in the frequency band, a minimum carrier frequency distance of 150 kHz is recommended with a power level difference  $\Delta P \geq 20$  dB.

A setup with a DRM+ transmitter next to a FM transmitter in the VHF Band II could be tested at the community radio station Líder FM in the Recanto dos Emas in the suburbs of Brazil's capital Brasília in 2012. The Ministry of Communication was testing different digital radio standards on its way of a digitalization of Brazil's radio landscape. As there are more than 4000 licensed community radio stations in Brazil, an important condition for a digital radio standard is its usability for small scale community radios. They are all licensed to 25 W of transmission power in FM with the purpose to cover a radius of 1 km around the radio station.

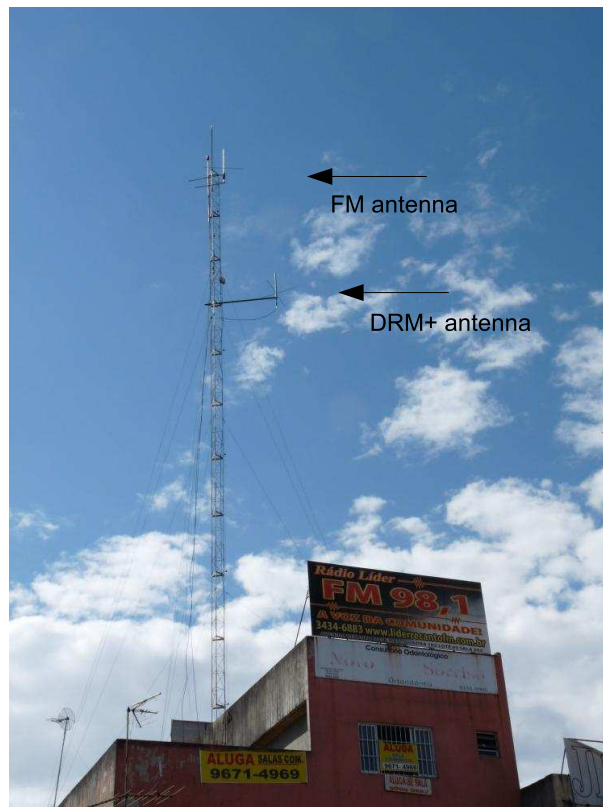
The initial plan to combine the analogue and the digital signal with a 3 dB combiner could not be followed as the FM antenna was not adapted very good to the impedance of the rest of the equipment. This resulted in a disturbance of the signal caused by intermodulation due to reflections from the antenna back to the combiner. Instead of using the combiner, a second antenna was then installed slightly lower than the FM antenna as can be seen in Figure 4.17.

The FM radio station was on air with 25 W at a frequency of 98.1 MHz, the digital signal was set to 5 W at 97.9 MHz. This makes  $\Delta f = 200$  kHz and  $\Delta P = 7$  dB, which fits into the protection ratio from ITU-R 1660, which is 3 dB at  $\Delta f = 200$  kHz as can be seen in Table 4.3. Another challenge was a pirate radio station transmitting on the same frequency as Líder FM disturbing the analogue signal in one direction. The measurements

were done with a robust 4-QAM mode with protection level 1 with a data rate of 49.8 kbps and a 16-QAM mode with protection level 2 resulting in a data rate of 149.3 kbps. In the 4-QAM mode, the live radio show from Líder FM was transmitted together with a Journaline news service stream. With 16-QAM additionally a surround sound signal was transmitted.

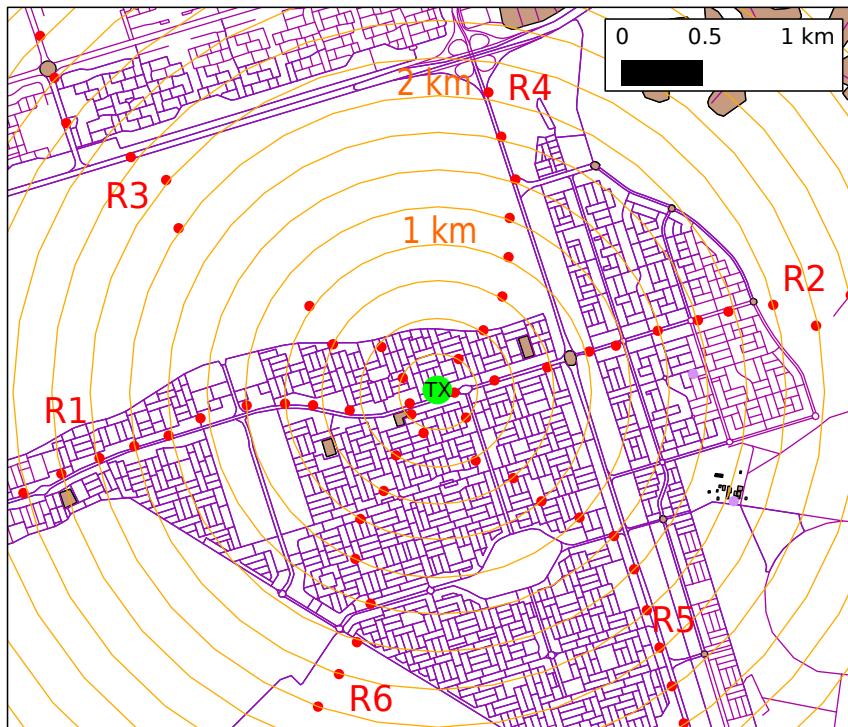
The planning of the Ministry of Communications was to conduct measurements on 6 radial routes (R1-R6) with measurement points at distances of 250 m (see Figure 4.18). There was the possibility to take stationary measurements on route 2, 3 and 6. The rest of the measurements were done by the Ministry of Communication. The main purpose was to compare the analogue and digital signal quality. In route 6 additional measurements, analysing the FM quality, while switching on and off the digital signal were conducted. Especially on route 2 towards the east, the FM signal was disturbed by the pirate FM station on the same frequency. On route 3 both digital modes, the 4-QAM and 16-QAM mode were measured, on the other routes the 4-QAM mode only.

Table 4.4 contains the measurement results from the combined mode measurements. In contrast to the FM signal, which was highly interfered by the pirate FM transmitter at the same frequency, the digital signal was not affected by interferences. The FM quality was analysed switching the digital signal on and off while the FM audio was recorded. No audible differences with the digital transmitter running and switched off could be observed



**Figure 4.17:** Community radio station Líder FM in Recanto dos Emas





**Figure 4.18:** Measurement routes and points in Recanto dos Emas (mapdata (c) Vectordata from OpenStreetMap and contributors, CC-BY-SA)

in the analogue FM signal.

The digital signal could be received in an area of the desired 1 km from the transmitter. With 4-QAM an error free reception could be achieved with a SNR and MER (Modulation Error Ratio) of 5 dB. With 16-QAM a MER of 6 dB and a SNR of 4 dB resulted in some errors in the audio data, whilst 12 dB MER and 14 dB SNR delivered still an error free signal.

Also mobile measurements were conducted with 4- and 16-QAM. Figure 4.19 shows the audio quality in the 4-QAM mode, Figure 4.20 the audio quality in the 16-QAM mode. With 4-QAM reception was mostly possible up to the desired 1 km radius. Towards the south shadowing effects resulted in a slightly worse coverage area. Towards the north-east, open environment and a hill were resulting in a coverage of up to 4 km. As expected with 16-QAM the coverage area was slightly smaller.

This trial showed that the setup of a DRM+ signal 150 kHz next to a FM signal as proposed in the ETSI standard worked as expected. The audio quality of the FM signal was not affected by the adjacent digital signal



**Table 4.4:** Results of the stationary measurements in combined mode in Recanto dos Emas

Route/ Point	Distance TX [km]	FM quality (digital on)	FM quality (digital off)	DRM+ qual. (4/16 QAM)	SNR/MER [dB]
<b>Route 2</b>					
R2P3	0.75	noisy	-	good/-	8/9
R2P4	1	different FM station	-	good/-	3.5/5.5
R2P6	1.5	different FM station	-	some errors/-	1/4
R2P7	1.75	different FM station	-	no signal	-
<b>Route 3</b>					<b>16-QAM</b>
R3P1	0.25	good	-	good/good	27/27
R3P2	0.5	good	-	good/good	17/18
R3P3	0.75	noisy	-	good/good	12/14
R3P4	1	noisy	-	good/some err.	6/5
<b>Route 6</b>					
R6P3	0.75	noisy	noisy, no diff.	good/-	6/7
R6P4	1	noisy	noisy, no diff.	good/-	5/5
R6P5	1.25	no signal	-	no signal	-
R6P6	1.5	no signal	-	no signal	-

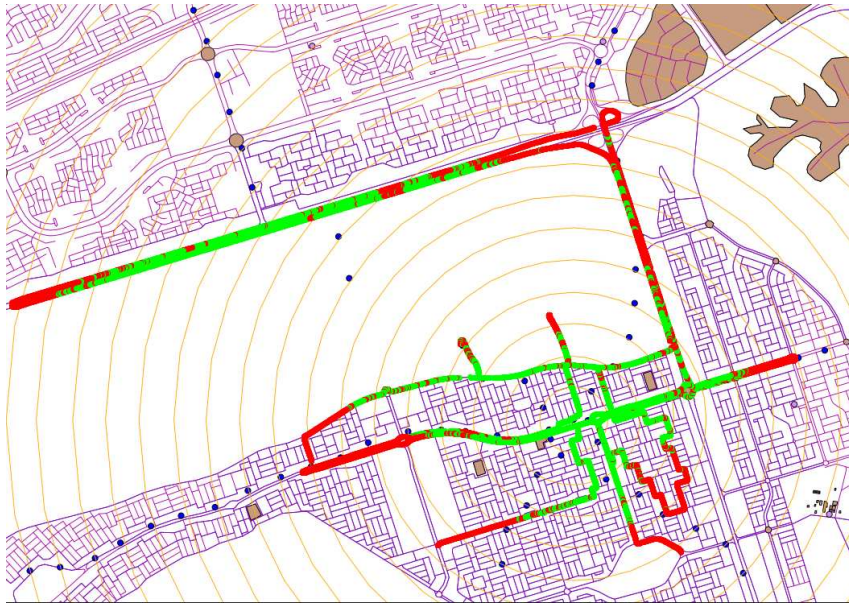


**Figure 4.19:** Mobile measurements in Recanto dos Emas with 4 QAM, green: audio frames ok, red: one or more audio frames corrupted (mapdata (c) Vectordata from OpenStreetMap and contributors, CC-BY-SA)

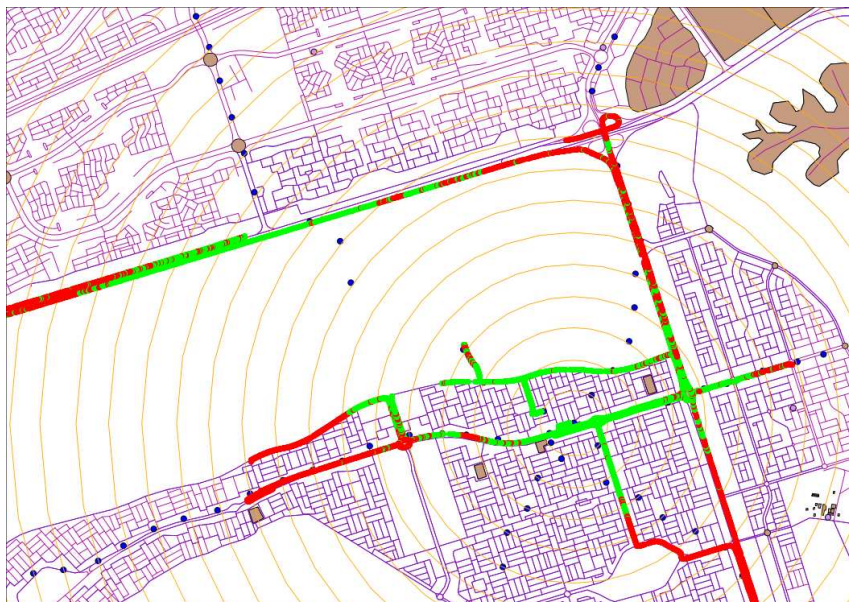


**Figure 4.20:** Mobile measurements in Recanto dos Emas with 16 QAM, green: audio frames ok, red: one or more audio frames corrupted (mapdata (c) Vectordata from OpenStreetMap and contributors, CC-BY-SA)

## 5 The DRM+ System in the VHF Band III

In Germany and other countries the VHF Band II (87,5-108 MHz) is fully occupied by analogue FM radio, which will probably not be switched off in the next years. At the same time, in the VHF Band III, which allocates the frequencies from 174 to 230 MHz, there is a lot of free spectrum intended for digital audio broadcasting. As DRM+ was originally designed to be used in the VHF Band I and II, evaluations about a usage at higher frequencies in the VHF Band III were conducted. In Band III DRM+ can coexist with the multiplex radio system DAB (Digital Audio Broadcast), offering local and community radios a cheap and flexible possibility to digitize their signals, which is hardly possible with DAB due to its multiplex structure [37] and [38].

To evaluate the possibility of using DRM+ in the VHF Band III the channel properties, especially in respect to high receiver velocities were analysed. Doppler shifts caused by movements of the receiver are the main constraint. Simulations of the effects of mobile reception for different receiver velocities at different frequencies have been conducted. Another aspect of the usage at higher frequencies are the pilot signals that are necessary for synchronisation and channel estimation. Additionally field-trials were conducted in the VHF Band III. The results were compared to the measurement results obtained from the field-trials in the VHF Band II. Those results were also submitted to the ITU Radiocommunication Study Group [39] and, together with measurements conducted by the University of Applied Sciences Kaiserslautern (see [31]) resulted in an expansion of the ETSI DRM standard to the VHF Band III.

### 5.1 Impact of the Mobile Channel

This Section gives an overview about the channel properties at different frequencies and receiver velocities and describes the parameters that are affecting the reception at higher frequencies.

#### 5.1.1 Inter-Carrier-Interference

A moving receiver causes Doppler shifts to the OFDM carriers. The shift depends on the direction of arrival of the wave and the direction of motion. If a moving receiver is combined with multipath propagation, reflections can arrive at the receiver from different directions. This can cause frequency dependent Doppler shifts and can result in Inter-Carrier-Interference (ICI).

In [40] the upper bounds of the normalized interference power for a classical (Jakes) channel model depend on the maximum Doppler shifts ( $f_d$ ) and the symbol duration ( $T_s$ ) are given as:

$$P_{ICI} \leq \frac{1}{12}(2\pi f_d T_s)^2. \quad (5.1)$$

The Doppler shift increases with higher carrier frequencies  $f_0$  and receiver velocities  $v$  as:

$$f_d = f_0 \cdot \frac{v}{c} \cdot \cos(\alpha). \quad (5.2)$$

with the speed of light  $c$  and the angle between the direction of arrival and the direction of motion  $\alpha$ .

To investigate the systems robustness against ICI at different velocities, simulations were made. The interference can be handled as additional near-Gaussian noise [41]. This was done for an angle  $\alpha = 0$  as the worst case scenario when the receiver is moving directly towards or away from the transmitter on a radial route.

To estimate the influence of ICI on the reception quality, the Bit Error Rate (BER) was calculated and plotted. The location probability was assumed to be 99 % as in [15] this probability is defined as the basis for 'good' mobile reception.

The simulations were conducted with loading 100 different sets of initial channel parameters. Each represents a different set of multipath components and can be seen as simulations of different locations. The details on the simulation process are given in Section 3.3.2. The approximation of the 99 % location probability can then be calculated as the average of the (in this case) 99 simulation calls, having the lowest BER. As the 'rural' and the 'SFN' channel profiles are defined to have the highest receiver velocities (see Annex A) the simulations have been conducted with those profiles.

### ICI in a 'rural' Channel

Performance simulations were conducted with a 'rural' channel profile with receiver velocities from 100 - 300 km/h.

Figure 5.1 shows the simulation results of the performance of a DRM+ system in the VHF Band III at a medium frequency of 200 MHz. For comparison Figure 5.2 shows the results for the VHF Band II at 100 MHz. Both were conducted with 16-QAM and a code rate of 0.5. The BER for a location probability of 99 % (in dashed lines) is plotted together with the values for 100 % location probability and for receiver velocities from 100 to 300 km/h. The coverage probability has no big effect on the system performance within the analysed velocities. At a frequency of 100 MHz and the lowest velocity, small differences can be seen at high SNR values, at 200 MHz there are no differences between the full coverage and a coverage probability of 99 %. This shows the influence of the coherence time of the channel at these frequencies, which is 0.072 sec. for 150 km/h at 100 MHz and 0.036 sec. at 200 MHz. The deep fades are short enough that the cell interleaver with a duration of 0.6 sec. and the bit interleaver with 0.1 sec. can handle them.

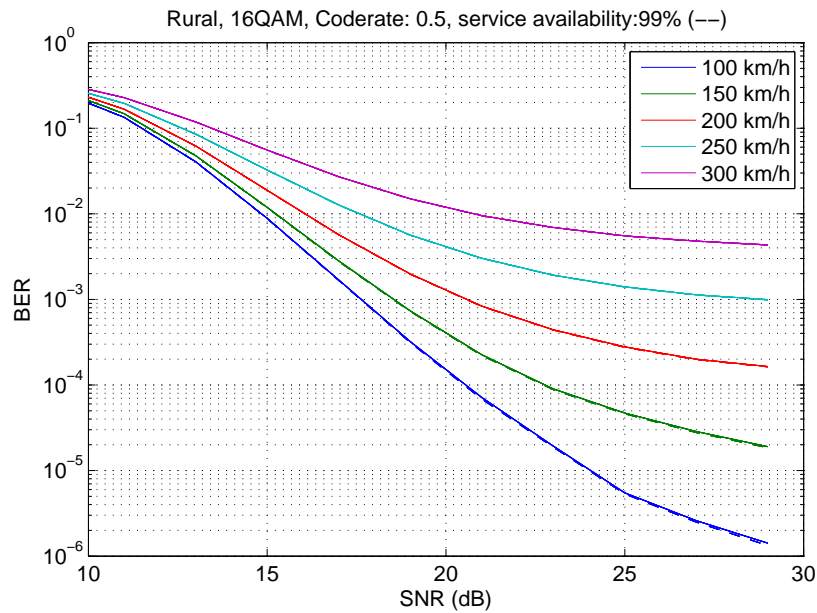


**Figure 5.1:** DRM+ performance in a 'rural' channel at different receiver velocities in the VHF Band III

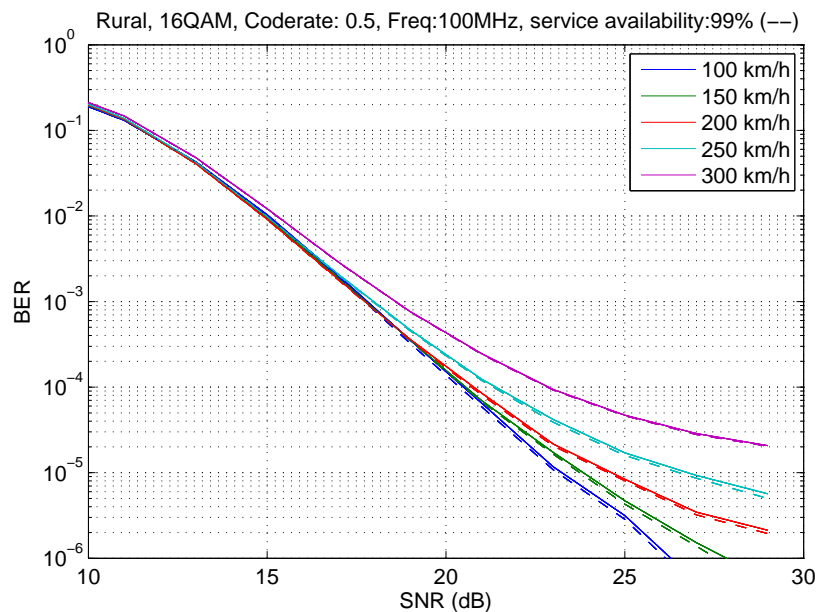


**Figure 5.2:** DRM+ performance in a 'rural' channel at different receiver velocities in the VHF Band II

In [42] a BER of  $10^{-4}$  is given as the maximum value for proper DRM reception. The simulation results in Figure 5.2 show that at 100 MHz a Signal-to-Noise Ratio (SNR) of 20 dB is necessary to reach this value at a velocity of 100 km/h. For 300 km/h a SNR of 22.5 dB is necessary. At 200 MHz in Figure 5.1 and 100 km/h the necessary SNR stays the same as at 100 MHz. Stepping up the receiver velocity, the impact of the ICI increases faster at 200 MHz. At 150 km/h a SNR of 22.5 dB is necessary for good reception, at 200 km/h the BER of  $10^{-4}$  is hardly achieved with around 30 dB. At higher



velocities this scenario doesn't achieve a Bit Error Rate of  $10^{-4}$  in this worst case scenario.

### ICI in a 'Single Frequency Network' Channel

A special case of propagation occurs in a 'Single Frequency Network' (SFN) as shown in Figure 5.3. It represents a network of transmitters sharing the same radio frequency to achieve a larger coverage area. As given in Annex A the delays for the simulation are chosen so that they are in the range of several hundreds micro seconds representing signals arriving from the different transmitter stations in the overlapping area.

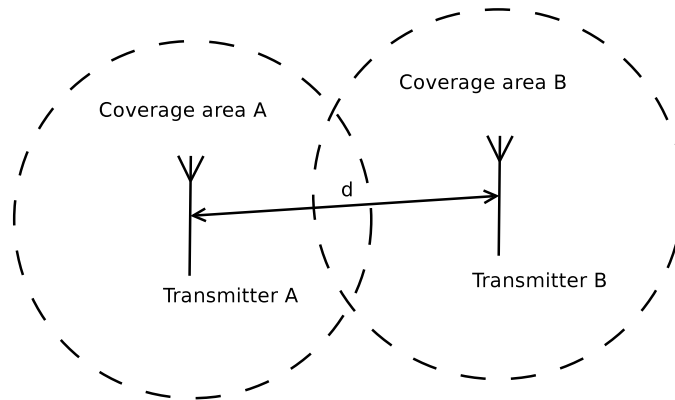


**Figure 5.3:** A 'Single Frequency Network' with two transmitters A and B in distance  $d$ . Each transmitter has its own coverage area which overlaps with the respective transmitter

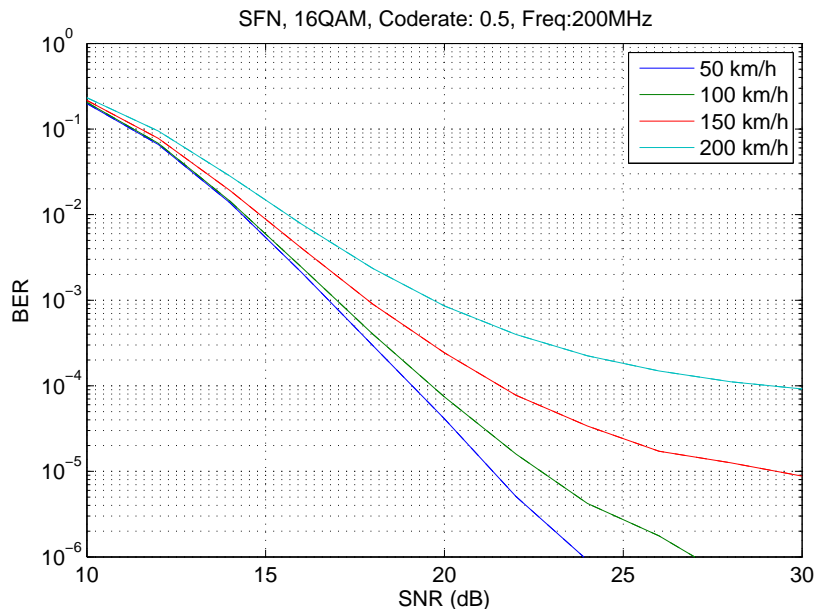


**Figure 5.4:** Performance in a 'Single Frequency Network' in Band III

Simulations were conducted with a 'Single Frequency Network' (SFN) channel profile for receiver velocities from 50 - 200 km/h. Figure 5.4 shows the performance of a 'Single Frequency Network' at a frequency of 200 MHz. It can be seen that for a receiver velocity

of 150 km/h a slightly higher SNR is needed as for 100 km/h to get a BER below  $10^{-4}$ . For 200 km/h it is still possible to get a proper reception, but a higher SNR is needed.

### 5.1.2 The Pilot Grid

The robustness of the signal with mobile reception also depends on the pilot grid [7]. The pilot symbols are needed for the channel estimation. If the channel changes too fast (short coherence time) as it does with a high speed receiver, the variation of the channel can no longer be reproduced by the pilots. As the coherence time is dependant on the carrier frequency this parameters are investigated in respect to the usage of DRM+ in the VHF Band III with fast moving receivers.

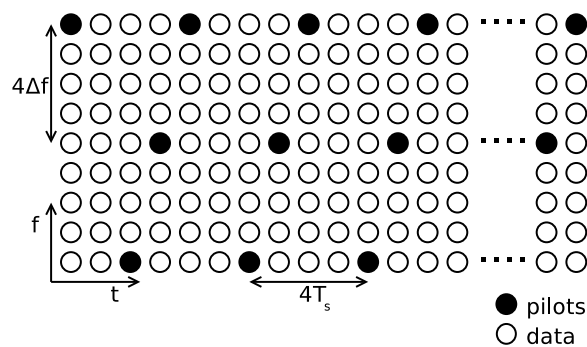


**Figure 5.5:** DRM + Pilot grid

Figure 5.5 shows the locations of the DRM+ pilots. Compared to the data carriers, the pilots are 'boosted'. In order to get consistent power over all carriers the pilot carriers are distributed diagonally over the frames.

The pilots are inserted on every fourth subcarrier and every fourth symbol. Considering the symbol duration of  $T_s=2.5$  ms, in time direction, the channel is measured every 10 ms ( $4 * T_s$ ). Assuming a Rayleigh channel, the coherence time is inversely proportional to the Doppler frequency  $f_d$  as shown in Section 3.3. Figure 5.6 shows the coherence time of the channel at different frequencies and velocities. Here again the the worst case scenario with the receiver driving directly towards or away from the transmitter on a radial route ( $\alpha = 0$  in equation 5.2) is assumed.

To be able to follow all channel variations, the coherence time of the channel should not be larger than the distance between two pilots. This value is also added to Figure 5.6. At 100 MHz the coherence time falls below this value at a velocity of 450 km/h, at 170 MHz at 270 km/h and at the upper bound of Band III, at 230 MHz at a velocity of 200 km/h.

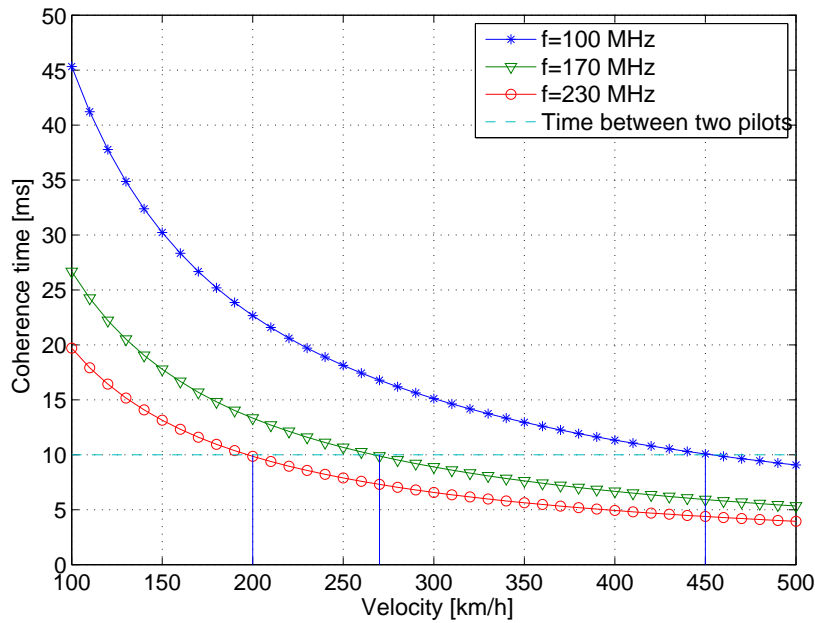


Figure 5.6: Coherence time over velocity at different frequencies

### 5.1.3 Flat Fading at Low Speed

For low receiver velocities in Band II fading over the whole signal bandwidth can lead to deep fades over the whole signal bandwidth, lasting longer than the cell interleaver (600 ms). This can result in signal drop-outs as there is no chance to recover the signal by the following error correction. As a shorter wavelength results in a higher spatial resolution of the interference pattern in the air and the coherence time becomes smaller, this results in less drop-outs due to slow fading.

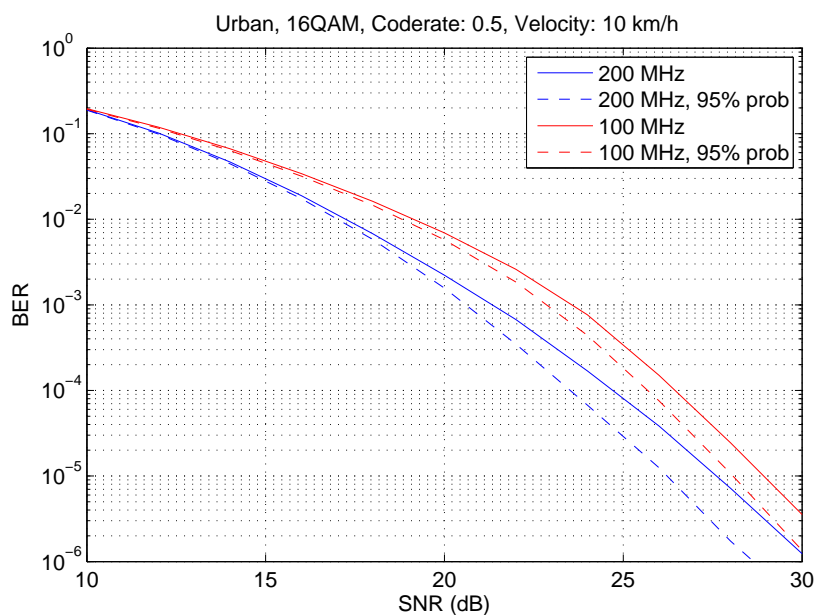


Figure 5.7: Comparison of the performance in a slow and flat fading environment



Figure 5.7 shows a comparison of the system performance with a slowly moving receiver at 10 km/h for carrier frequencies of 100 and 200 MHz. As can be seen, the performance is better at 200 MHz. In addition an error probability of 95 %, calculated as described in Section 5.1.1, is plotted with dashed lines. The differences between full 'coverage' and a coverage probability of 95 % in this slowly changing channel clearly exceeds the differences in the fast channel, especially for the lower frequency.

## 5.2 Measurements in the VHF Band III

Measurements were conducted in the inner-city of Hannover and on a radial route in direction of the main antenna beam as in Band II. The purpose of the measurements was to analyse the DRM+ performance in the VHF Band III and to compare the results to the measurements made in Band II. Again the tests were conducted with the robust 4-QAM modulation and the 16-QAM modulation with high data rates as listed in Table 4.1. Vertical polarization and a ERP of 30 W as in Band II were used.

### Equipment

The following equipment was used for the measurements:

- Fraunhofer Content Server
- RFmondial Modulator/Exciter
- Thomson linear amplifier (VHF amplifier Band III, 54 dB gain)
- Transmit antenna: Kathrein K 52 40 5, 5- Element Yagi directional antenna
- Receive antenna: Kathrein K 51 16 4 / BN 510 351 adapted to Band III, monopole, an antenna-factor of 13 dB/m was measured at 176.64 MHz, the antenna was mounted on the roof of a van at a height of around 2 m
- HF-Frontend: Rhode & Schwarz measuring receiver (ESVB), IF: 10.7 MHz
- Field strength measurements: ESVB, BW: 300 kHz
- A/D converter Ettus USRP, daughterbord: BasicRX
- RFmondial software Receiver

### Transmission Content

The transmission content in both modes consisted in an AAC encoded stereo audio stream and a synchronous pseudo random bit sequence (prbs), that was used for the calculation of the Bit Error Rate (BER) (see [9] for details).

### Measurement Parameters

The following parameters were recorded and analysed during the measurements:

- RMS field strength (Rhode & Schwarz ESVB Measuring receiver, BW: 300 kHz)

- GPS coordinates
- Bit Error Rate
- Signal-to-noise ratio (calculated via the time correlation/synchronisation, see [28])
- Receiver status information (RSTA), the status of the audio decoding that shows if one or more audio frames are corrupted within one DRM multiplex frame and the FAC CRC are evaluated, see [9] for details)

### 5.2.1 Measurements in Urban Environment

The measurements in urban environment were conducted in 16-QAM mode (code rate 0.5). In order to analyse the effect of flat fading, measurements were conducted with a low receiver velocity of around 15 km/h. As this area is located in the main beam of the transmitter the results for Band II and III are comparable.

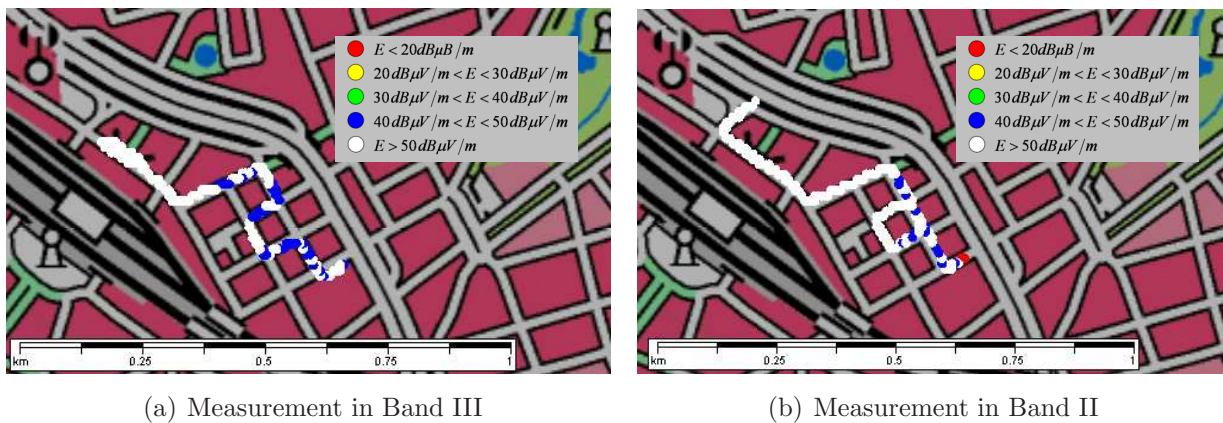


**Figure 5.8:** Field strength in urban environment (map source: Bundesamt für Kartographie und Geodäsie)

Figure 5.8 shows the field strength in Band III compared to Band II, in the vicinity of Hannover main station. Figure 5.9 shows a plot of the receiver status information (rsta) which describes whether all audio frames are ok (green) or one or more audio frames are corrupted (red). The reception was almost error free here in Band III as well as in Band II. More details can be seen in Figure 5.10 and 5.11. Here the results are plotted against the time. In the first row the field strength is shown. Additionally the mean field strength (mean fs) and the standard deviation of the field strength (std fs) are added to the Figures. They show that the field strength in Band II is slightly higher than in Band III, the standard deviation is a bit lower in Band III which can be caused by the differences in slow and flat fading due to the different frequencies as evaluated in Section 5.1.3. The second row shows the BER, which is slightly lower in Band III than in Band II. The third row shows the calculated SNR, which is slightly higher in Band III. This could be caused by less interferences as at the time of the measurement in the VHF Band III only

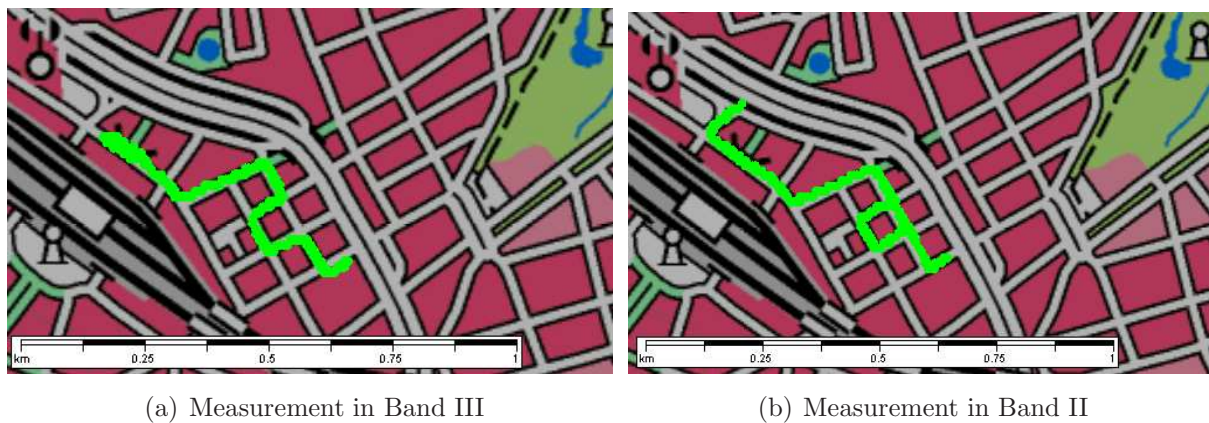


**Figure 5.9:** Measurement of the audio data in the urban environment (green: Audio OK, red: one or more audio errors)(map source: Bundesamt für Kartographie und Geodäsie)

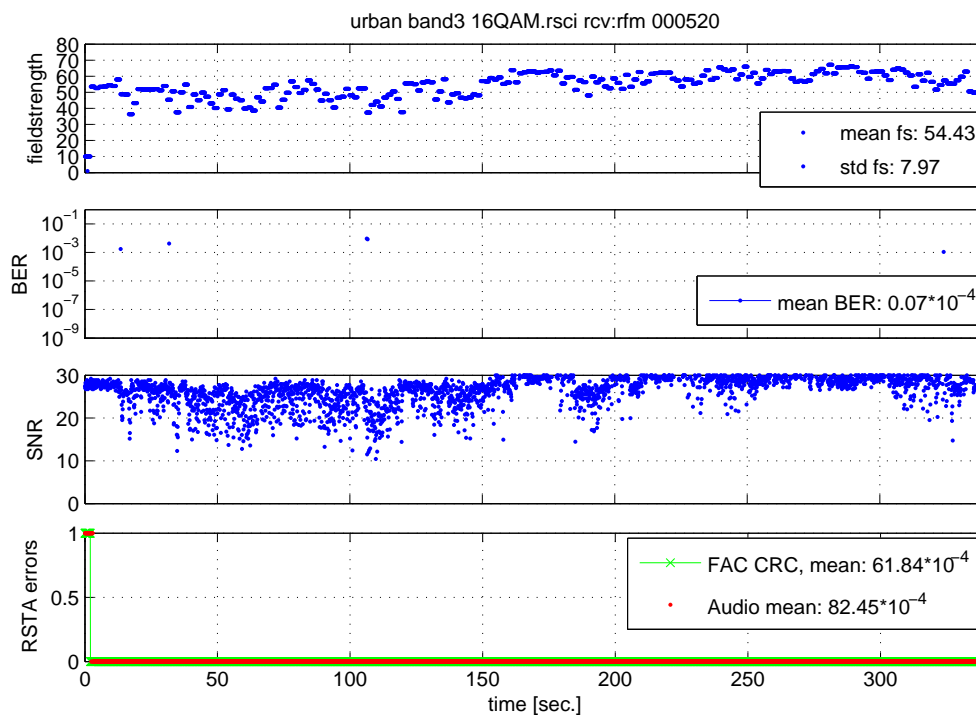


**Figure 5.10:** Measurement results with 16-QAM in 'urban' environment in the VHF Band III

block 12A (around 223 MHz) was used for DAB in the region of Hannover. In Band II interferences from other FM transmitters might effect the reception and degrade the SNR. The last row shows the status of the Cyclic Redundancy Check (CRC) of the Fast Access Channel (FAC) and the audio decoder errors (0: errorfree, 1: one or more audio frames corrupted). Here some more errors show up in Band III.

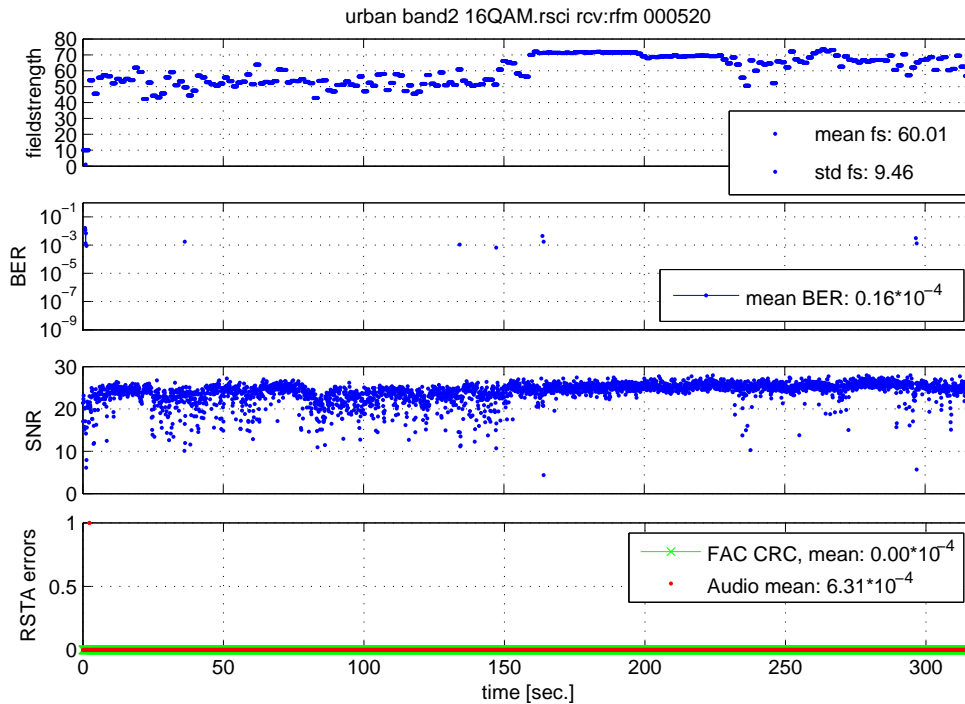


**Figure 5.11:** Measurement results with 16-QAM in 'urban' environment in the VHF Band II

## 5.2.2 Measurements of the Coverage Limit

Measurements of the coverage limit were conducted in the main beam of the transmitting antenna with 16- and 4-QAM modulation. The route was chosen to be on the B65, a rural road located mostly in the main beam of the antenna to compare the results with Band II. The measurement was continued until the audio quality became bad.

### Measurements with 4-QAM

Figure 5.12 shows the field strength measured on the route, Figure 5.13 the audio status. Figure 5.13 shows clearly, that with more distance to the transmitter, passing villages, the audio becomes erroneous, whereas passing the countryside with almost no obstacles (the countryside in Hannover is quite flat) reception quality was still good at low field strength values.

Figure 5.14 shows the reception parameter plotted against the time in the direction away from the transmitter. On the radial route reception was possible down to a field strength of around 35 dB $\mu$ V/m with a SNR of around 12 dB. The measurement was stopped at a distance of around 30 km from the transmitter, where audio quality became bad also in the free countryside. In general there was little difference to the measurement in the VHF Band II (see Section 4.1.2).





**Figure 5.12:** Field strength measurement of the coverage limit 4 QAM mode (code rate: 0.5) in the VHF Band III (map source: Bundesamt für Kartographie und Geodäsie)



**Figure 5.13:** Measurement of the coverage limit in 4 QAM mode (code rate: 0.5) in the VHF Band III (green: audio frames ok, red: one or more audio frames corrupted (map source: Bundesamt für Kartographie und Geodäsie)

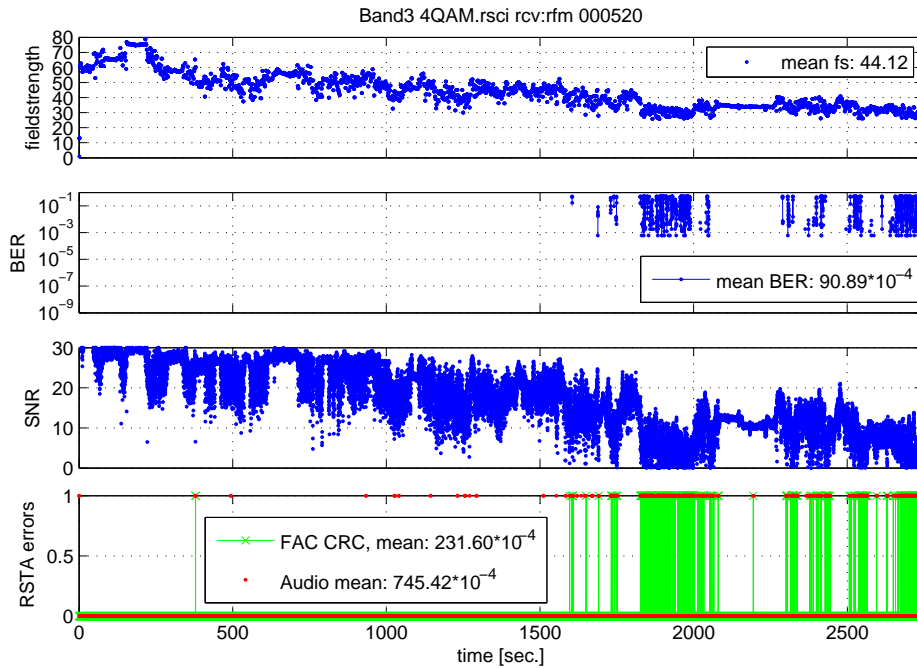


**Figure 5.14:** Reception parameter on the B65 with 30 W ERP and 4 QAM mode (code rate: 0.5) in the VHF Band III, measurement while moving towards the transmitter (map source: Bundesamt für Kartographie und Geodäsie)

### Measurements with 16-QAM

On the way back to Hannover city, measurements in the 16-QAM mode were conducted. The measurement was started in the village Sehnde. Figure 5.15 shows the measured field strength in the 16-QAM mode, Figure 5.16 shows the audio status. While the reception in the open (flat) environment was still good, errors came up passing villages. Compared to Band III, in Band II (Figure 4.11) some more errors occurred while leaving the city of Hannover and in the small village before Sehnde. This could be caused again by higher interferences with FM in Band II. At this location due to a four-lane road velocities up to 100 km/h could be achieved.

In Figure 5.17 the field strength is plotted in comparison to the receiver Signal-to-Noise Ratio (SNR), the Bit Error Rate (BER) and the Receiver Status Information (RSTA) against the time. The mean field strength here is higher compared to Figure 5.13 because the measurement with 16-QAM started closer to the transmitter than 4-QAM. It shows that the reception was acceptable down to a field strength of around 48 dB $\mu$ V/m at a calculated SNR of around 20 dB in the 16-QAM mode.



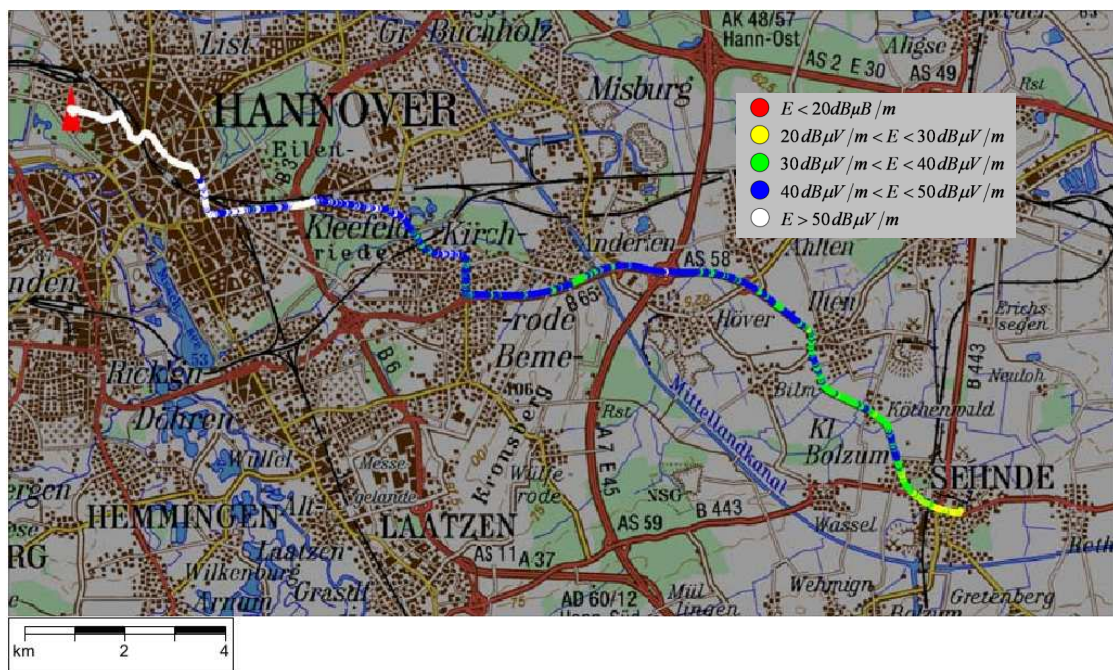


**Figure 5.15:** Field strength measurement of the coverage limit in 16 QAM mode (code rate: 0.5) in the VHF Band III (map source: Bundesamt für Kartographie und Geodäsie)

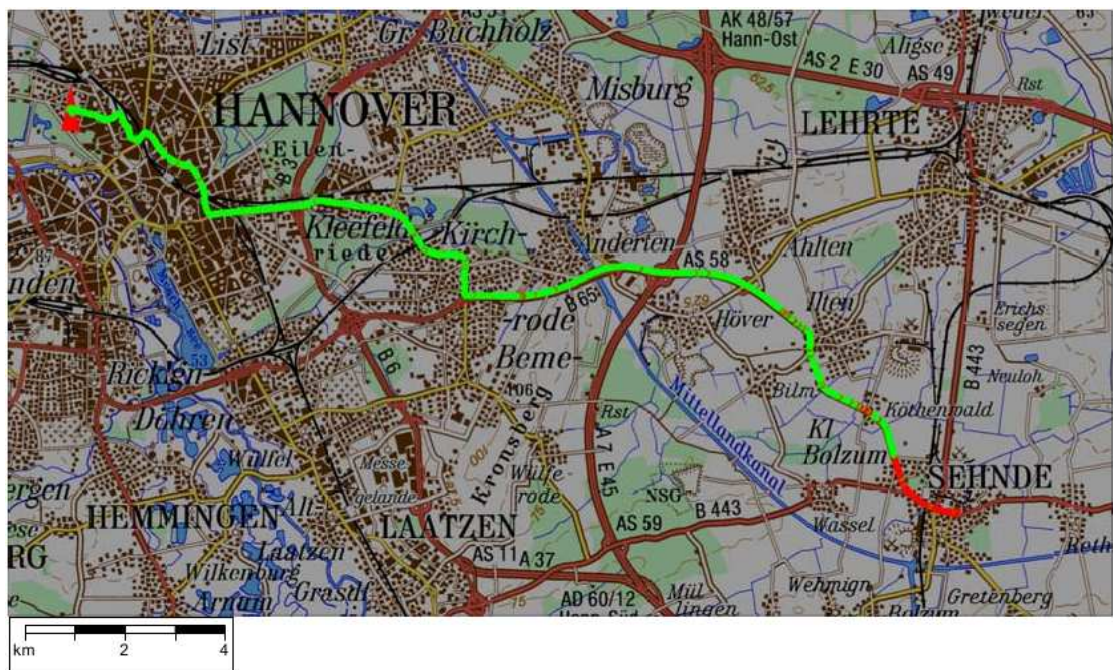


**Figure 5.16:** Measurement of the coverage limit in 16 QAM mode (code rate: 0.5) in the VHF Band III (green: audio frames ok, red: one or more audio frames corrupted (map source: Bundesamt für Kartographie und Geodäsie)

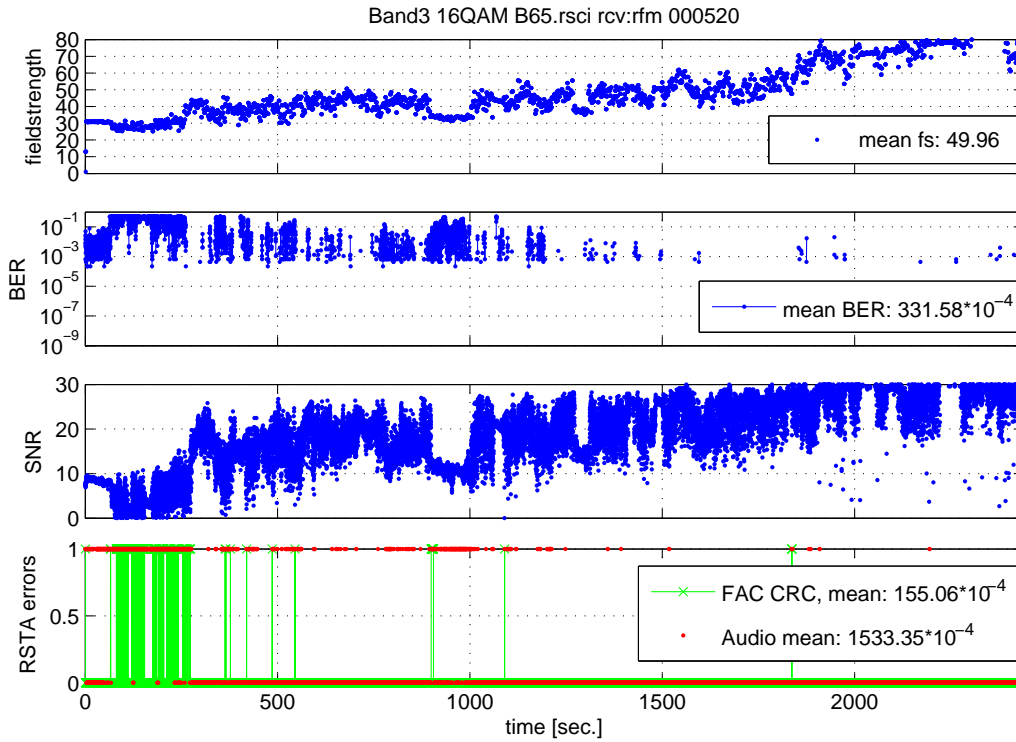


**Figure 5.17:** Reception parameters on the B65 with 30 W ERP and 16 QAM mode (code rate: 0.5) in the VHF Band III (map source: Bundesamt für Kartographie und Geodäsie)

### 5.3 Conclusions on DRM+ in the VHF Band III

In general, the measurements conducted in Band II and III show no significant differences. While measuring the coverage limit, less errors were recorded in Band III, which can be caused by less interferences in Band III in Hannover as it was quite unoccupied at the time of the measurement while the FM Band II was and is heavily used.

A real speed test could not be conducted due to speed limits on the streets around the transmitter and the lack of a suitable vehicle. As the ICI only becomes a problem when different carriers are affected by different Doppler shifts due to multipath propagation, this tests should be made in a region with obstacles in the countryside. The region of Hannover is a quite flat area and thus not suited for testing multipath propagation in the countryside.



## 6 Transmitter Diversity Techniques

Due to its small bandwidth DRM+ is especially interesting for local and community radio stations, which are often licensed for low power transmission and low antenna facilities. Therefore techniques to enhance the reception quality without transmitting more power can be interesting for a better coverage area [43].

To enhance system performance, the DRM+ channel coding offers the possibility to take advantage of the channel diversity. Especially with slow receiver velocities, destructive interference can produce channel attenuation over the whole signal bandwidth for a time period which exceeds the ability of the interleaver and the Viterbi decoder to recover the erroneous data.

Different diversity techniques are already used to enhance the performance in many OFDM based systems as IEEE 802.11, DAB or DVB-T. An overview of different spatial transmitter diversity techniques is given in [44]. As a diversity system without the necessity of applying changes to the receiver, the (cyclic) transmit delay diversity system was proposed for DRM+ in [45]. A comparison between the well known Alamouti transmit diversity scheme [46] and (cyclic) delay diversity (C)DD is given in [47]. It has been shown that the Alamouti scheme is leading to significant performance gains. For (C)DD, the gains are slightly smaller. On the other hand, the Alamouti scheme is very sensitive against fast fading and changes have to be applied to the receivers, which are not part of the standard.

Therefore a transmitter delay diversity system was set up to evaluate the promising results in a real environment. As the performance enhancement is highly dependent on the correlation between the transmission paths, the wavelength in the VHF Band II is quite big and space is mostly a problem at antenna facilities, further evaluations on the spatial correlation and antenna distances at different antenna heights have been conducted.

### 6.1 Transmitter Delay Diversity

A common experience listening to FM radio in the car and stopping at a traffic light is hearing it degenerating, while the signal is reacquired if the vehicle moves a fraction of a meter out of the destructive interference, which is caused by multipath propagation. A possibility to overcome this problem is the introduction of additional diversity to the channel. Transmitter diversity applications have the advantage that two (or more) antennas have to be installed only once at the transmitter. The cost and size of the receivers do not increase.

In the DD system a second (or more) antenna transmits the same OFDM signal with a small time delay  $\delta$  added after adding the cyclic prefix. The signals are weighted according to the number of TX branches in a way that the overall power level stays the same (see Figure 6.1).

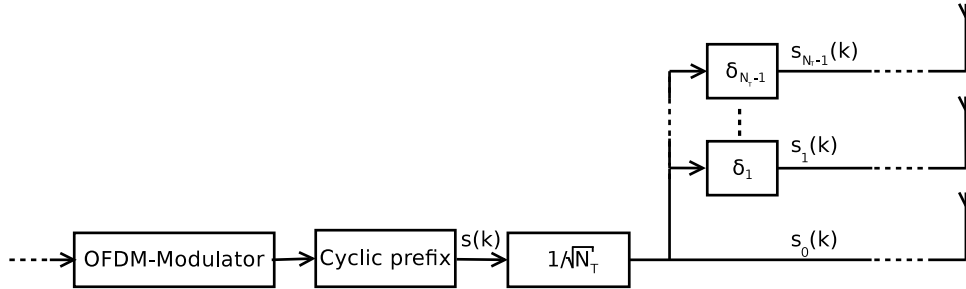


**Figure 6.1:** Frontend of an OFDM transmitter with Delay Diversity

A variant of Delay Diversity is called Cyclic Delay Diversity (CDD). Here the delay is added before the cyclic prefix. The advantage of this is that the delay does not minimize the length of the guard interval. Both CDD and DD yield the same signal at the receiver after guard interval removal as long as the received signal is free of Inter-Symbol-Interference (ISI) [48]. As the Delay Diversity mode was easier to implement and the guard interval of the DRM+ system is large enough to run DD without ISI in our low power setup, the DD mode was used for the trial and evaluations. Therefore the following equations refer to DD.

Referring again to Figure 6.1 the system model for Delay Diversity can be derived.  $s_i(k)$  denotes a sequence of time domain OFDM symbols including the guard intervals. For practical reasons the time delay should be a multiple of the sampling time otherwise it will be difficult to implement it in hardware.

The TX DD signals can be written as [49]:

$$s_i(k) = \frac{1}{\sqrt{N_T}} \cdot s(k - \delta_i), \quad 0 \leq i \leq N_T - 1 \quad (6.1)$$

Passing the transmission channel, the signal at the receiver is given as:

$$r(k) = \sum_{i=0}^{N_T-1} \sum_{l=0}^{L_{max}} h_i(l) \cdot s_i(k - l) + n(k), \quad (6.2)$$

$h_i(l)$  is the channel impulse response from TX antenna number  $i$  to the RX antenna with a maximum delay spread of  $L_{max}$ .  $n(k)$  is complex Gaussian noise with a variance of  $\sigma^2/2$  and  $N_T$  the number of transmit antennas.

In [49] the definition of an 'effective channel' is introduced. It includes the effect of the DD system into the channel properties. The impulse response of the effective channel is given as:

$$h(l) = \frac{1}{\sqrt{N_T}} \cdot \sum_{i=0}^{N_T-1} h_i(l - \delta_i). \quad (6.3)$$

Using this, the RX signal can be written as:

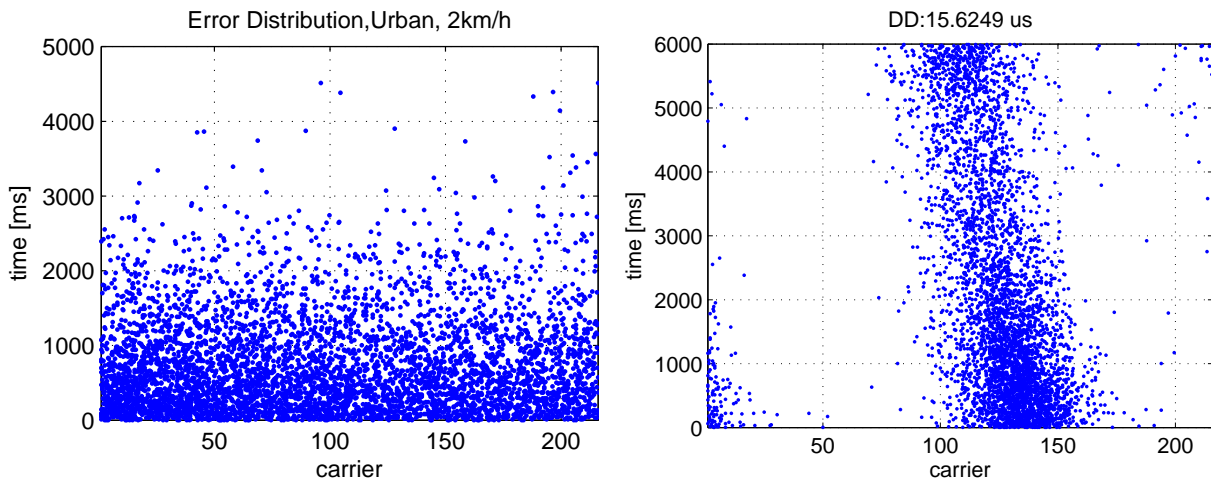
$$r(k) = \sum_{l=0}^{L_{max} + \delta_{max}} h(l) \cdot s(k - l) + n(k). \quad (6.4)$$

With

$$\delta_{max} = \max \{ \delta_i \}, \quad i \in [0, N_T - 1]. \quad (6.5)$$

At the receiver the signal can be seen as a superposition of the signals from the different branches with an increased delay spread. As the introduced delay reduces the size of the effective guard interval, the delay should be chosen sufficiently small.

In the field trial delay times of 15.625  $\mu$ s and 31.25  $\mu$ s were used. These values could be easily implemented by delaying one signal branch by 3 or 6 samples at the sample rate of 192 kHz. The corresponding coherence bandwidth is 64 kHz/32 kHz. With this choice flat fading can be prevented as the frequency response has at least one maximum and one minimum within the signal bandwidth of 96 kHz.



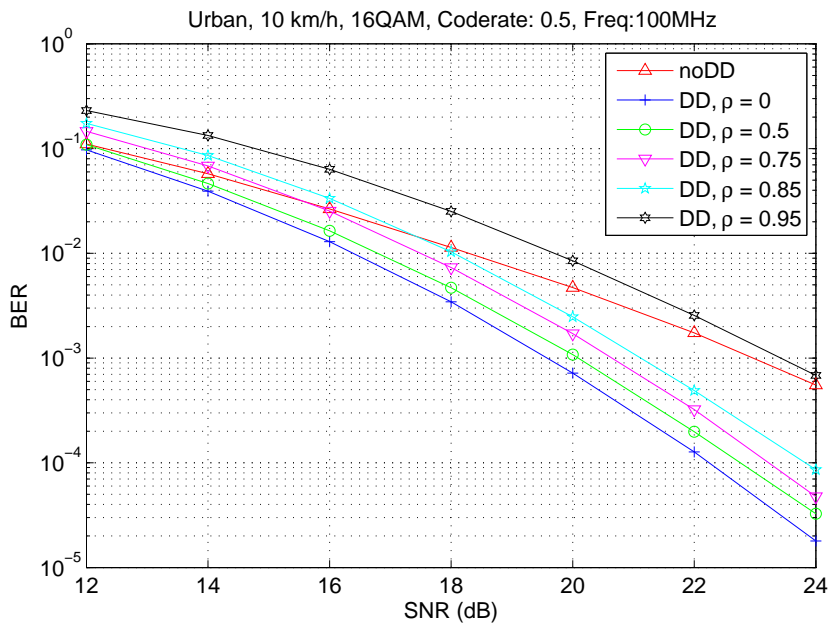
**Figure 6.2:** Distribution of bit errors (blue dots) in an uncoded system with slow receiver velocity in an urban channel (left: without DD, right: with DD)

Figure 6.2 shows the simulation result of the distribution of the bit errors in an uncoded system over the time and carriers (frequency). On the left the signal was filtered by a tapped delay line filter, representing an 'urban' channel at a very slow receiver velocity of 2 km/h with a center frequency of 100 MHz. The channel parameters are given in Annex A. The bit errors are distributed over all carriers and, due to the slow velocity, over a long time. The error correction won't be able to correct all the bit errors. On the right a DD system was simulated with the same channel parameters and a delay of 15.625  $\mu$ s. The

errors appear over the whole time but only affect part of the carriers. With an appropriate interleaving and error correction the signal can be decoded properly.

## 6.2 Dependency of the System Performance on the Correlation between the Propagation Paths

Simulations of a DRM+ system with (cyclic) transmitter delay diversity are presented in [47] and [45]. They show a diversity gain between 3 and 6 dB for an urban channel at different velocities, but only with fully decorrelated transmission paths. In a transmitter diversity setup with an elevated transmitter the antenna distance has to be considerably greater than in a receiver diversity setup to get uncorrelated transmission paths [12]. To evaluate this, simulations with a delay diversity setup with two transmitter branches and different correlations between the paths were conducted.



**Figure 6.3:** Simulation of the DD performance in an 'urban' channel with different correlation between the paths

The channel was implemented as a tapped delay filter as described in Section 3.3.2 with the properties of the 'urban' channel given in Annex A with a velocity of 10 km/h. With this low velocity flat fading becomes a major problem. Simulations were conducted with a correlation coefficient  $\rho$  of 0, which is uncorrelated, 0.5, 0.75, 0.85 and 0.95. Additionally the results of a one TX antenna setup (noDD) are shown in Figure 6.3.

The simulation shows that up to a quite high correlation of  $\rho = 0.85$  the performance shows only small degradations. For higher correlations a significant degradation of the system performance can be seen. For  $\rho = 0.95$  the performance is worse than in the one

antenna setup (noDD). Here the diversity gain can no longer compensate the degradation of the channel caused by the introduced delay. The 3-dB loss between the one antenna setup and the DD setup with  $\rho = 0.95$  for low SNR can also be explained with the deep fades introduced by the delay with nearly equal paths.

Fully correlated paths also can be present if there is only line-of-sight propagation between the transmitter antennas and the receiver and the receiver is located at the broadside direction of the antennas. One method to overcome the degradation of system performance in case of correlated paths is the implementation of Soft Delay Diversity.

### Soft Delay Diversity

While DD increases the diversity gain in the Rayleigh fading channel, in the case of pure line-of-sight (LOS) propagation the channel is transformed into a static frequency selective one, which can degrade the system performance. With pure line-of-sight propagation the correlation between the signal paths is normally high, as for uncorrelated paths very large distances between the transmission antennas are necessary. To overcome this problem the signal power at each transmit antenna branch can be weighted by a different factor, as proposed in [50]. This is called Soft Delay Diversity. After this weighting process the signals are normalized such that the total transmitted power remains constant [51].

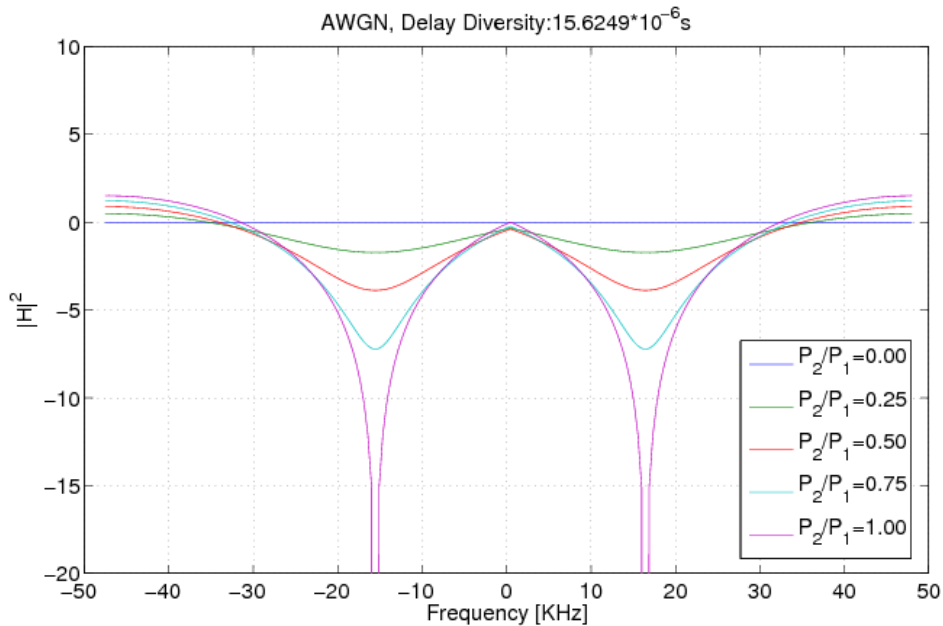


**Figure 6.4:** Frequency response of two correlated paths with different power ratios

Figure 6.4 shows the frequency response of a static line-of-sight channel with Delay Diversity and different ratios of the power level.  $P_1/P_2$  denotes the ratio between the signal power on antenna 2 and 1. With only power at one branch ( $P_2/P_1 = 0$ ) the channel becomes frequency flat. Increasing the power level at the second branch, the fading increases. Simulations have been conducted with a 2 TX antenna DRM+ DD system with a delay

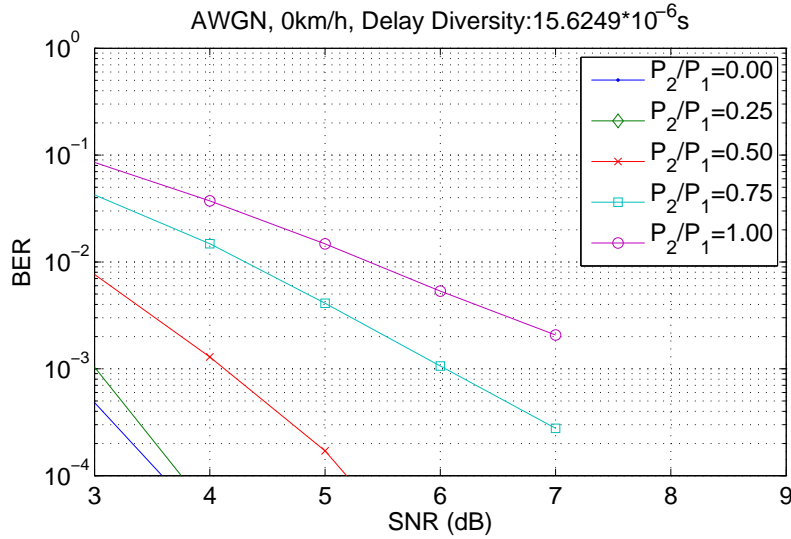


**Figure 6.5:** Soft Delay Diversity BER simulation in an AWGN channel with different power ratios

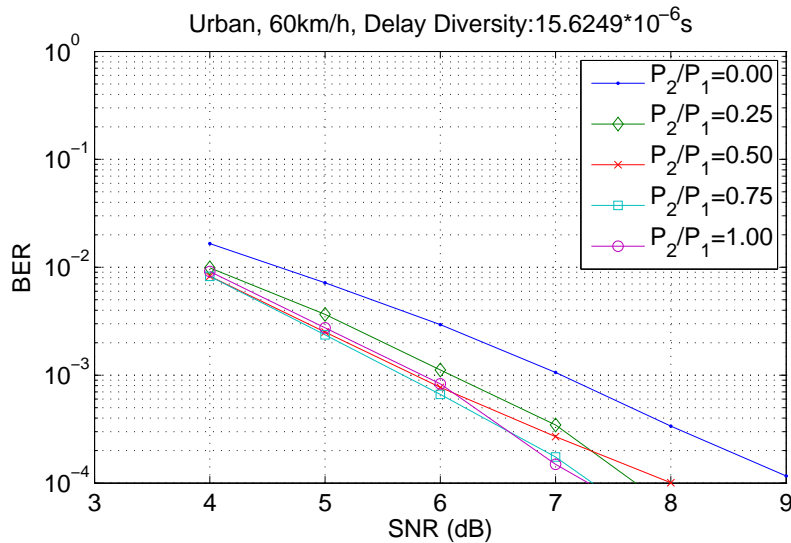


**Figure 6.6:** Soft Delay Diversity BER simulation in a mobile 'urban' channel with different power ratios

time of  $15.625 \mu\text{s}$  with optimal channel estimation and 4-QAM with a code rate of  $1/3$ .

The line-of-sight scenario can be simulated with an AWGN channel. Only white, Gaussian noise at different power levels is added to the diversity signal. Simulation results in the AWGN channel depicted in Figure 6.5 show that increasing the power of the second antenna yields to an increase of the BER. The deep fades here disturb the reception as no diversity gain can be exploited.

On the other hand, in the Rayleigh fading 'urban' channel with a receiver velocity of  $60 \text{ km/h}$ , increasing the power on the second antenna, reduces the BER as shown in Figure 6.6. The diversity gain here exceeds the additional frequency selectivity. This results

simulated with a DRM+ system are comparable to the results for DVB-T given in [50].

A setup with Soft Delay Diversity could be interesting for example if a transmitter is located on the outskirts. The power ratios could be implemented by using antennas with different pattern, providing equal power towards the city (Rayleigh Fading) and different power levels towards the more open environment (LOS).

## 6.3 Correlation between the Transmission Paths

As the correlation between the transmission path from the different antennas is important for the diversity gain as shown in Section 6.2, methods to evaluate the correlation are presented in this Section.

### 6.3.1 2D Model

The correlation coefficient in a broadcast situation with an elevated transmitter is highly dependent on the scatterers in the receivers surrounding. A simple 2D model with all scattering assumed in a horizontal plane with the horizontally spaced transmit antennas was given by Jakes in [14]. The model is shown in Figure 6.7. The scatterers are assumed

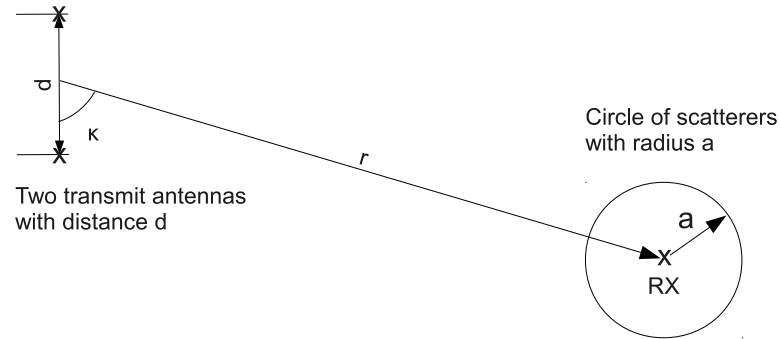


**Figure 6.7:** Scattering model for calculating the correlation

to lie on a circle around the receiver, as the main scatterers contributing to the signal are those within the first Fresnel zone [12]. The distance between the transmitter and the receiver is assumed to be greater than the radius of the scatterers so that the transmitter does not lie within this circle.

With the radius of the scatterers  $a$ , the distance between the transmitter and receiver  $r$ , the angle toward the scatterers  $\kappa$  and the distance between the transmit antennas  $d$  and with  $k = \frac{a}{r}$  the correlation coefficient can be calculated as [14]:

$$\rho(d) = J_0^2 \left( \frac{2\pi d k}{\lambda^2} \sin \kappa \right) J_0^2 \left( \frac{\pi d k}{\lambda^2} \sqrt{1 - \frac{3}{4} \cos^2 \kappa} \right) \quad (6.6)$$

Figure 6.8 shows the correlation plotted against the distance between the transmit antennas. It assumes the receiver to be in the broadside direction of the transmit antennas ( $\kappa = 90^\circ$ ). The radius of the scatterers was deduced as the distance of wave propagation in the time of the delay spread of the 'urban' channel ( $0,8 \mu\text{s}$ ). This results in a radius of 240 m.

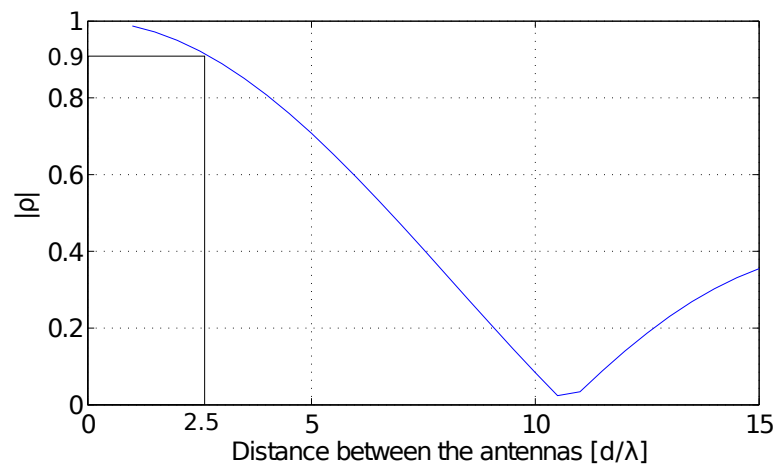


**Figure 6.8:** Correlation for horizontally spaced transmit antennas with a distance of 2 km between the transmitter and the receiver

The available space for the two transmit antennas in the field trial setup is 8 m. At the transmission frequency of 95.2 MHz this corresponds to approx.  $2.5 \lambda$ . With this distance this very simplified model gives a correlation of 0.9.

### 6.3.2 Raytracing Calculations

As the 2D model does not take into account vertical propagation and computational power nowadays allow the calculation of site-specific models as described in Section 3.2.3, a city model was created with the radio propagation software 'Wireless InSite' to get an idea of the parameters with different antenna heights. This also offers the possibility to further analyse the behaviour of the system with different TX antenna distances as the possibilities of the real-world transmit antenna setup were quite restricted.

A model of a city was created of around 4000 m x 800 m. Two routes of 58 transmitters each were installed at one end at a height of 35 m and 70 m over ground. The houses in the TX surrounding have heights between 30 and 42 m so the lower transmitter route (35 m) is located at around the height of the roofs to provoke reflections near the transmitters. This low antenna setup shall represent the situation of many local radio stations using the given infrastructure of rooftops to setup the TX antenna.

The other setup is adapted to the situation in the field trial with an antenna elevation of 70 m over ground. The distance between the transmitting antennas was set to 0.7 m, so



transmitting antenna distances up to 40.6 m (corresponding to  $13.5 \lambda$  at 100 MHz) have been evaluated.

Four receiver routes were configured at a distance of 3500 - 4000 m from the TX at a height of 2 m over ground. The RX routes consisted of 200 - 300 single receivers, with a distance of 2 m. The height of the buildings in the surrounding of the RX is 10 - 50 m, so there was little LOS propagation, the majority of the reflections occurred in the surroundings of the receivers.

The complex RX power at each receiver location was calculated as the summation of the complex impulse response. In order to evaluate the correlation coefficient, the complex power of each point of a receiver route, resulting from the first transmitting antenna ( $x_i$ ) was combined to the complex power at the same receiver route arriving from the second transmitting antenna ( $y_i$ ). The correlation coefficient for the  $n$  reception points is then calculated as:

$$\rho(x, y) = \frac{\sum_{i=1}^n (x_i - \bar{x})(y_i - \bar{y})}{\sqrt{\sum_{i=1}^n (x_i - \bar{x})^2 \cdot \sum_{i=1}^n (y_i - \bar{y})^2}} \quad (6.7)$$

with  $\bar{x} = \frac{1}{n} \sum_{i=1}^n x_i$  and  $\bar{y} = \frac{1}{n} \sum_{i=1}^n y_i$ .

This was repeated for the other TX antennas at rising distances from the first antenna.

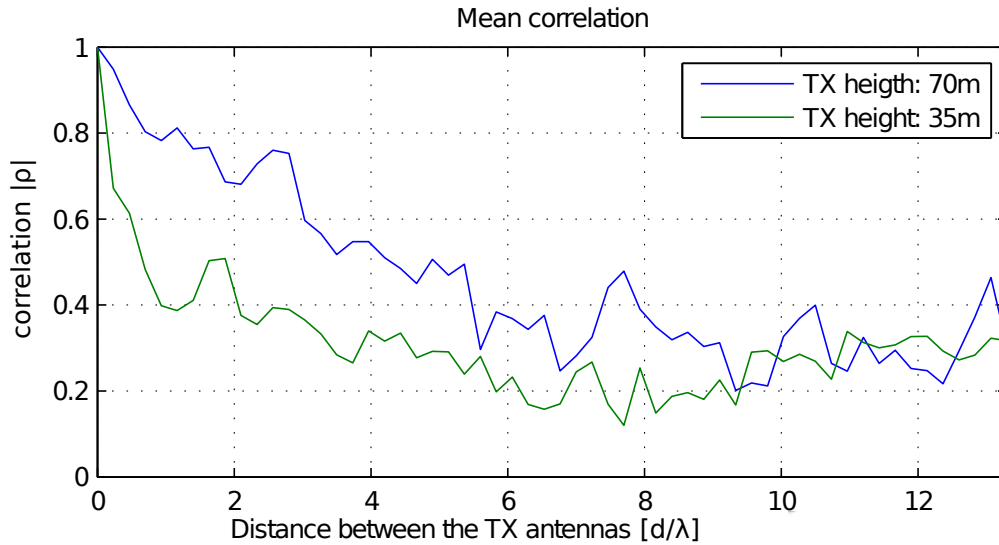


**Figure 6.9:** Mean correlation between the RX signals in urban environment from 2 vertically polarized TX antennas over distance between the TX antennas

Figure 6.9 shows the mean correlation between the vertically polarized TX antennas versus the distance between the TX antennas at different heights of the TX antennas. As expected, the correlation is much lower with lower TX antennas as reflections already take place close to the transmitter. At the TX height of 70 m a correlation lower than 0.8 was achieved with a distance of approx.  $1.5 \lambda$ . With the lower TX height this was already achieved with a distance of less than  $1 \lambda$ .

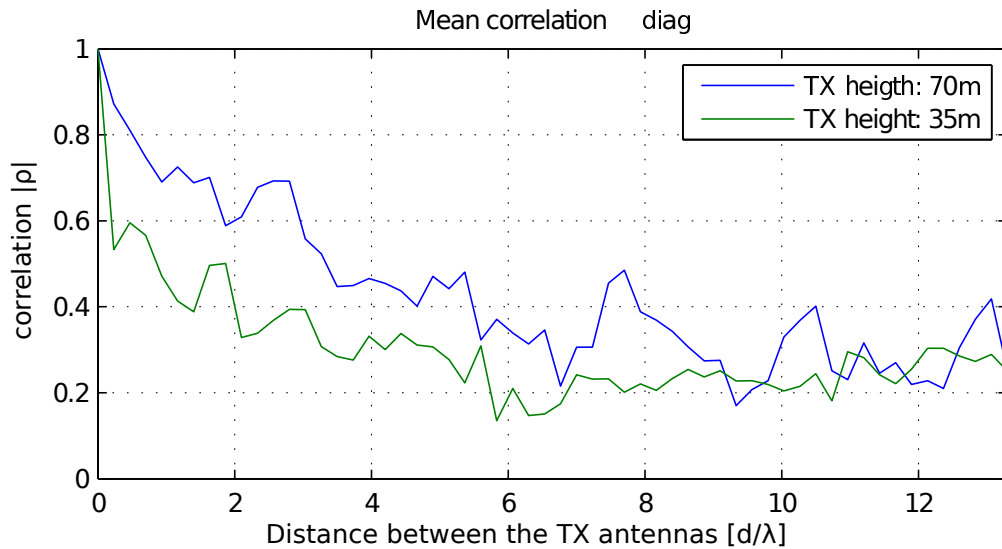


**Figure 6.10:** Mean correlation between the RX signals in urban environment from 2 diagonal ( $\pm 45^\circ$  slanted) TX antennas over the distance between the TX antennas

As the space at a transmitter tower is often limited, polarization diversity, as often used in mobile communication [52], was evaluated. A setup with a diagonal polarization diversity antenna setup was tested with two antennas slanted by  $\pm 45^\circ$ . Figure 6.10 shows, that in this setup the correlation is significantly lower than with two vertically polarized antennas, especially for the 70 m height TX setups up to a distance of  $2\lambda$ . A correlation coefficient below 0.8 can be achieved at a distance of  $1\lambda$  for the 70 m setup. Another advantage of this setup is that it offers comparable reception quality for vertical and horizontal RX antennas.

A polarization diversity setup with vertical/horizontal polarized antennas also showed good decorrelation. However the cross polar discrimination (XPD) was very high in this setup with vertical RX antennas so the performance enhancement is quite low. Another possibility could be circular polarization as evaluated for example in [53].

## 6.4 Field Trial

In a joint industry-academy project a field test was set up to analyse the transmitter delay diversity system in the real world. To evaluate the enhancement of delay diversity, measurements with one antenna were conducted and compared with measurements at the same route with two antennas and delay diversity. Different delay lengths have also been tested. The measurements have been conducted with a low velocity (approx. 10 km/h) where fading can become a major problem.

### 6.4.1 Transmitter Hardware Setup

The hardware setup was done at the IKT in close collaboration with the industry partner RFmondial. The main challenge for the hardware setup was the exact synchronization of the two transmitters. As the setup also had to work for a Single Frequency Network (SFN) test (see Chapter 7), the synchronization also has to work when the transmitters are located at different locations. Therefore synchronization with very stable GPS receivers was implemented.

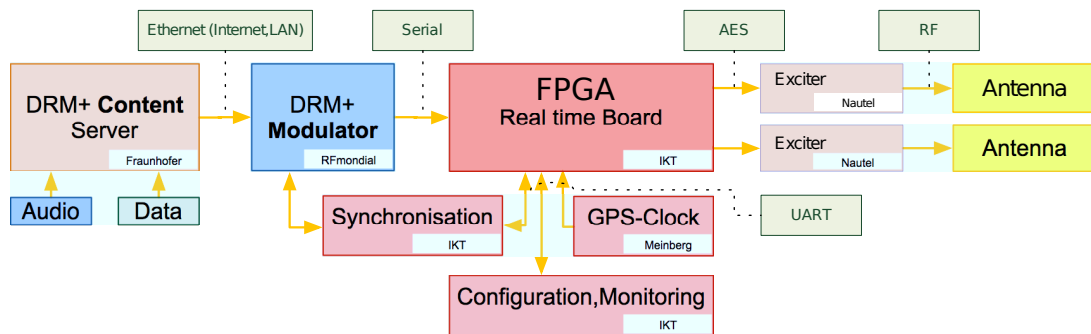


**Figure 6.11:** Block diagram of the Delay Diversity transmitter hardware setup

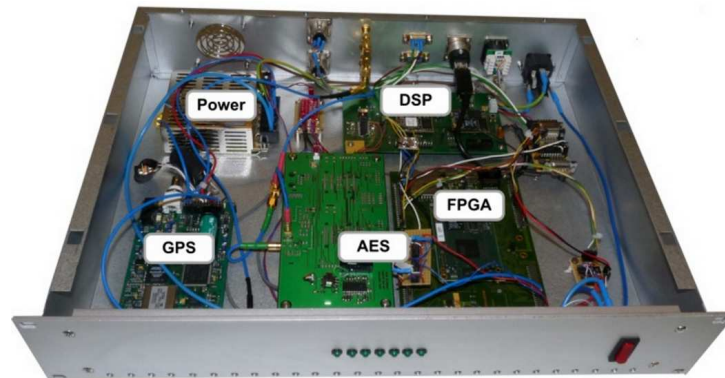


**Figure 6.12:** The hardware setup of the DRM+ Delay Diversity transmitter

Figure 6.11 shows the block diagram of the transmitter setup. The program relevant data like audio, text messages, pictures etc. are encoded by the content server. The prepared data stream is sent via LAN or Internet to the DRM+ modulator. The modulator adds the channel coding and modulation to the data stream.

For the synchronization of the two baseband signals, a FPGA based 'Realtime Board' was developed. As it should also work in a Single Frequency Network with distant transmitters, the 'Realtime Board' is synchronized via GPS and the FPGA is driven by a stable 10 MHz clock which was used to synchronize the two transmitters and to add a constant delay to the signals. The delay can be chosen in multiples of the sampling period. Figure 6.12 shows the hardware setup of the modulator including the 'Realtime Board' on the FPGA

and the GPS clock. The modulated data, one with a delay, is then sent to the two exciters that are used for modulation onto the carrier frequency and final amplification.

### 6.4.2 Measurement Locations

The measurements with Transmitter Delay Diversity were conducted in 2010 in the city of Hannover. The transmitter was located on the roof of the university building at a height of 70 m over the ground. An ERP (Effective Radiated Power) of 30 W (2x15 W in case of DD) was transmitted at a frequency of 95.2 MHz. The two vertically polarized Yagi antennas were mounted at a distance  $d$  of 8 m ( $2.5 \lambda$ ) as this was the maximum available space on the roof. The antenna setup is shown in Figure 6.13. Compared to the calculations in Section 6.3.2 and 6.2 this distance should already provide enough decorrelation to enhance the reception quality. The direction of the main beam directs to an azimuth (clockwise angle to the north) of  $130^\circ$ . In the measurements 4-QAM subcarrier modulation with a code rate of  $R_0 = 0.33$  was used.

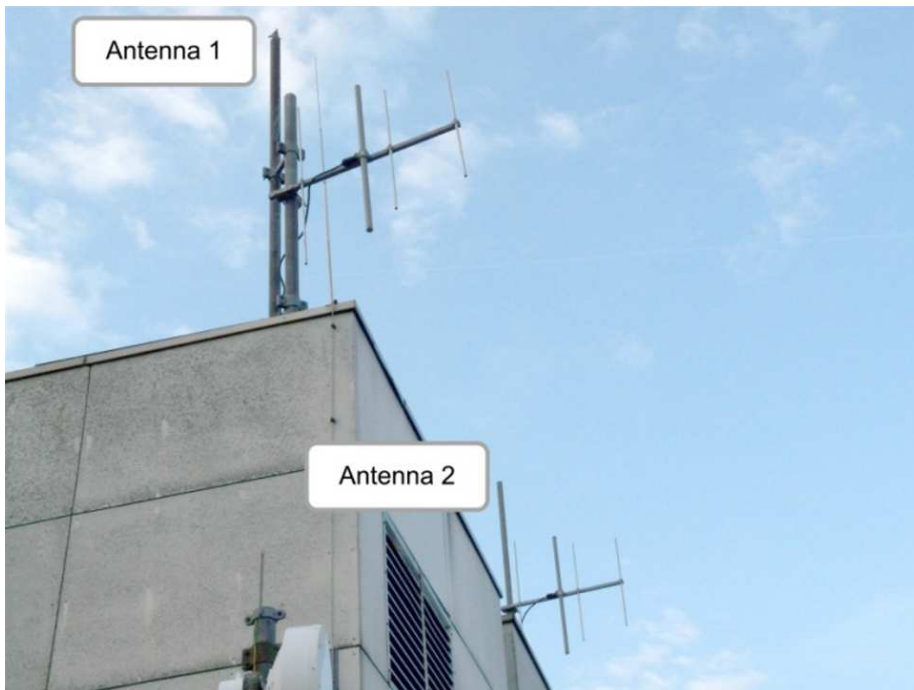


**Figure 6.13:** Transmit antennas for delay diversity mounted on the roof of the university

Measurements have been conducted at five locations at different distances from the transmitter and angles to the antennas broadside direction at a receiver velocity of around 10 km/h. Depending on the angle between the broadside direction of the antennas and the direction of the measurement location  $\alpha$ , the effective antenna distance varies as  $d_{eff} = d \cdot \cos(\alpha)$ . Table 6.1 shows the measurement locations in the city of Hannover, their average distance from the transmitter, the effective antenna distance and their environmental characteristics. Figure 6.14 shows the locations together with a field strength

prediction calculated with the freeware program 'Radiomobile'. Most of the locations are 'urban', which are 5-6 story buildings in Hannover. Only 'R. Koch-Platz' is 'suburban' with one family houses. The measurements on each route took a time of approximately 5 minutes.

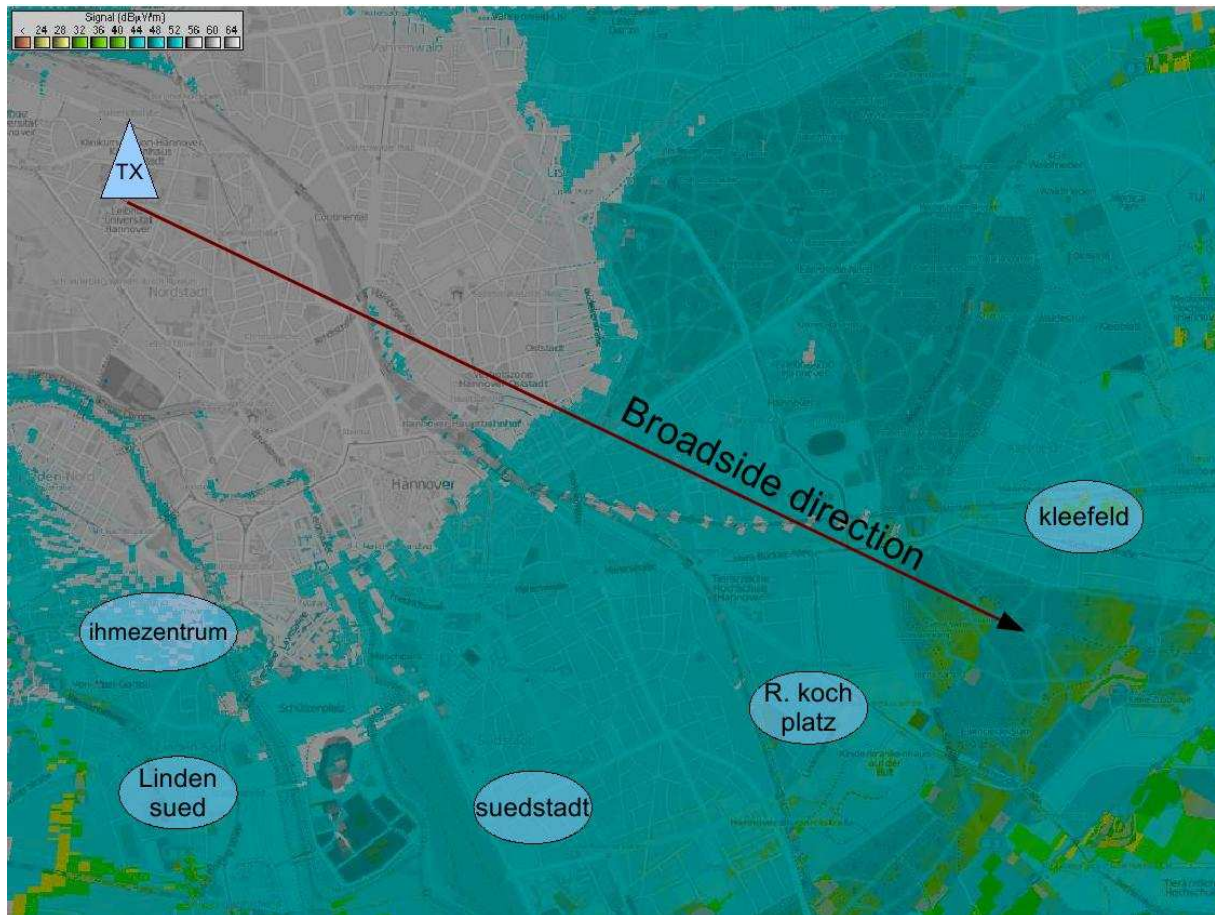


**Figure 6.14:** Measurement locations (mapdata (c) OpenStreetMap and contributors, CC-BY-SA, <http://www.openstreetmap.org>)

For comparison the transmitter setup was switched between one transmitter, two transmitters with a delay of 3 samples resulting in  $15.625 \mu\text{s}$  delay and two transmitters with a delay of 6 samples resulting in  $31.25 \mu\text{s}$  delay.

In some cases as there were very few errors to combine, AWGN-noise was added to the recorded IQ-data and the IQ-data were decoded again. The Signal-to-Noise Ratio (SNR) was chosen to be in relation to the mean power of the whole recorded data stream, which gives a setup comparable to a transmitter with lower power.

### 6.4.3 Measurement Equipment and Parameters

A magnetic monopole reception antenna from Kathrein was mounted on the roof of a van at a height of 2 m. As RF-Frontend a Rhode & Schwarz test receiver (ESVB) was



**Table 6.1:** Measurement locations overview

Location	Distance to TX	Effective antenna dist.	Environment
Ilmezentrum	2 km	$d_{eff} = 4 m$	<b>Urban</b> area with 5-6 story buildings behind a big block of buildings
Linden Sued	3.2 km	$d_{eff} = 4 m$	<b>Urban</b> area with 4-5 story buildings
Suedstadt	4.2 km	$d_{eff} = 7 m$	<b>Urban</b> area with 4-5 story buildings
Kleefeld	6 km	$d_{eff} = 7.8 m$	<b>Urban</b> area with 5-6 story buildings
R.-Koch Platz	4.4 km	$d_{eff} = 7.8 m$	<b>Suburban</b> area with one-family houses

used, providing band-pass filtering with a bandwidth of 300 kHz at the IF output. The IF output was connected to an Universal Software Peripheral (USRP, Ettus Research LLC), for A/D conversion and re-sampling. The DRM+ signal was then decoded by a software receiver (RFmondial). Some measurements included the field strength, which was recorded also with the ESVB, triggering the measurement via GPIB. The IQ data was recorded and the power spectrum density (PSD) was analysed offline on its standard deviation. The receiver records all kind of reception parameters, see details in [9]. Here, the mean FAC (fast access channel) CRC and the mean audio errors (when available) have been analysed.

#### 6.4.4 Measurement Results

The measurement results against the time in 'Suedstadt' are plotted in Figure 6.15 and 6.16. The Figures show the Bit Error Rate (BER), the calculated SNR and the RSTA data. The mean error rates are added. Figure 6.16 also includes the field strength values measured with the ESVB. In this example the reception gets significantly better with transmit diversity, the audio error rate decreases from 0.048 to 0.007.

Table 6.2 provides the measurement results of all locations in an overview. 'Nondiv' means only one transmitter is running, 'DD3' means two transmitters with half power and a delay of 3 samples (15.625  $\mu$ s) and 'DD6' means two transmitters with half power and a delay of 6 samples (31.25  $\mu$ s). In the second column the standard deviation of the power spectral density (PSD) is given. The PSD describes the variation from the average power and gives

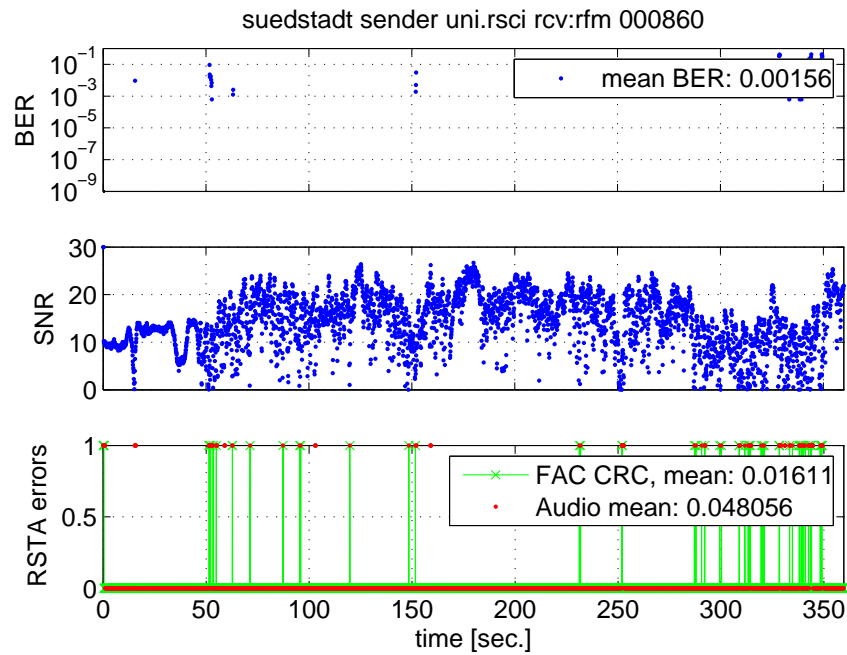


Figure 6.15: Measurement results in 'urban' area (Suedstadt) without DD

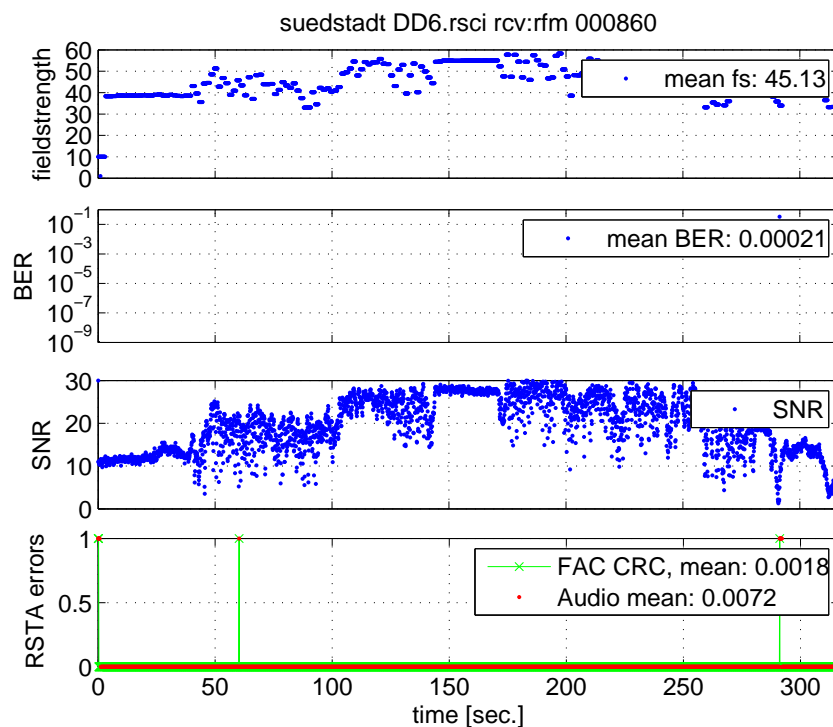


Figure 6.16: Measurement results in 'urban' area (Suedstadt) with DD

an indication for the amount of frequency flat fading. Additionally the FAC CRC error rate and, if measured, the audio error rate are given to compare the reception quality.

The results show, that the standard deviation decreases in the DD mode at every measure-

**Table 6.2:** Measurement results of the transmitter Delay Diversity trial

Location/Mode	Std. PSD	FAC CRC	Audio
<b>'Urban'</b> ('Ihmezentrum')			
nondiv	5.64000	0.00588	x
div DD3	5.03000	0.02313	x
div DD6	4.78000	0.00441	x
<b>'Urban'</b> ('Linden Sued')			
nondiv	6.00170	0.02690	0.07440
div DD3	5.49	0.01220	0.02950
div DD6	5.48580	0.00540	0.01775
<b>'Urban'</b> ('Suedstadt')			
nondiv	5.47000	0.01610	0.04800
div DD3	4.76000	0.00240	0.00890
div DD6	5.22000	0.00189	0.00760
<b>'Urban'</b> ('Kleefeld')			
nondiv	5.63000	0.00120	0.00481
div DD3	5.22000	0.00213	0.00273
div DD6	5.18000	0.00152	0.00485
<b>'Suburban'</b> ('R. Koch-Pl.')			
nondiv	5.26000	0.00407	x
div DD3	4.02000	0.07560	x
div DD6	4.90000	0.01650	x

ment location, which indicates, that fading is decreasing. In most of the 'urban' measurement locations the reception was getting better with DD. Exceptions are the FAC-CRC DD3-Ihmezentrum and Kleefeld and the audio errors of DD6-Kleefeld, which are slightly increasing compared to the one-TX setup. The 'suburban' measurement at 'R. Koch Platz' is worse with DD compared to the single transmitter case. An explanation for this can be the lower buildings in this area, resulting in less multipath propagation and as a result, less fading than in an area with higher buildings. This is supported by the lower standard deviation for all modes at 'R. Koch Platz'.

As the measurements are not dependent on the effective distance between the antennas, the angle to the broadside direction does not seem to have an influence on the measurement results.



## 6.5 Conclusions on Transmitter Delay Diversity with DRM+

Performance simulations show the dependency of the diversity gain on the spatial correlation of the channel paths. A significant diversity gain could be achieved up to a correlation coefficient of 0.85.

Raytracing calculations of two transmitter setups with different distances between the TX antennas have been conducted. The low transmitter setup, as it could be used by small local and community radio stations using the rooftop to install the antennas, shows a very fast decrease of the correlation, offering an enhancement of the performance with distances of less than a wavelength between the transmit antennas.

The higher transmitter antennas, as used in the field trial show that a correlation coefficient lower than 0.8 can be achieved with antenna distances of approx.  $1.5 \lambda$  with two vertical polarized TX antennas. Lower correlation could be achieved in both cases with additional polarization diversity with two diagonal,  $\pm 45^\circ$  slanted antennas.

The measurement results of a field trial show that reception could be enhanced in most 'urban' locations with the DD setup. In some cases reception quality slightly decreases, specially in the 'suburban' environment where the field strength has a lower standard deviation over the locations.



## 7 Single Frequency Networks

As a digital COFDM radio system, DRM+ is capable of transmitting in a Single Frequency Network (SFN) with several transmitters working on the same frequency. Due to a guard interval added after every symbol, differences in time of arrival from the different transmitters do not result in Inter-Symbol-Interference (ISI) if all signals arrive within the guard interval at the receiver. Attenuations of carriers due to the time delay can mostly be compensated by the SFN gain. This offers the possibility of covering a big area with several transmitters on only one frequency which saves bandwidth and simplifies frequency planning significantly. It also enhances the reception quality in areas with obstacles as buildings, hills or mountains. Other uses for SFN are gap filling transmitters and coverage extenders [54].

The DRM+ symbol duration is 2.25 ms followed by a guard interval of 0.25 ms. This guard interval duration allows a theoretical distance between the contributing transmitters of 75 km. First studies and simulations about using a DRM+ SFN are described in [55]. It states that compared to FM, DRM+ Single Frequency Networks have a higher coverage reliability even at lower TX powers.

The principle of Single Frequency Networks is already used in other digital broadcasting systems as DVB-T or DAB. Principles on SFN planning for DAB and DVB-T are given e.g. in [56], dealing with cost optimization and [57], developed by the ITU Regional Radiocommunication Conference to carry out compatibility analyses.

Recent studies about Single Frequency Networks for broadcasting systems focus on planning optimization as in [58] or on advantages of hierarchical modulation as in [59].

As the DRM+ signal bandwidth of 96 kHz is quite small, compared to e.g. DVB-T (7-8 MHz) and DAB (approx. 1.5 MHz), frequency flat fading in the overlapping area can occur and degrade the reception quality. As already described in Chapter 6 this is caused by small time delays of the signals arriving from different transmitters with similar power. Adding a delay at one transmitter station was proposed in [60] to solve this problem and will be further analysed in this Chapter.

### 7.1 Propagation Conditions in a SFN

In this Section a closer look at the effect of interferences between signals arriving from different transmitters is taken.

In a two TX-SFN as depicted in Figure 7.1, the vertically polarized amplitude of the

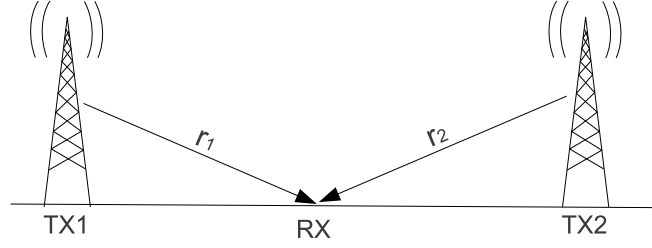


**Figure 7.1:** A Single Frequency Network of two transmitters

E-field as the interference of signal  $E_1(r_1)$  arriving from TX1 and  $E_2(r_2)$  arriving from TX2 can be derived from the well known wave equation for a single carrier at frequency  $f_0 + f_\Delta$  at reception point  $r$  [60].

$$E_1(r_1, t) = \hat{E}_1(r_1) e^{j2\pi(f_0 + f_\Delta)(t + \frac{r_1}{c_0})} \quad (7.1)$$

$f_\Delta$  denotes the distance from the carrier frequency and should be a multiple of the sub-carrier distance in an OFDM system.  $E_2$  can be calculated respectively.

With  $E_{12}(r_1, r_2, t) = E_1 + E_2$  and assuming constant levels within one symbol duration the mean sum power level is given by:

$$\begin{aligned} |E_{12}|^2 &= \hat{E}_1(r_1)^2 + \hat{E}_2(r_2)^2 \\ &+ 2\hat{E}_1(r_1)\hat{E}_2(r_2) \cos\left(2\pi\frac{(f_0 + f_\Delta)}{c_0}(r_2 - r_1)\right) \end{aligned} \quad (7.2)$$

The power level of the interference of all carriers within the OFDM bandwidth  $B$  is then given to:

$$P_{12} = \int_{-\frac{B}{2}}^{+\frac{B}{2}} |E_{12}|^2 df_\Delta, \quad (7.3)$$

which leads to the following equation [60]:

$$\begin{aligned} \frac{P_{12}}{B} &= \hat{E}_1(r_1)^2 + \hat{E}_2(r_2)^2 + \\ &+ 2\hat{E}_1(r_1)\hat{E}_2(r_2) \cos\left(2\pi\frac{f_0}{c_0}(r_2 - r_1)\right) \cdot \\ &\cdot \text{si}\left(\pi\frac{B}{c_0}(r_2 - r_1)\right) \end{aligned} \quad (7.4)$$

In Figure 7.2 the sum power level of the two signals is plotted together with the power level of signals from the separate transmitters, assuming free space loss ( $\hat{E}(r) \sim 1/r$ ).

The DRM+ signal bandwidth of 96 kHz,  $f_0 = 100$  MHz and a distance of 10 km between the transmitters was used for the calculation. TX1 is located at 0 m on the x-axis, TX2 at 10000 m, as the power level is symmetrical, the plot only shows the part between 0 and 5000 m.

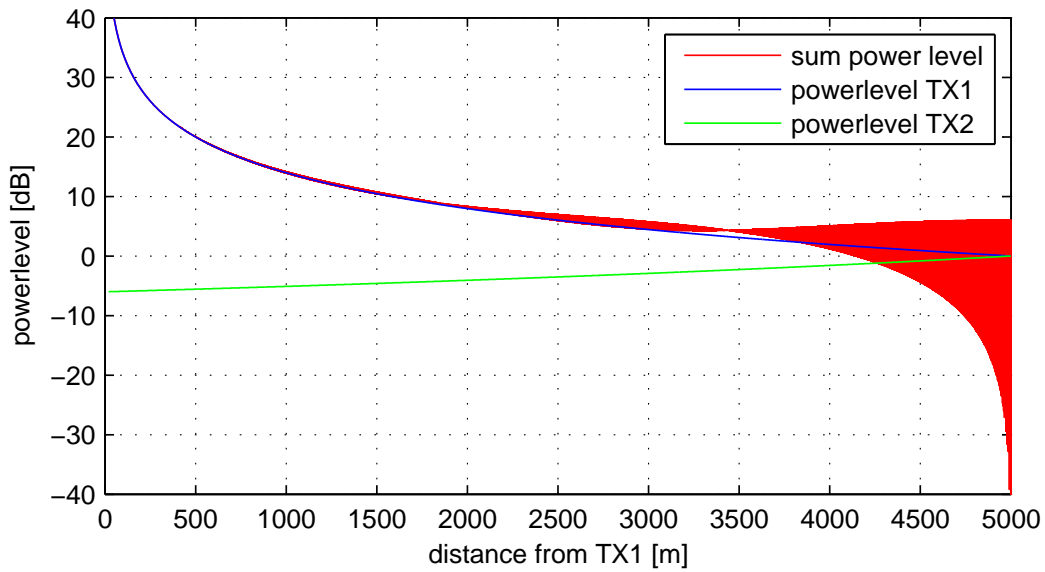


**Figure 7.2:** Sum power level in a perfectly synchronized SFN

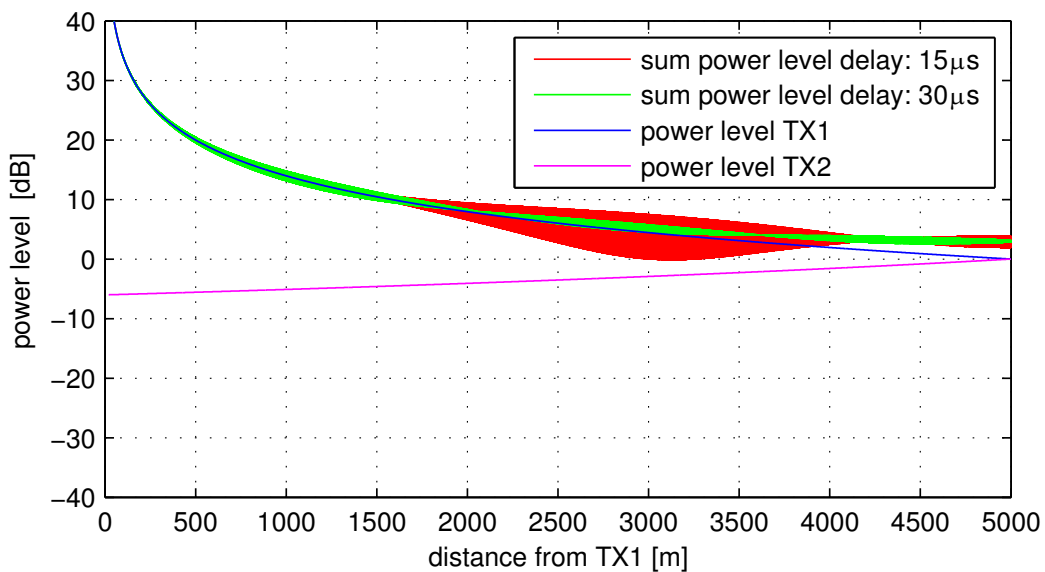


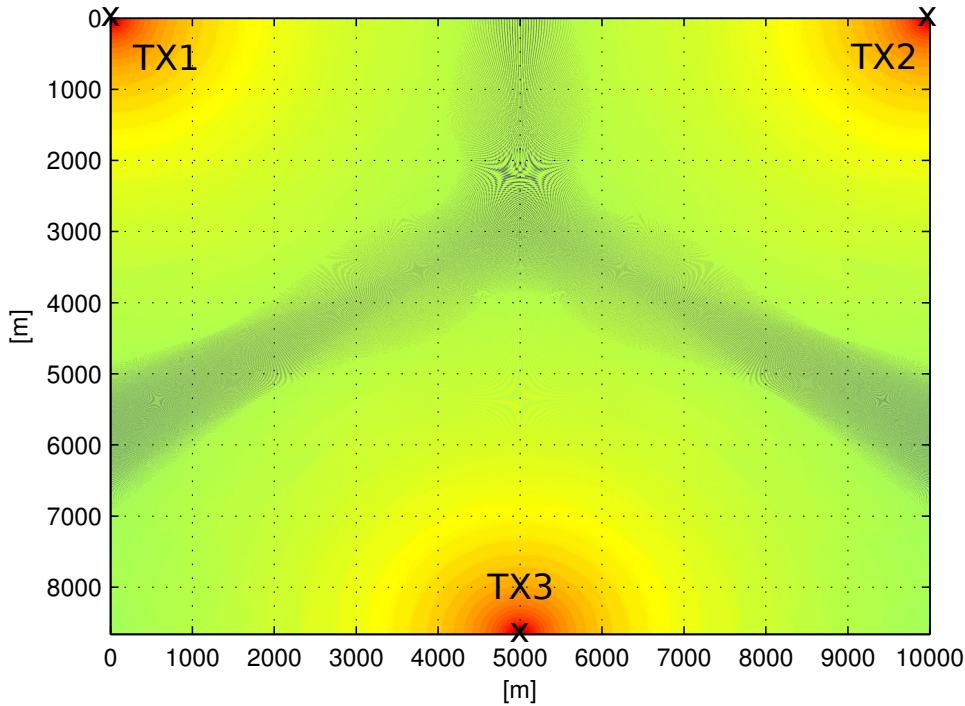
**Figure 7.3:** Sum power level in a SFN with different delays added to TX1

It shows clearly that additive interferences as well as deep fades up to -40 dB will occur in the middle between the two transmitters at a distance of around 5000 m from TX1 and TX2. Here equal power levels from both transmitters can be expected and the signals are arriving nearly simultaneously. As the coherence bandwidth is proportional to the reciprocal of the delay in the channel, it can become wider than the signal bandwidth and result in frequency flat fading. This occurs at distances in the range of half a wavelength. Adding a delay at TX1, the region of simultaneous arrival of the signals is shifted to the delayed TX. Here the power levels of both transmitters are not equal any more and as a result the fading is not as distinctive as shown in Figure 7.3 for delays of 15  $\mu\text{s}$  and 30  $\mu\text{s}$ .

Adding the E-field of a third transmitter to (7.2), the sum power level can be calculated as:

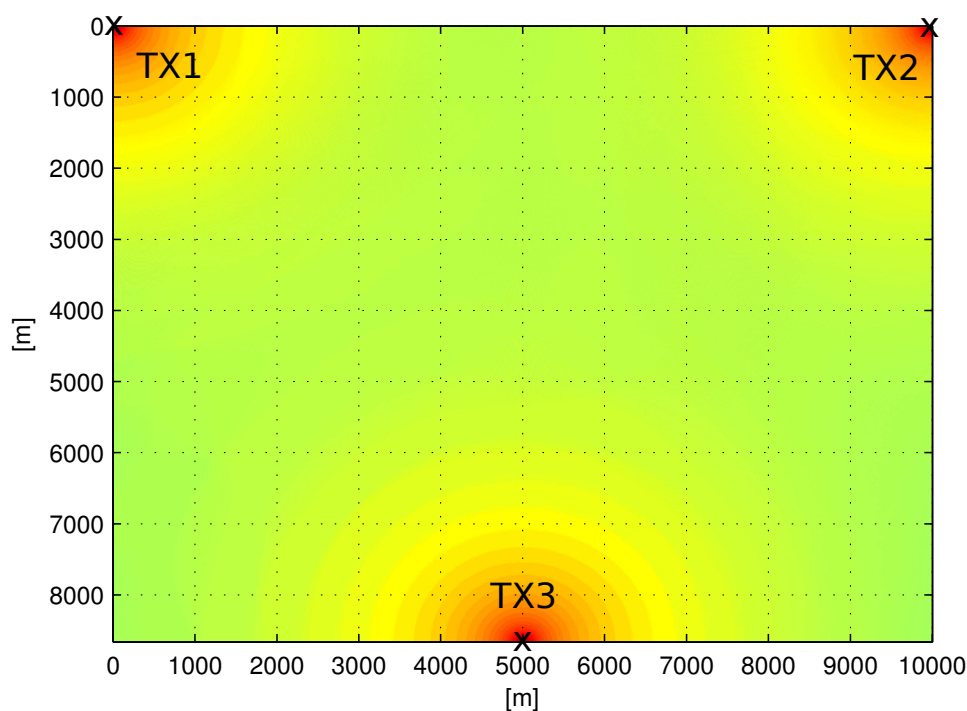
$$\begin{aligned} \frac{P_{123}}{B} &\sim \hat{E}_1(r_1)^2 + \hat{E}_2(r_2)^2 + \hat{E}_3(r_3)^2 + \\ &+ 2\hat{E}_1(r_1)\hat{E}_2(r_2) \cos\left(2\pi\frac{f_0}{c_0}(r_2 - r_1)\right) \cdot \text{si}\left(\pi\frac{B}{c_0}(r_2 - r_1)\right) + \\ &+ 2\hat{E}_2(r_2)\hat{E}_3(r_3) \cos\left(2\pi\frac{f_0}{c_0}(r_3 - r_2)\right) \cdot \text{si}\left(\pi\frac{B}{c_0}(r_3 - r_2)\right) + \\ &+ 2\hat{E}_1(r_1)\hat{E}_3(r_3) \cos\left(2\pi\frac{f_0}{c_0}(r_3 - r_1)\right) \cdot \text{si}\left(\pi\frac{B}{c_0}(r_3 - r_1)\right) \end{aligned} \quad (7.5)$$

Figure 7.4 shows the sum power level of a three transmitter setup with a distance of 10 km between each TX without any added delay. The TX are located at  $[0, 0]$  (TX1),  $[10000, 0]$  (TX2) and  $[5000, \sqrt{3}/2 \cdot 10000]$  (TX3). From red to green the power level decreases. The dark blue moiré pattern between the three transmitters shows fades of more than 6 dB compared to the mean power level.



**Figure 7.4:** Sum power level in a 3 TX SFN, regions with an attenuation of more than 6 dB compared to the mean power level are marked dark blue

In Figure 7.5 the sum power level of the three TX setup with a delay of  $15 \mu\text{s}$  added to TX1 and  $30 \mu\text{s}$  added to TX2 is shown. The moiré pattern is still present due to the interferences between the signals but the deep fades (dark blue) can be prevented with the delays.



**Figure 7.5:** Sum power level in a 3 TX SFN with a delay of  $15\ \mu\text{s}$  added to TX1 and  $30\ \mu\text{s}$  added to TX2

Further evaluations with different delays showed that with smaller delays, the areas of the fading pattern widens. Higher delays are also not recommended, because the delays have to be subtracted from the guard interval resulting in less robustness against multipath propagation and restricting the maximum distance between the transmitters.

Other possibilities to prevent flat fading are different power levels at the transmitters or directional antennas as already described in Chapter 6.

## 7.2 A Single Frequency Network Field Trial

A field test was set up in 2011 to test the SFN setup and especially the behaviour in the overlapping area. To compare the reception in the overlapping area, measurements were conducted without delay and with a delay added to one transmitter. Additionally some measurements were conducted with only one transmitter switched on. All test results were gathered in urban area with low velocity as well as on a motorway and in mixed surrounding.

The very detailed results of this trial have also been submitted to the ITU (see [61]). This Section follows up the main results of the trial and gives examples on how the measurements were conducted and the results obtained.



### 7.2.1 Hardware Setup

The transmitter setup for the SFN test has already been described in Section 6.4.1. The difference to the transmitter diversity system is that two GPS synchronized modulators have been used due to the distant transmitter locations. A block diagram of the setup is given in Figure 7.6.

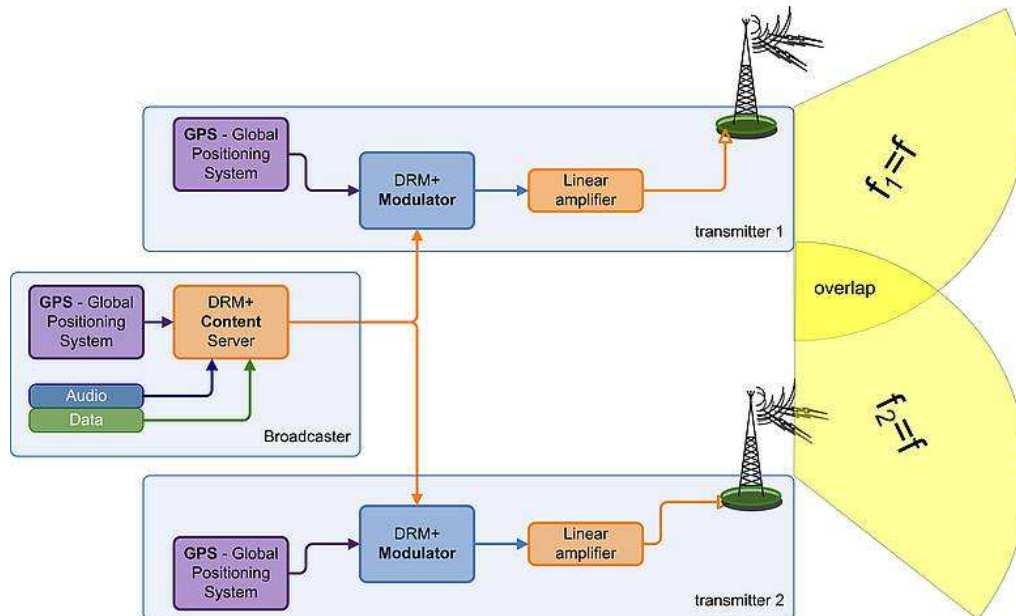


**Figure 7.6:** Block diagram of the Single Frequency Network transmitter setup

One transmitter (TX1) was located at the University of Hannover at a height of 70 m above ground, the other transmitter (TX2) at the headquarters of the Trade Fair Hannover at a height of 100 m above ground) at a distance of 9.2 km. The transmission frequency was 95.2 MHz. For the measurements a robust 4-QAM modulation with protection level 1 (49.7 kbps) was chosen.

Some test measurements were conducted to look for reasonable places and a proper power level. In order to get some errors to compare, the transmitter power was set to 1 W at each transmitter in the SFN mode and 2 W in the single transmitter mode.

### 7.2.2 Field Strength Prediction and Measurement Locations Overview

A field strength prediction was calculated with the free radio propagation simulation program 'Radio Mobile'. 'Radio Mobile' is based on the ITS (Longley-Rice) propagation model. The program uses topographic data (SRTM data from the Space Shuttle Radar Terrain Mapping Mission), but no morphology (buildings, woods, etc.).

The prediction was conducted with 1 W power at each transmitter. In the map in Figure

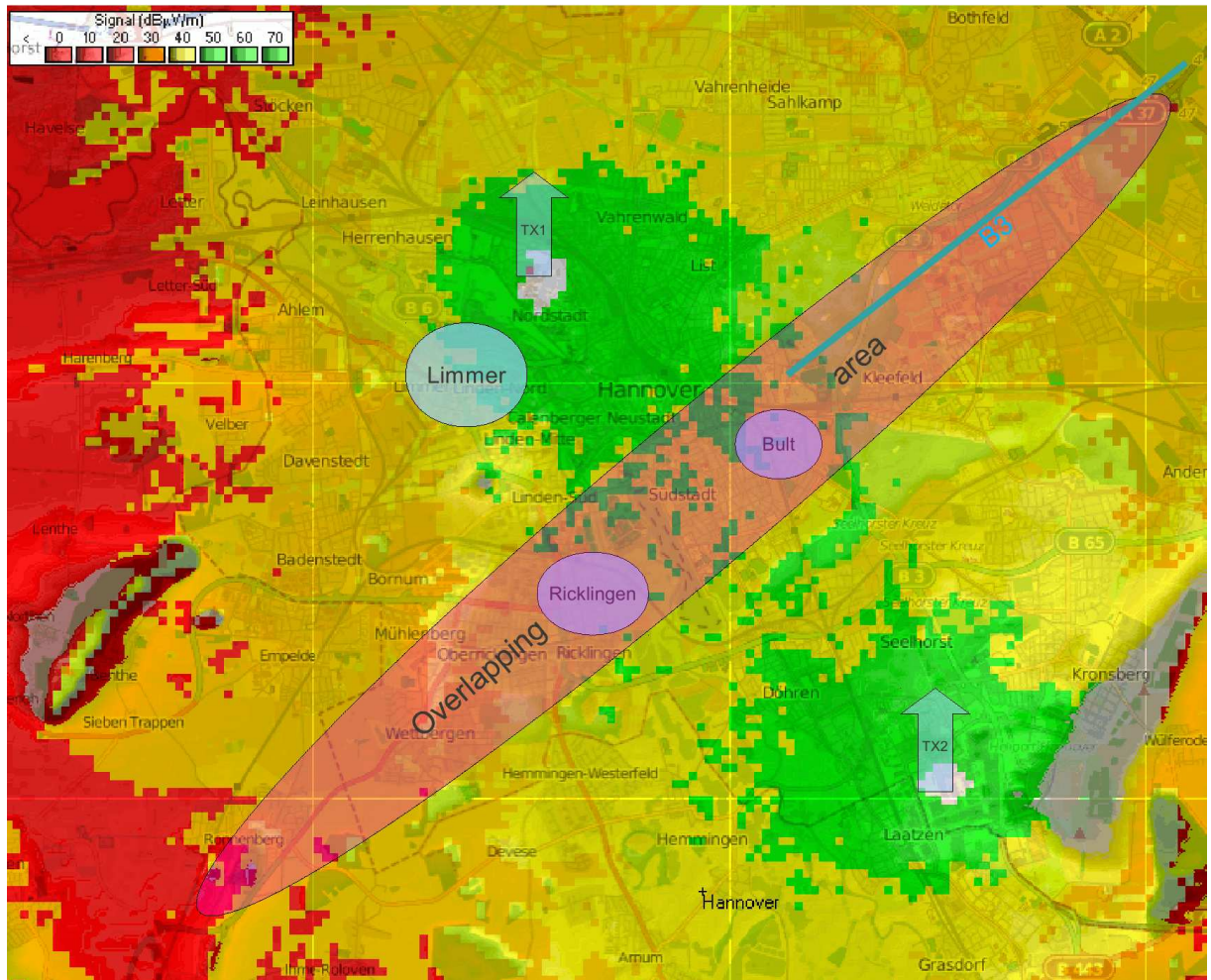


**Figure 7.7:** Field strength prediction and measurement locations (Map data (c) OpenStreetMap and contributors, CC-BY-SA)

7.7 the different measurement locations are marked. One route was chosen on a city highway ('B3') to perform tests with high speed (approx. 100 km/h). Two routes in urban area in the overlapping area were chosen ('Bult' and 'Ricklingen'). Here the trial was conducted with low speed (approx. 10 km/h) to analyse the flat fading that can be caused in the overlapping area by interferences.

For comparison, tests with and without delay have been conducted. Additionally one route outside the overlapping area in mixed environment (city highway/urban) was measured ('Limmer') with velocities of 50-70 km/h.

### 7.2.3 Measurement of the Coverage Area

First measurements of the coverage area were conducted to test the setup. Figure 7.8 shows the audio errors with the SFN setup. TX2 (TX Messe) was delayed by 6 samples (approx. 31  $\mu$ s). With only 1 W at each transmitter, reception was possible up to a distance of



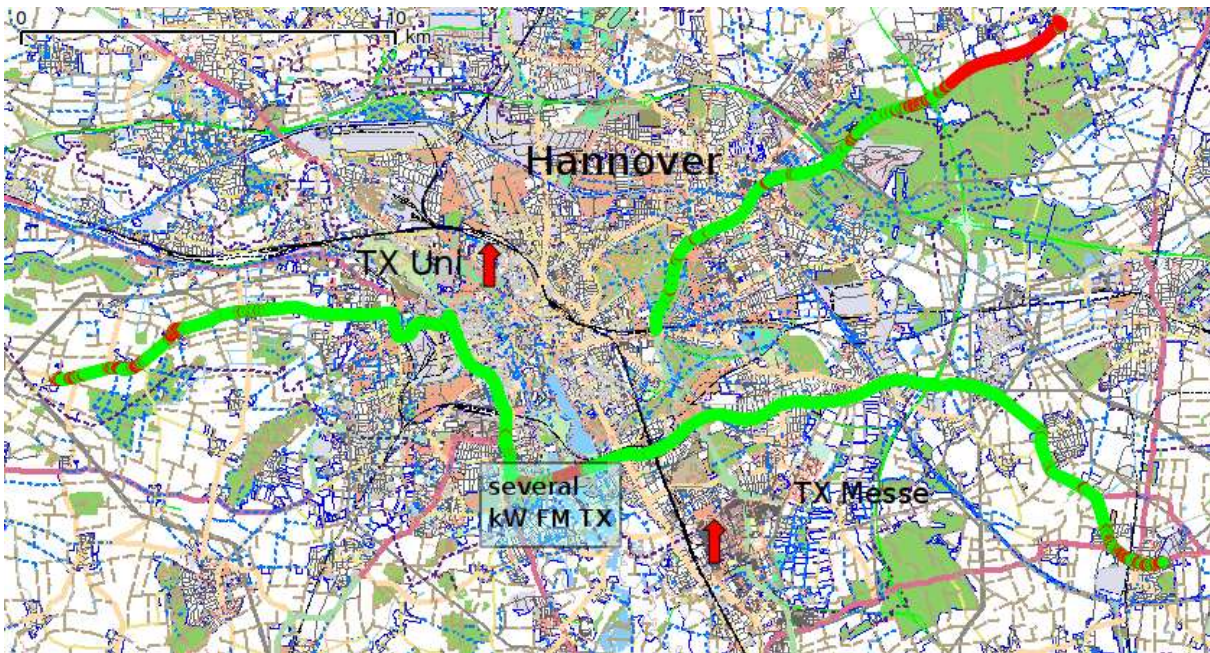


**Figure 7.8:** Measurement of the coverage area (red: one or more audio errors, green, no audio error, Map data (c) OpenStreetMap and contributors, CC-BY- SA)

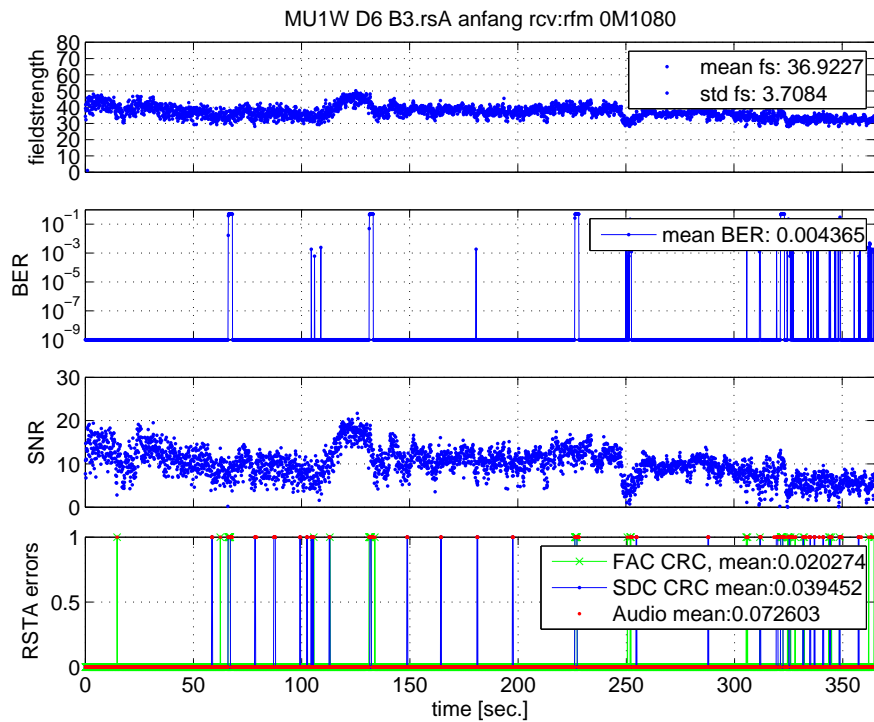
around 10 km from the point equidistant from the two transmitters. At one location an FM transmission site with several kW transmission power on different frequencies right beside the street causes disturbances to reception due to an overload of the receiver front end. Comparing this measurement with measurements conducted with only one transmitter with 2 W, an extension of the coverage area could be achieved.

### 7.2.4 High Velocity Measurements

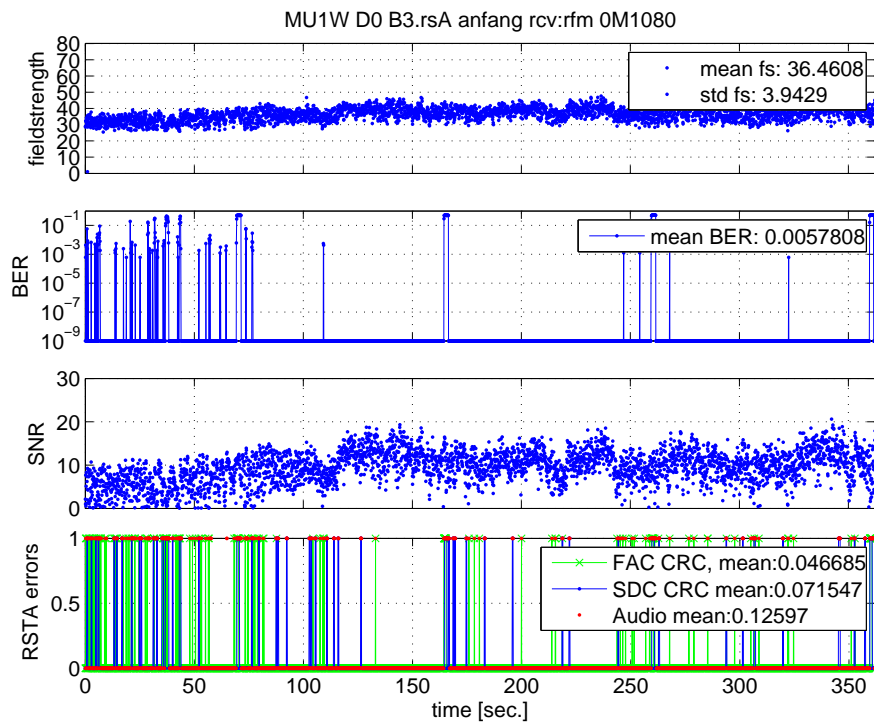
As the route to the north-east (B3) lies in the overlapping area, the reception with and without delay was compared.

Figure 7.9 shows the measurement results with a delay of 6 samples ( $31 \mu\text{s}$ ) added to TX1. The reception parameters field strength, Bit Error Rate (BER), Signal-to-Noise Ratio (SNR), the mean FAC (Fast Access Channel) error rate, the mean SDC (Service Description Channel) error rate and the mean audio error rate are plotted against the time.

The same route in the other direction was measured without delay. In Figure 7.10 shows the measurement results of this trial. As the B3 lies mostly in the overlapping area, as expected the standard deviation and the errors increase without added delay. An overview of the measurement results is given in Table 7.1.



**Figure 7.9:** High velocity measurement in the overlapping area of the SFN with a delay of 31  $\mu$ s added to TX1



**Figure 7.10:** High velocity measurement in the overlapping area of the SFN without delay

### 7.2.5 Low Velocity Urban Measurements

Measurements on two different routes have been conducted in urban areas with low speed. Both places are located within the overlapping area, thus the SFN mode was tested with and without delay to test the effect of fading in the overlapping area. The measurements were conducted, driving slowly (approx. 10 km/h) by car, the results are given in Table 7.1.

The results in 'Bult' show an enhancement of reception quality for the SFN mode with a delay of 6 samples compared to the single transmitter modes. Besides the BER and audio error rate, also the standard deviation decreases significantly. The last measurement was conducted in the SFN mode without added delay. Here the reception quality decreases compared to the SFN mode with delay. The standard deviation is higher, which could indicate more flat fading.

**Table 7.1:** Measurement results of the SFN trial

Location/ Mode	Median field strength [dB $\mu$ ]	Standard deviation of the field strength	Mean BER	Mean audio error rate
<b>City highway ('B3'), high velocity test in overlapping area</b>				
with delay	36.9	3.7	0.0043	0.073
no delay	36.5	3.9	0.0057	0.126
<b>Urban area ('Bult'), low velocity test in overlapping area</b>				
TX1 only	40.3	5.7	0.0063	0.103
TX2 only	39.5	4.8	0.0017	0.057
SFN delay	40.1	3.4	0.0002	0.029
SFN no delay	37.9	4.9	0.0025	0.059
<b>Urban area ('Ricklingen'), low velocity test in overlapping area</b>				
TX1 only	35.3	4.9	0.021	0.233
TX2 only	42.9	5.4	0.0005	0.224
SFN delay	40.9	4.3	$5 \cdot 10^{-6}$	0.011
SFN no delay	38.6	4.9	0.004	0.072
<b>Mixed surrounding ('Limmer'), outside overlapping area</b>				
TX1 only	34.26	7.9	0.0023	0.056
TX2 only	37.15	9.0	0.0077	0.14
SFN delay	36.5	8.2	0.0004	0.007

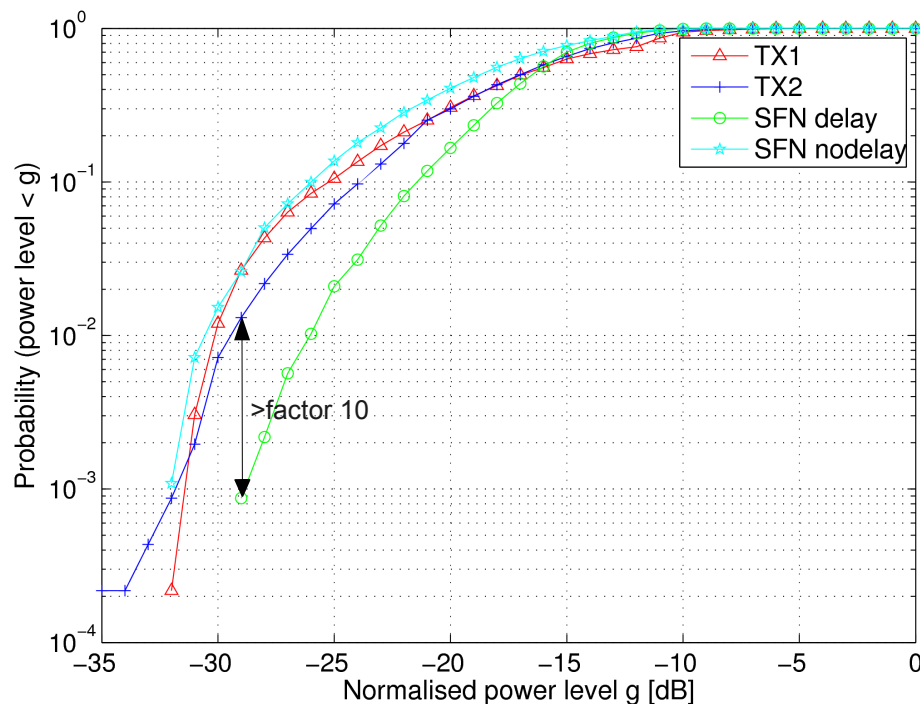


**Figure 7.11:** Culmulative distribution function in 'Bult'

As the median field strength levels from each transmitter at the location 'Bult' are almost equal, a cumulative distribution function (CDF) of the field strength levels was calculated as seen in in Figure 7.11.

The cumulative distribution function gives the probability that the power level is below a certain value  $g$ . Figure 7.11 clearly shows, that while the CDF of the SFN without delay is even worse than the CDF of the single transmitter modes, the CDF of the SFN with delay shows a lower probability of deep fades by a factor of approx. 10 for the power level of around -30 dB.

At the measurement location 'Ricklingen' some more power of TX2 arrived, as the antenna at the university is quite directional and the location is not located in the main beam. The results are also given in Table 7.1. Due to the difference in the median field strength of over 7 dB in the single transmitter modes, the SFN modes result in a lower median field strength than with only TX2. However the SFN mode with delay still enhances the reception quality. With no delay implemented in the SFN mode, the standard deviation is getting higher and therefore reception quality is getting worse here compared to the SFN mode with delay.

### 7.2.6 Measurements in Mixed Surrounding

On the route in 'Limmer' measurements have been conducted with only TX1 and only TX2 and in the SFN mode with delay.

The results in Table 7.1 clearly show the enhancement of reception quality in the SFN mode. Although the median reception field strength was not equal from both transmitters, Bit Error Rate (BER) and audio error rate decrease with both transmitters switched on at half power. Due to the different median field strength the standard deviation of the SFN mode is in between the ones with one transmitter. However the results indicate that the second transmitter can fill deep fades which occur in the propagation path from one side.

### **7.3 Conclusions on a DRM+ Single Frequency Network**

The results of the evaluations on propagation in a Single Frequency Network and of the field trials show, that due to the small bandwidth of the DRM+ system, care has to be taken in the planning to avoid flat fading in the overlapping area, when transmitting with the same power from each TX. Adding a different delay to transmitters located side-by-side is one solution to overcome the flat fading. A delay  $>15 \mu\text{s}$  is necessary for the DRM+ signal bandwidth of 100 kHz to avoid flat fading.

In the field trial conducted with two TX, the reception performance in the SFN have been enhanced by adding a delay of  $31 \mu\text{s}$  to one of the transmitters. The probability of deep fades became smaller by a factor of approx. 10. Comparing the reception of the SFN with delay, with the results of an single transmitter setup with equal power in different environments, the SFN enhanced the reception performance significantly.



## 8 Receiver Diversity Techniques

Besides the usage of diversity techniques at the transmitter, receiver diversity techniques can provide a significant enhancement of the reception quality. The signals from several antennas at the receiver are combined and contribute to the performance.

Different diversity techniques are already being used to enhance the performance in OFDM based systems as IEEE 802.11, DAB or DVB-T. An overview of different receiver and transmitter diversity techniques is given in [62]. [63] shows the results of diversity reception for the Digital Audio Broadcasting system.

This chapter evaluates the possibilities and parameters of a receiver diversity system for DRM+. Simulations have been conducted to evaluate the expected gains and parameters of different receiver diversity and combining techniques in different environments. Then a field trial has been prepared. The possibilities of setting up the antennas on the measurement vehicles have been evaluated and a field trial has been conducted with a Selection Combining (SC) as well as a Maximum Ratio Combining (MRC) receiver diversity setup. A description of the system with receiver diversity is also given in [64].

### 8.1 Combining Methods

There are different possibilities to combine the incoming signals of the antennas in a receiver diversity system. The following methods have been evaluated in terms of diversity gain and performance cost.

**Switched Combining (SWC):** With SWC always one reception branch is decoded. If this branch falls below a given SNR threshold, the receiver switches to the other branch. This has the advantage that only one branch has to be decoded, which reduces computational needs. However, taking a closer look at the implementation for the DRM+ system shows, that needed synchronisation processes such as frequency and frame synchronisation are done with values gathered from the previous frames. Switching on a frame basis is not possible without doing this synchronisation also in the second branch.

This method was analysed in terms of the optimal threshold and the optimal timing to analyse the SNR. Figure 8.1 shows the simulation results of a 16-QAM mode with code rate 0.5 in an urban channel with a receiver velocity of 60 km/h. To evaluate the impact of different SNR-thresholds on the performance, simulations with different SNR-thresholds (TH) have been conducted. It can be seen that the optimal threshold is at round 12 dB for the considered mode. For a higher SNR-threshold the performance for lower SNR

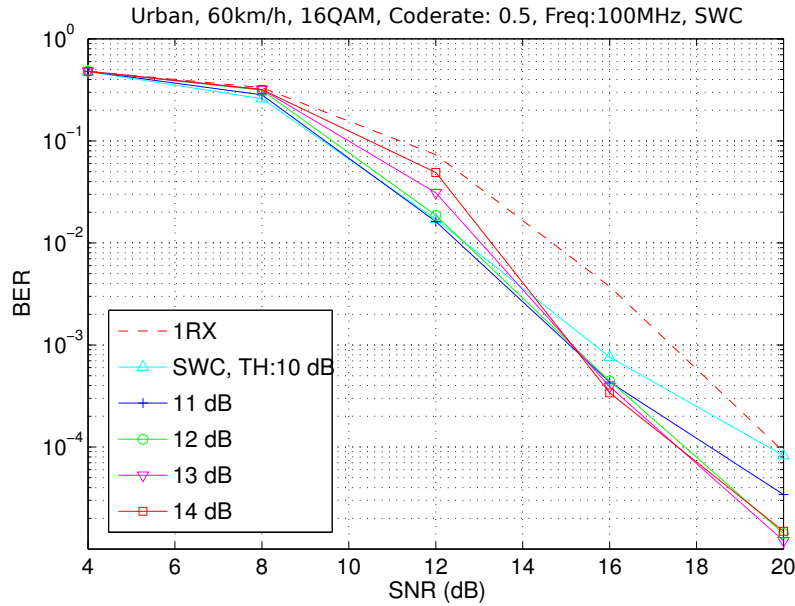


**Figure 8.1:** Impact of different SNR-thresholds on the performance of Switched Combining receiver diversity

decreases, for a lower threshold the performance at higher SNR decreases. The 12 dB SNR complies with the minimal necessary SNR in a static AWGN-channel for a BER smaller than  $10^{-4}$  in the simulation system.

**Selection Combining (SC):** The SNR of both branches is estimated and the branch with higher SNR is decoded. In theory two branches have to be decoded up to the time synchronisation, as the SNR estimation is done via the time correlation/synchronisation as described in [28]. Here the statement about frequency and frame synchronisation from SWC is also valid and therefore synchronisation up to a frame level has to be performed.

**Maximum Ratio Combining (MRC):** The gain of each branch is made proportional to the RMS signal level and inversely proportional to the mean square noise level in that branch. For this combining method the exact knowledge of the channel response of each branch is necessary. Two decoding stages up to the channel estimation have to be implemented. To reduce the computational complexity and power consumption of the MRC scheme, different methods are given for example in [65].

**Equal Gain Combining (EGC):** Two signals are combined with equal gain. This offers a very simple implementation with good performance when used in conjunction with differential detection. As DRM+ uses QAM, phases have to be corrected before combining. This also needs two decoding stages up to the channel estimation.

**Simulations** Simulations have been conducted in different channels and different velocities with 16-QAM modulation at a code rate of 0.5. The channels were implemented as tapped delay filters with the properties of the 'urban' and 'rural' channel as described in Section 3.3.2 and a velocity of 10, 60 and 150 km/h. The threshold for SWC has been

set to an SNR of 12 dB as this has shown the best results. For the simulations fully uncorrelated transmission paths are assumed.

Figure 8.2 shows the results of a very slow urban channel at a receiver velocity of 10 km/h.

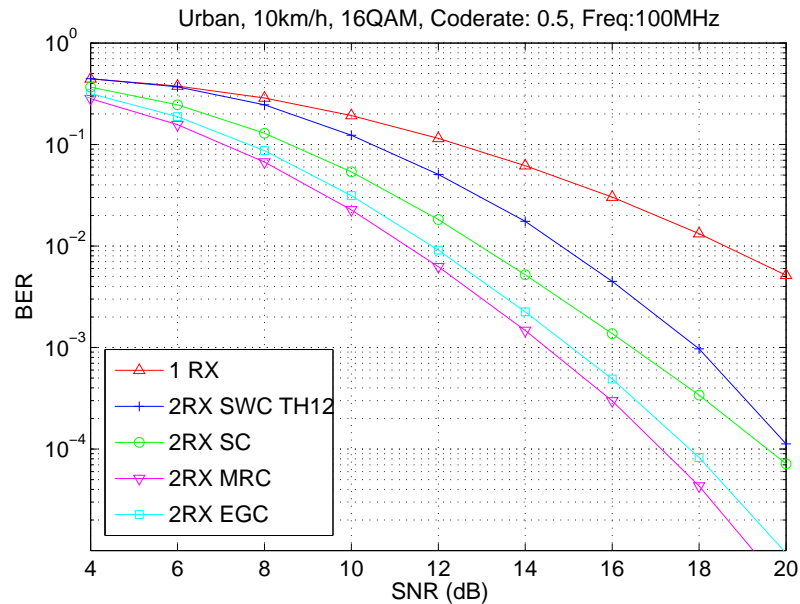


Figure 8.2: Simulation results for a very slow urban channel

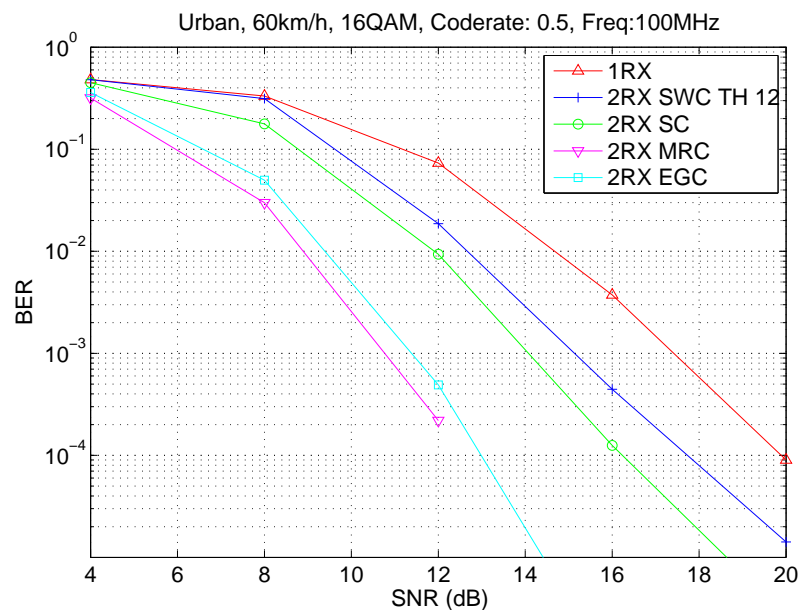
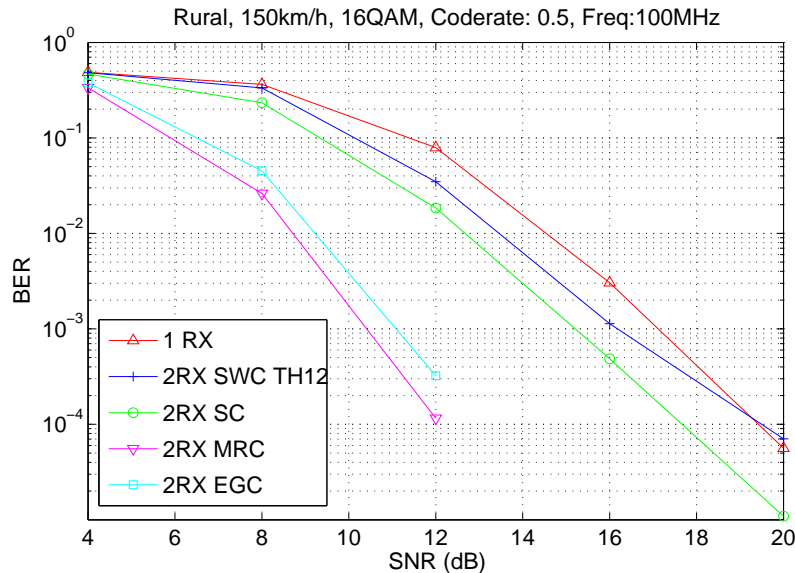


Figure 8.3: Simulation results for an urban channel

As the slow speed of the receiver results in slow and flat fading and the cell interleaver can only work properly up to a duration of 600 ms, this results in high error rates. Receiver diversity enhances the performance up to 8 dB with MRC, slightly less with EGC, SC performs somewhere in between and SWC has a gain of around 4 dB.

Higher receiver velocities result in better performance, as the interleaver can work properly. The results in an urban channel with 60 km/h receiver velocity can be seen in Figure 8.3. The diversity gain in this performance simulation in an urban channel at a velocity of 60 km/h for MRC is also approx. 8 dB, EGC slightly less, SC around 3 dB and SWC results in a gain of only approx. 2 dB.



**Figure 8.4:** Simulation results for a rural channel

Figure 8.4 shows the simulation results for the rural channel. At a receiver velocity of 150 km/h the gain of SC and SWC compared to the 1RX mode is very low. As a consequence of the high velocity, the channel variation within one frame is significant. The evaluation of the SNR is done only at the beginning of a frame, which is not enough to follow the variation of this channel. Theoretically this could be done more often, resulting in a higher diversity gain for SC and SWC at high velocities, but the implementation effort of the channel estimation would be very high, as this is based on a frame level. The gain of MRC is again around 8 dB, slightly less with EGC.

As SC performs better than SWC and the implementation effort is comparable due to the recursive frequency and frame synchronisation, it has been used for the measurements. As a second system MRC was used for the measurements. It performs better than EGC with the same implementation cost and therefore has been chosen.

The results for MRC cannot directly be compared to the results for DAB in [63] and DVB-T in [62] due to different system parameters, code rates and channel properties. But the tendency that the diversity gains with DRM+ are higher than the ones between 4 and 5 dB, depending on the channel, for DAB and approx. 2 dB for DVB-T in the outdoor channel seems reasonable. Those higher values can be explained with the smaller signal bandwidth of 100 kHz compared to DAB with a bandwidth of 1.5 MHz and DVB-T with the simulations conducted with a signal bandwidth of 8 MHz. Due to the smaller bandwidth the DRM+ signal is more affected by frequency flat fading. The receiver di-

versity setup thus is especially interesting for this system as it can help very effectively to overcome this problem.

## 8.2 Antenna Diversity Methods

The antenna diversity methods mostly used are space diversity and polarization diversity. The main purpose of the antenna setup is to get sufficiently uncorrelated input signals with equal mean input levels.

### 8.2.1 Space Diversity

In case of space diversity the two antennas are distributed in space to take advantage of the spacial diversity of the signal levels in a multipath environment. For receiver diversity with horizontal distributed antennas the correlation between the antennas in a Rayleigh fading environment, with the scatterers uniformly distributed around the receiver can be approximated by a Bessel-function [12]:

$$\rho(d) = J_0\left(\frac{2\pi d}{\lambda}\right) \quad (8.1)$$

with the Bessel function of the first kind and zeroth order  $J_0$ , the distance  $d$  between the antennas and the wavelength  $\lambda$ . For restricted angles of arrival the correlation for a given spacing is increasing. In [12] a distance of  $0.5 \lambda$  is given as a reasonable compromise between the available space and the correlation. Figure 8.5 shows the correlation with uniformly distributed scatterers plotted against the distance between the antennas in wavelengths. For distances larger than  $0.5 \lambda$  the correlation is smaller than 0.5.

If the antennas are moved further together the coupling effects between the antennas are becoming significant. On the one hand this reduces the correlation between the antennas [66], on the other hand if the adaption is not changed, this can reduce the efficiency up to a level higher than the diversity gain.

To analyse the behaviour of two antennas on a van, calculations have been conducted with 4NEC2, a free program using the open source Numerical Electromagnetics Code (NEC), an antenna modelling software developed by the Lawrence Livermore Labs in 1981, under contract to the US navy. NEC2 was later released to the public domain. The code is based on the Method-of-Moments solution of the electric-field integral equation for closed, conducting surfaces [67].

Figure 8.6 shows the antenna setup with two monopole antennas, each with a length of  $\lambda/4$  on the model of the van that was used for the measurement. The evaluation then was done by moving the antennas to different positions on the van.

For comparison first one monopole antenna was set to the middle of the van. Figure 8.7 shows on the left side the 3D far field antenna pattern of this setup.  $\Theta$  defines the

angle between the z-axis and the horizontal pattern that is plotted on the right side. The evaluation was done at an angle of  $70^\circ$  to the z-axis, which is visualized as the non-transparent surface within the transparent pattern in the 3D pattern on the left side of Figure 8.7.

The impact of the car structure can clearly be seen. A monopole over infinite perfect ground would be perfectly omnidirectional in the horizontal plane, the pattern in Figure 8.7 shows several lobes. The car structure results in an attenuation of the antenna gain towards the front and back of the car.

Additionally to the pattern the impedance of the antennas was evaluated. Table 8.1 gives an overview of the results.

The 'one antenna in the middle of the van' setup shows an impedance of  $57.5+j2.1$ . Which is a good adaption to the 50 Ohm feed line and the input of the receiver. If the antenna and the feed line do not have matching impedance, some of the energy will be reflected by the receiver and the efficiency of the antenna will be diminished. A common parameter to measure the reflection is the Voltage Standing Wave Ratio (VSWR). The calculation is done in two steps. First the reflection factor  $\Gamma$  is calculated as:

$$\Gamma = \frac{Z_r - Z_0}{Z_r + Z_0} \quad (8.2)$$

With the impedance at the reflection (here the antenna)  $Z_r$  and the characteristic impedance  $Z_0 = 50$ . The VSWR is then calculated as:

$$VSWR = \frac{1 + |\Gamma|}{1 - |\Gamma|} \quad (8.3)$$

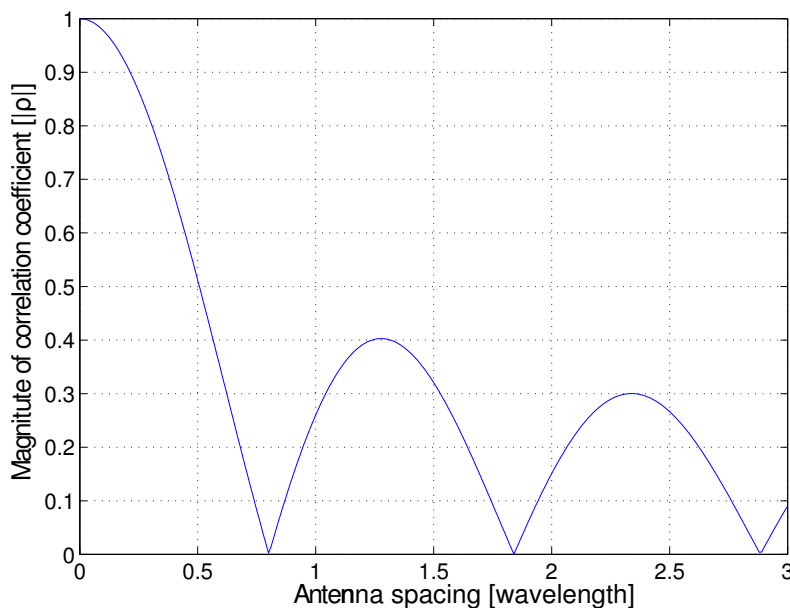


**Figure 8.5:** Correlation between two horizontally spaced antennas in a Rayleigh fading environment



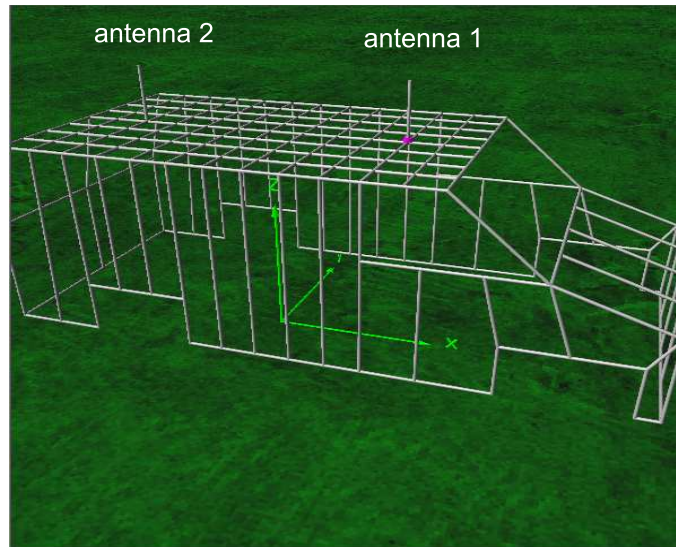


**Figure 8.6:** Antenna setup for the calculation of the antenna pattern

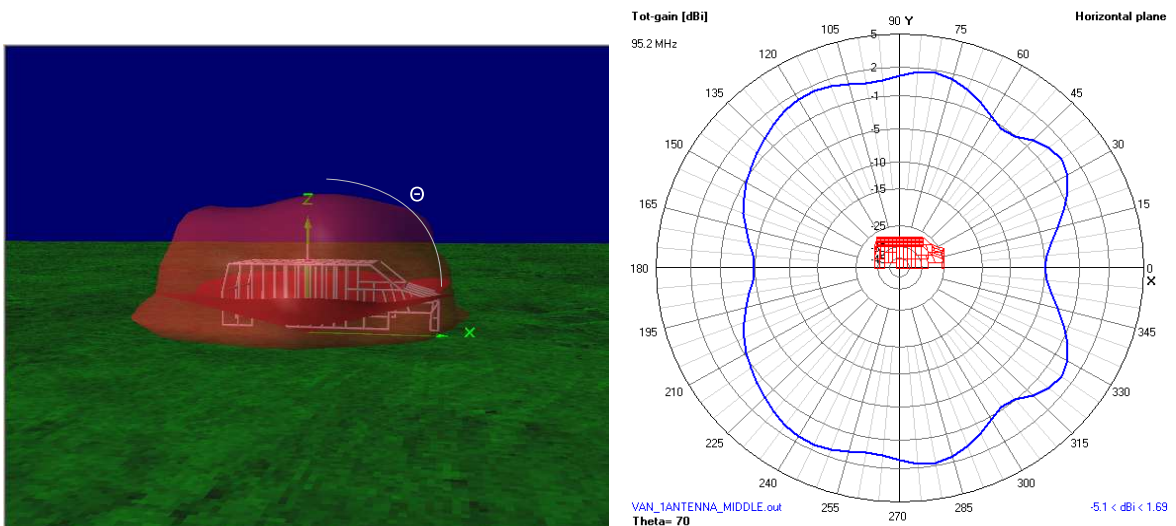


**Figure 8.7:** 3D far field antenna pattern with a one antenna setup

As a next step one antenna was moved to the front of the van until the front edge of the van at 240 cm. Figure 8.8 shows the effect on the antenna pattern, the corresponding colors of the antenna patterns are given in Table 8.1. While moving the antenna more to the front more lobes show up in the antenna pattern. The impedance and VSWR in Table 8.1 are increasing for the locations 80 cm and 240 cm. For 160 cm the impedance is quite good adapted to the  $50 \Omega$  of the feeder.

Figure 8.9 shows the setup and antenna patterns if the antenna is moved towards the back of the van. In this direction the pattern is not affected that much but the impedance is also higher at -80 cm and especially at -240 cm. With a VSWR of 2 the efficiency of the antenna is diminished significantly.

Figure 8.10 shows the setup and pattern with a second antenna added. The antenna in



the front is first located at  $x_1 = 160$  cm, the antenna in the back at  $x_2 = -80$  cm. The antennas are then moved towards the middle of the van. At  $x_1 = 80$  cm,  $x_2 = -80$  cm a notch in the antenna pattern comes up. Moving them further together more notches occur and the VSWR is becoming higher. Taking a closer look at the setup with a distance of around half the wavelength shows that the notch can be reduced by small variations of the distance (see Figure 8.11). The VSWR stays below 1.3.

For the trial the antennas were mounted at a distance of 1.5 m, equally to approx.  $\lambda/2$  between the antennas. This distance offers a good compromise between the correlation, the antenna pattern and the limited space on the roof.

**Table 8.1:** Evaluation of the antenna properties

Location of antenna 1 [cm] (color of pattern)	Location of antenna 2 [cm]	Distance between the antennas [cm/ $\lambda$ ]	Impedance [ $\Omega$ ]	VSWR
One antenna in the middle of the van (Figure 8.7)				
0	-	-	57.5+j2.1	1.15
Moving one antenna to the front of the van (Figure 8.8)				
0 (purple)	-	-	57.5+j2.1	1.15
80 (green)	-	-	79.2+j7.35	1.6
160 (red)	-	-	48.5+j2.4	1.06
240 (blue)	-	-	85.3+j19.9	1.84
Moving one antenna to the back of the van (Figure 8.9)				
0 (purple)	-	-	57.5+2.1j	1.15
-80 (green)	-	-	68.5+j7.2	1.4
-160 (red)	-	-	48.5+j2.4	1.2
-240 (blue)	-	-	99.8+j9.9	2.02
Two antennas (Figure 8.10)				
-160 (brown)	80	240/0.76	59.4+j11.1	1.3
-80 (purple)	80	160/0.51	63.4-j3.9	1.22
-80 (green)	40	120/0.38	70.4+j6.87	1.43
-40 (red)	40	80/0.25	58.1+j25.8	1.64
0 (blue)	40	40/0.13	17.5+j13	3.1

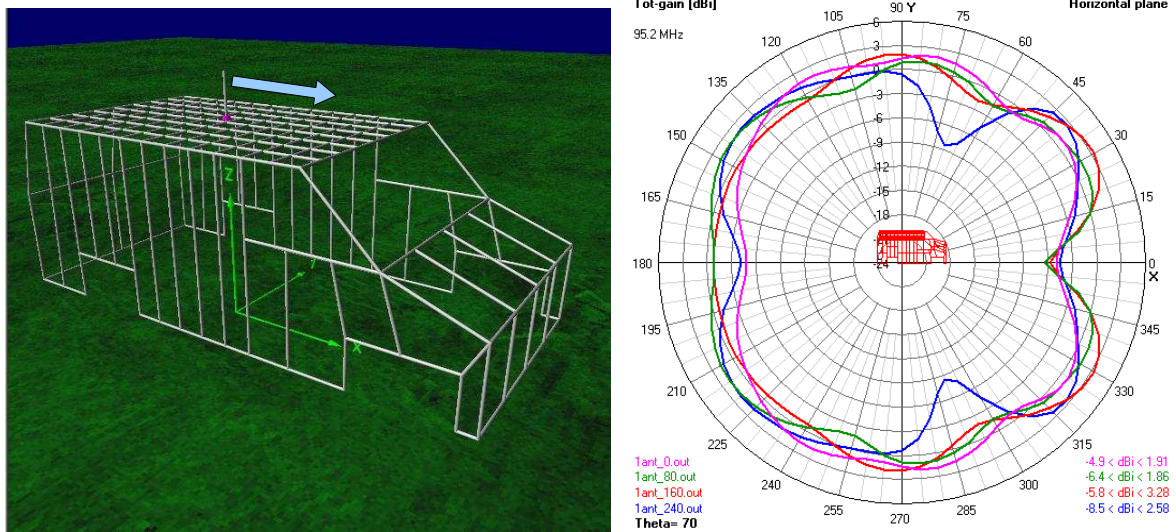


Figure 8.8: Moving one antenna to the front of the van

### 8.2.2 Polarization Diversity

As polarization diversity is known to offer a good diversity gain, evaluations about the implementation possibilities have been conducted. The use of polarization diversity with one antenna in horizontal polarization and one antenna in vertical polarization could be realised with a vertical monopole and a magnetic antenna in horizontal polarization. Anyway as the transmission is only possible in vertical or horizontal polarization a polarization discrimination of 10 dB can be expected as given in [29]. This means that the antenna orthogonal to the transmission polarization will receive a 10 dB lower mean signal strength than the antenna with equal orientation. Therefore one antenna will only have a minor influence on the diversity gain and thus this approach was dropped for the field trial.

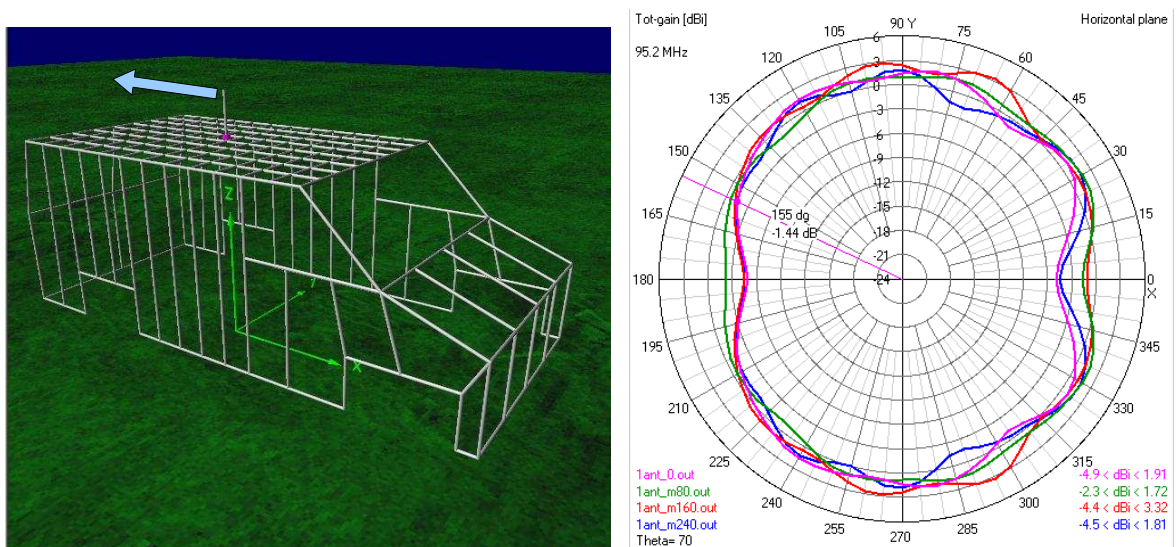


Figure 8.9: Moving one antenna to the back of the van

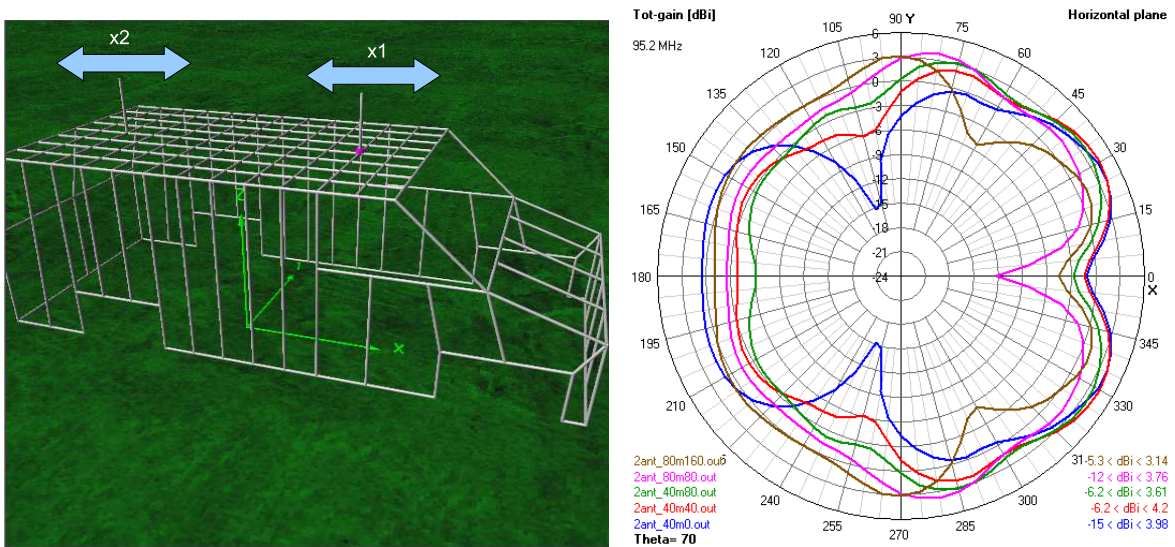


Figure 8.10: Setup with two antennas and different distances in between

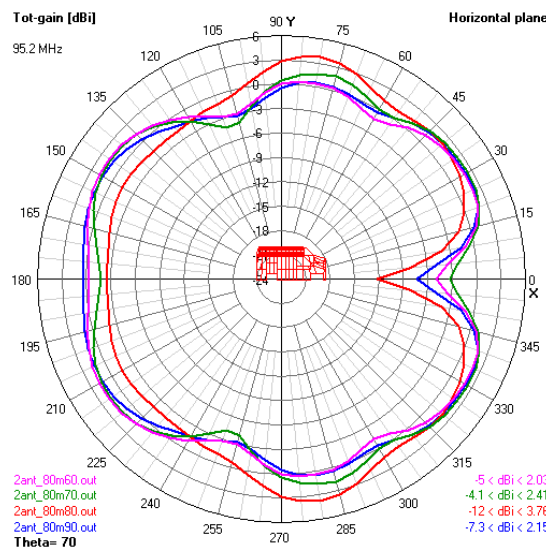


Figure 8.11: Pattern of two antennas at distances from 140 cm to 170 cm

Diagonal polarizations could be created with windscreen antennas. Here the metallic car components have a significant influence on the antenna pattern and adaption, thus this approach was also dropped.

### 8.3 Measurements

For the measurement two vertically polarized magnetic antennas were mounted on a van at a distance of 1.5 m, which equals approx.  $\lambda/2$ . As stated before, the combining was done with Selection Combining (SC) and Maximum Ratio Combining (MRC).

A prototype measurement receiver as shown in Figure 8.12 was developed by RFmondial.



**Figure 8.12:** Diversity DRM+ receiver prototype

It consists of two frontends, each with a 14 bit Analog-Digital converter and a Digital-Down-Converter (DDC). An Automatic Gain Control (AGC) loop was implemented to increase the dynamic range. After down-conversion, the sampled signal is re-sampled to the sample frequency of 192 kHz, needed by the receiver software. The prototype RX sends the IQ-data from both antennas via USB to the software receiver. For the measurements the IQ data of both antennas was stored and the decoding for the different modes was done offline. The software receiver records all kind of reception parameters, see details in [9]. For this trial the mean errors of the cyclic redundancy check (CRC) of the FAC (fast access channel), the mean audio errors and the Bit Error Rate (BER) have been analysed. Additionally in the Selection Combining mode, the switching between the antennas was monitored.

**Table 8.2:** Details of the measurement locations for the receiver diversity trial

Location	Distance to TX	Environment
Bahnhof	2 km	<b>Urban</b> area with 5-6 story buildings
Linden Sued	3.2 km	<b>Urban</b> area with 4-5 story buildings
Ihmezentrum	2 km	<b>Urban</b> area with 5-6 story buildings behind a big block of buildings
Bult	4.4 km	<b>Suburban</b> area with one-family houses

The measurements with DRM+ and receiver diversity were conducted at four urban locations in the city of Hannover. The transmitter was located on the roof of the university building at a height of 70 m above ground. An ERP (Effective Radiated Power) of 3 W was transmitted in vertical polarization at a frequency of 95.2 MHz. Figure 8.13 shows the



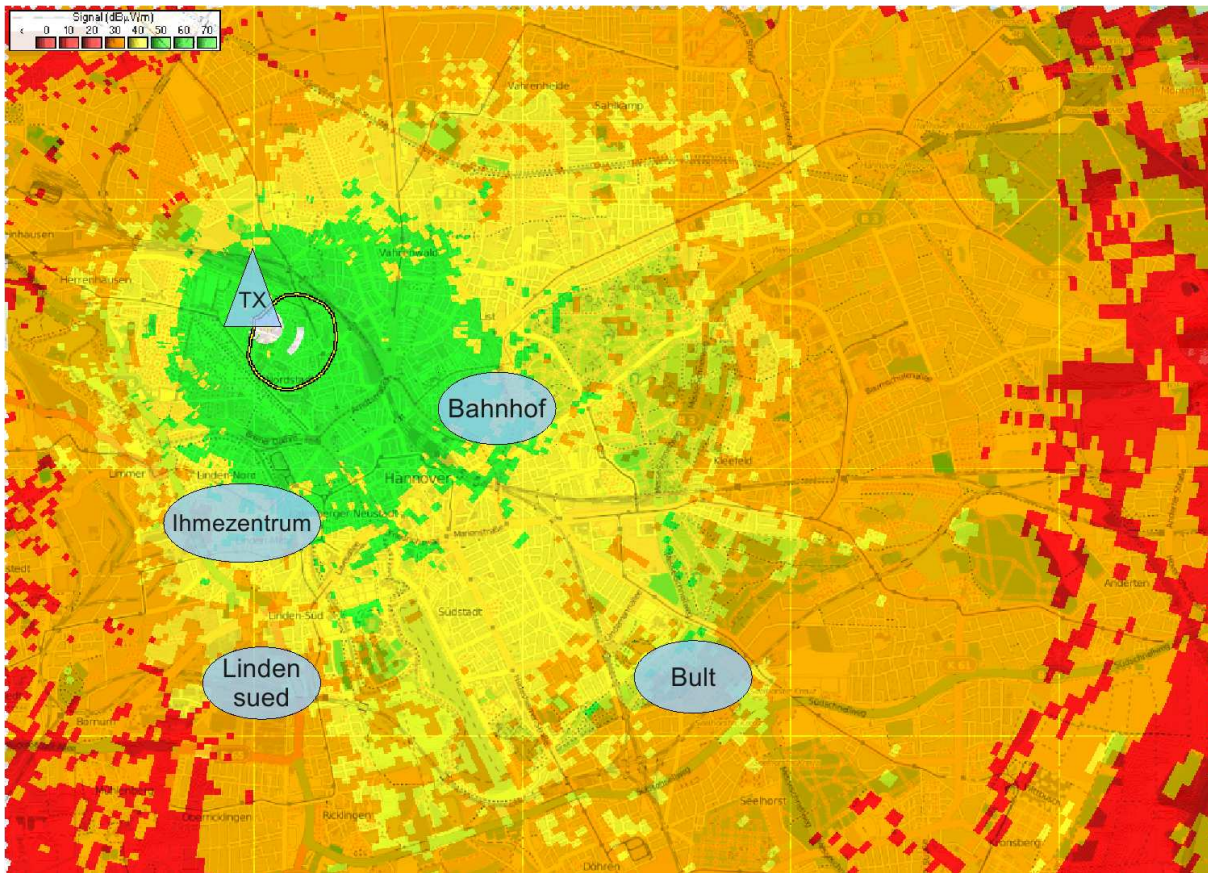


**Figure 8.13:** Measurement locations for the receiver diversity trial

transmitter, the measurement locations and a field strength prediction. Table 8.2 gives an overview about the environment of the locations and the distance to the transmitter.

Some of the locations were chosen to be at the edge of the coverage area in order to have some errors to compare the reception modes. Additionally the possibility of driving very slowly (approx. 10 km/h) without causing too much problems for the traffic was given at these locations. At this slow velocities fading can disturb the reception and the enhancement of reception quality with receiver diversity should become obvious.

Each route had a length of around 3 minutes. For the measurements a robust 4-QAM modulation with protection level 1 (data rate: 49.7 kbps) was chosen.

### Measurement Results

Figures 8.14 to 8.17 show the measurement results from the different antennas and modes at the measurement location 'Linden Sued'. Figures 8.14 shows the results, only decoding the data coming from antenna A. The first row shows the distribution of the bit errors, together with the mean Bit Error Rate (BER). The next row shows the Modulation Error Ratio (MER) together with the Signal to Noise Ratio (SNR). As the MER is calculated after the OFDM demodulation and the SNR in the process of time synchronization, the

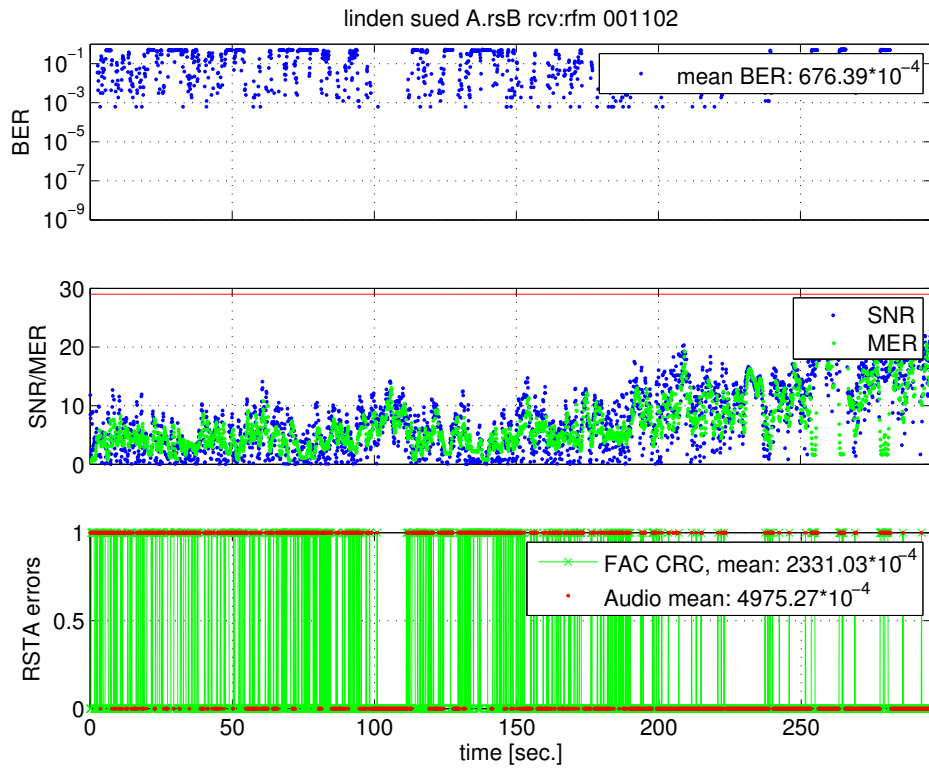


**Figure 8.14:** Measurement results at the location 'Linden Sued' with RX antenna A

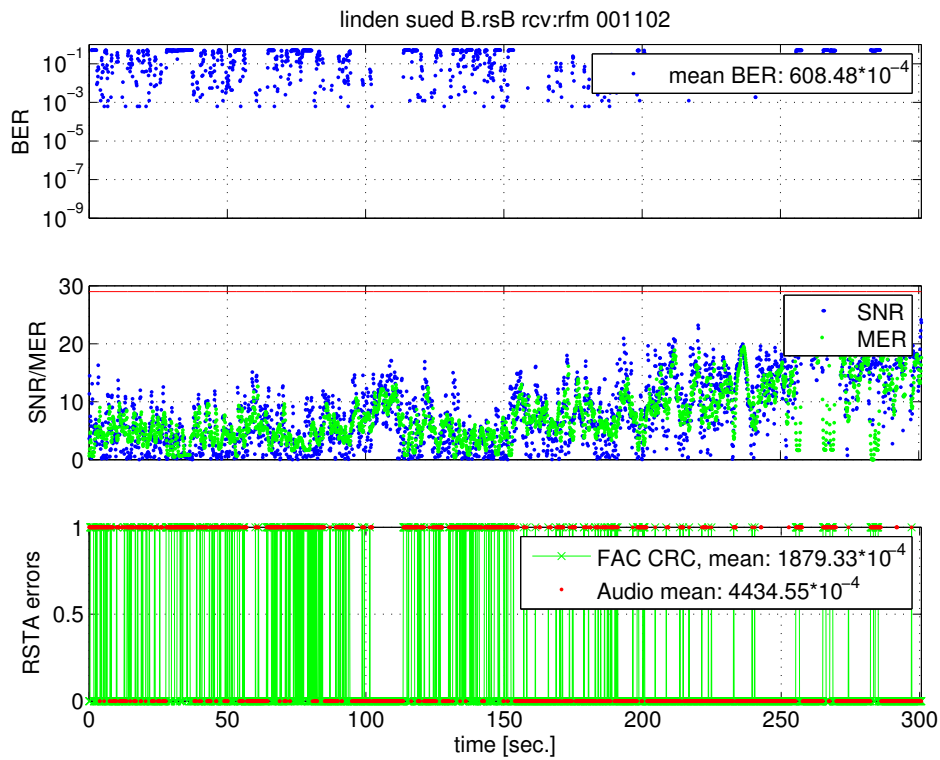


**Figure 8.15:** Measurement results at the location 'Linden Sued' with RX antenna B



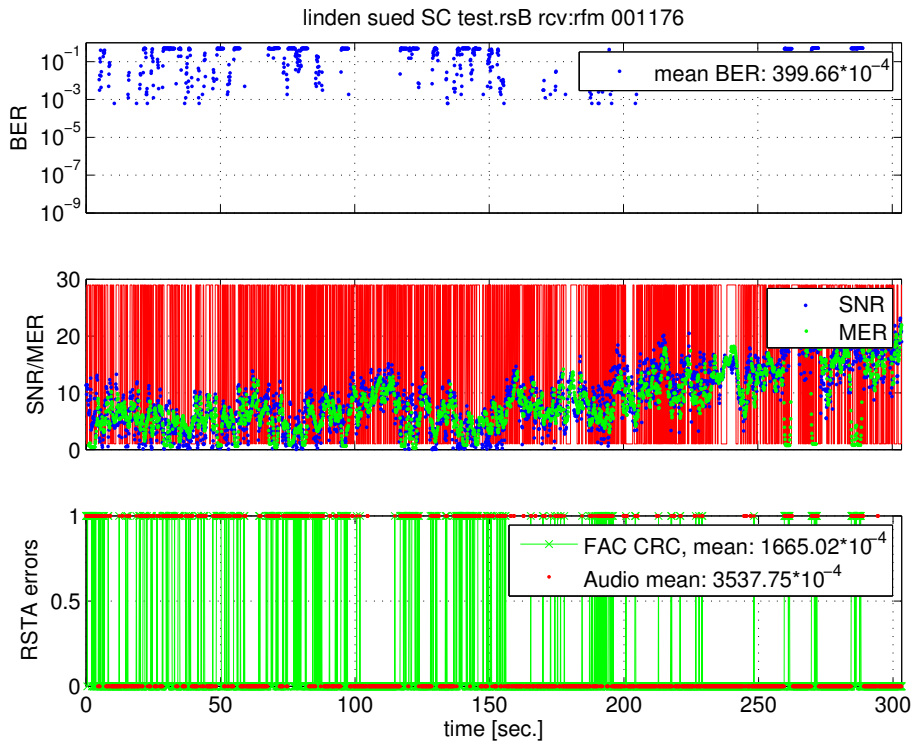


**Figure 8.16:** Measurement results at the location 'Linden Sued' with Selection Combining

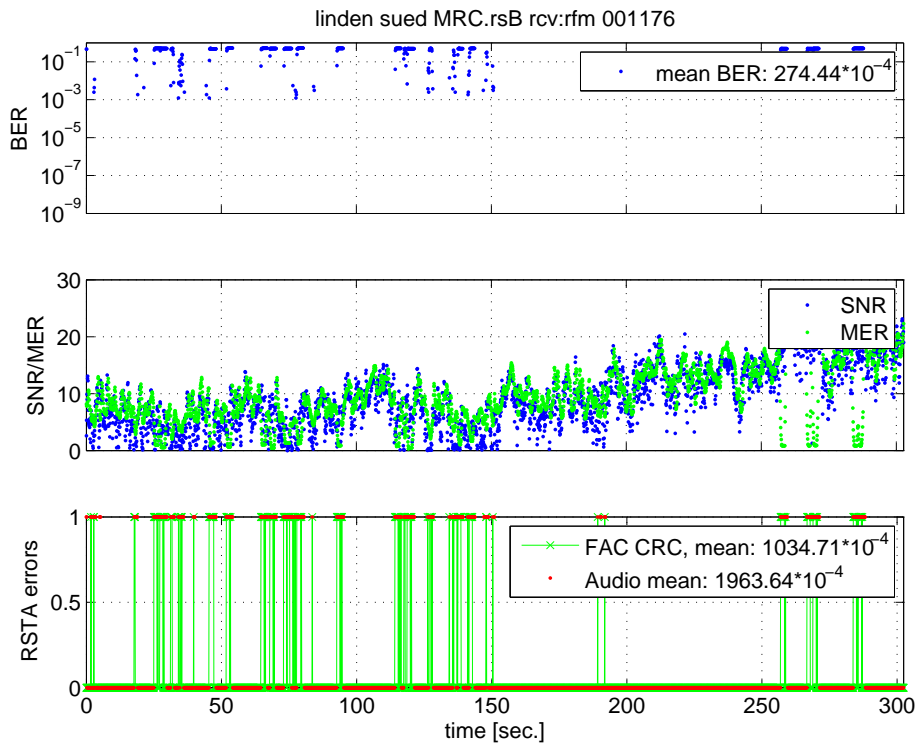


**Figure 8.17:** Measurement results at the location 'Linden Sued' with Maximum Ratio Combining

**Table 8.3:** Measurement results of the receiver diversity trial

Location/ Mode	Mean BER [ $\cdot 10^{-4}$ ]	FAC CRC mean error rate [ $\cdot 10^{-4}$ ]	Mean audio error rate [ $\cdot 10^{-4}$ ]
<b>Urban area ('Bahnhof')</b>			
Antenna A	584	1399	2587
Antenna B	1501	4683	7670
SC	259	1161	2549
MRC	217	993	2434
<b>Urban area ('Linden Sued')</b>			
Antenna A	676	2331	4975
Antenna B	608	1879	4434
SC	399	1665	3537
MRC	274	1034	1963
<b>Urban area ('Ihmezentrum')</b>			
Antenna A	227	1059	2538
Antenna B	173	378	746
SC	91	489	999
MRC	83	360	635
<b>Suburban area ('Bult')</b>			
Antenna A	420	1559	3316
Antenna B	936	3028	5639
SC	334	1405	2852
MRC	283	1435	2841

differences between the MER and SNR can reveal interesting information. E.g. if the receiver is overloaded by a nearby strong FM transmitter or if the transmitting antenna is badly matched to the transmitter and the reflected power is producing intermodulation in the transmitter, the MER goes down significantly while the SNR stays at a higher level.

Figure 8.15 shows the results with only antenna B and Figure 8.16 the results of the Selection Combining mode. The red line within the SNR-MER plot in the SC plot shows the receiver switching the input signal from one antenna to the other. Figure 8.17 shows the results in the MRC mode. Looking at the mean values for example of the BER a significant enhancement can be seen between the single antenna reception ( $420 \cdot 10^{-4}$  with antenna A,  $936 \cdot 10^{-4}$  with antenna B), the SC mode ( $334 \cdot 10^{-4}$ ) and the MRC mode ( $283 \cdot 10^{-4}$ ). The same tendency can be seen with the FAC CRC and the mean audio error

rate.

Table 8.3 provides an overview of the measurement results from the different locations. As expected, in most of the results an enhancement of the reception quality can be seen with SC and even more with MRC compared to the one antenna receiver modes. Exceptions are the FAC CRC error rate and audio error rate at 'Ihmezentrum' which is slightly higher in the SC mode than with only antenna B and the FAC CRC error rate at Bult, which is slightly higher with MRC than with SC. The differences between BER, audio errors and FAC errors are caused by the different length of the evaluated CRCs and bit sequences.

## 8.4 Conclusions on the use of Receiver Diversity Techniques for DRM+

In this Chapter simulations and measurements of a receiver diversity system for DRM+ have been presented. Simulations show that a significant diversity gain can be achieved with receiver diversity. Different combining methods were compared, the best results could be achieved with Maximum Ratio Combining. Another promising method, that needs less computational time is Selection Combining.

The measurement results show that reception could be enhanced in most urban and suburban locations with receiver diversity. Maximum Ratio Combining provides better results at all locations compared to reception with the single RX antenna. With Selection Combining at three out of four locations the reception quality could be enhanced.

As already used in other digital systems, receiver diversity techniques can also be implemented to the DRM+ receivers and offer a way to enhance the reception quality at the receivers end.

## 9 Summary

The DRM+ system offers an interesting new digital radio technology. As it has a very small bandwidth it is especially suitable for small scale local and community radios where a flexible frequency planning with an individual coverage area is necessary.

To analyse the DRM+ system performance and evaluate the functionality, a lot of measurements have been conducted in Hannover and in other parts of the world. The measurement results of this thesis show the minimum necessary field strength and SNR in different environments. Compared to analogue FM radio a comparable area can be covered with less power in a smaller bandwidth, which makes it more frequency efficient. The results served as contributions for the ITU standardization process for the DRM extension DRM+. Since the end of 2011 DRM+ is part of Recommendation ITU-R BS.1114-7: 'Systems for terrestrial digital sound broadcasting to vehicular, portable and fixed receivers in the frequency range 30 - 3000 MHz'. Additionally these measurements and evaluations about the planning of DRM+ contributed to the Recommendation ITU-R BS.1660-5: 'Technical basis for planning of terrestrial digital sound broadcasting in the VHF band'. DRM+ also was included into the CEPT (Conférence Européenne des Administrations des Postes et des Télécommunications) document on 'Possibilities of Future Terrestrial Delivery of Audio Broadcasting Services'.

Another focus was set on the compatibility with existing analogue FM broadcasting. Laboratory measurements as well as a field trial were conducted in a combined FM-DRM+ mode. The evaluations of this thesis contributed to define the protection ratios necessary to plan digital and analogue radio systems in the same frequency band.

Analysing the possibilities of a transition from analogue to digital, a parallel operation of FM and DRM+ in the VHF Band II in Germany turns out to be hardly possible due to a lack of free frequencies. An alternative could be the use of frequencies already assigned to digital broadcasting in the VHF Band III for DRM+. As the former DRM+ ETSI standard assigned DRM+ only up to 174 MHz, evaluations and measurements about the technical capabilities of DRM+ in the VHF Band III have been conducted. The main challenges with higher frequencies are the increased Doppler shifts resulting in Inter-Carrier-Interference and the increased variability of the channel. The evaluations and measurements showed that reception in the VHF Band III (174 - 230 MHz) is possible also at high speed. The results of these evaluations and measurements were also contributed to the ITU and the DRM+ system is standardized for the whole VHF Band now. After the standardization at the ITU also the frequency range of DRM+ in the ETSI standard was adapted to the whole VHF Band.

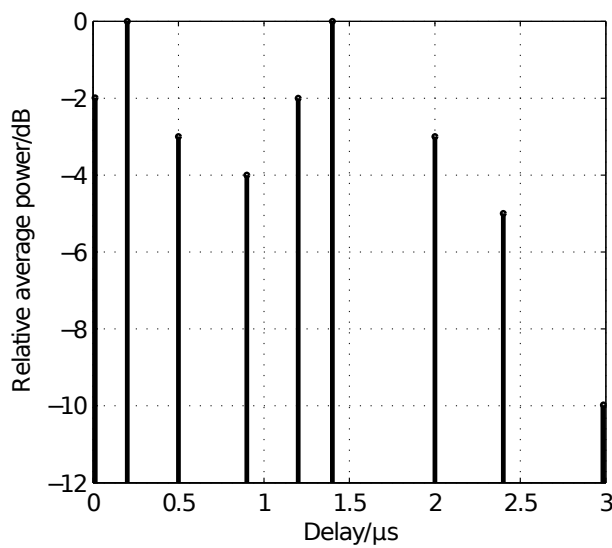
As local and community radios are often licensed with very low power, methods to enhance the performance without increasing the total transmitting power are of interest. As an OFDM system there are different methods for taking advantage of and enhancing the channel diversity. The possibilities of using Transmitter Delay Diversity for DRM+ have been evaluated. Particularly the correlation between the transmission paths were analysed as in a broadcasting system the requirements regarding the distance between the transmitting antennas are quite high. For different models and environments the correlation has been calculated. This showed, that especially for lower antenna heights uncorrelated paths can be achieved with an adequate antenna distance. Performance simulations of a Transmitter Delay Diversity system with correlated paths show that correlation up to a certain level still provides a good performance enhancement. Especially in a slow urban channel where frequency flat fading over a long time is a major problem. Additionally a field trial has been conducted to evaluate the transmitter Delay Diversity system in the real world. The results of this trial showed that at most places the performance could be enhanced using Transmitter Delay Diversity compared to transmitting with only one antenna and twice as much power as each antenna in the diversity mode.

Another method of enhancing the system performance, as well as for increasing the coverage area is the usage of Single Frequency Networks. As DRM+ is a system with a small bandwidth, care has to be taken in the overlapping areas. If the signals from different transmitters arrive at similar time with the same power, destructive interferences can cause problems. A solution is to add an additional delay to the signal at one transmitter (or more in a multi transmitter SFN) to avoid very small delays causing large coherence bandwidth and thus destructive interferences. The necessary parameters have been evaluated, a SFN was set up and a field trial confirmed the expected behaviour without and with different delays.

Finally the possibilities of performance optimizations at the receiver have been evaluated. Different methods of receiver diversity and combining techniques have been tested in simulations. Two different combining methods have been implemented into the software receiver and measurements showed an enhancement of the reception quality for most places with Maximum Ratio Combining as well as a smaller enhancement with Selection Combining compared to the reception with one antenna.

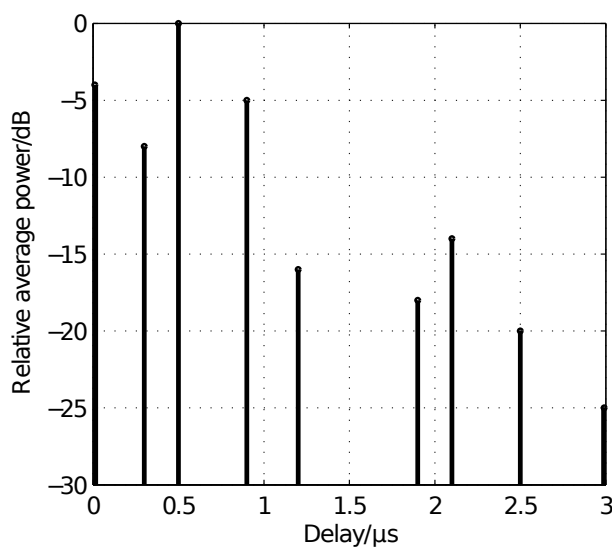
Different evaluations show that the digital radio system DRM+ as an OFDM modulated system has a lot of potential to overcome problems caused by the physical constraints of wave propagation. The coding, interleaving, error correction and system parameter in the DRM+ standard are adapted to the propagation conditions in the VHF Band and are still working in the VHF Band III. Different receiver and transmitter diversity techniques can add more diversity to the channel and help to increase the coverage area.

# A Channel Profiles for the Evaluation of the DRM+ System



Channel profile 'Urban'			
Velocity: 2 and 60 km/h			
max. Doppler freq: 0,2 and 5,5 Hz			
Path Nr.	Delay in $\mu\text{s}$	Power level in dB	Doppler spectrum
1	0	-2	JAKES
2	0,2	0	JAKES
3	0,5	-3	JAKES
4	0,9	-4	JAKES
5	1,2	-2	JAKES
6	1,4	0	JAKES
7	2,0	-3	JAKES
8	2,4	-5	JAKES
9	3,0	-10	JAKES

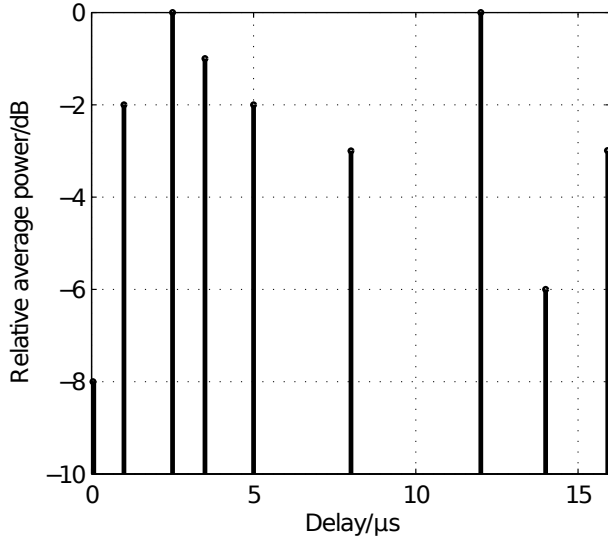
Delay Spread: 0,8  $\mu\text{s}$ , Coh. BW: 2,3 MHz



Channel profile 'Rural'			
Velocity: 150 km/h			
max. Doppler freq: 13,9 Hz			
Path Nr.	Delay in $\mu\text{s}$	Power level in dB	Doppler spectrum
1	0	-4	JAKES
2	0,3	-8	JAKES
3	0,5	0	JAKES
4	0,9	-5	JAKES
5	1,2	-16	JAKES
6	1,9	-18	JAKES
7	2,1	-14	JAKES
8	2,5	-20	JAKES
9	3,0	-25	JAKES

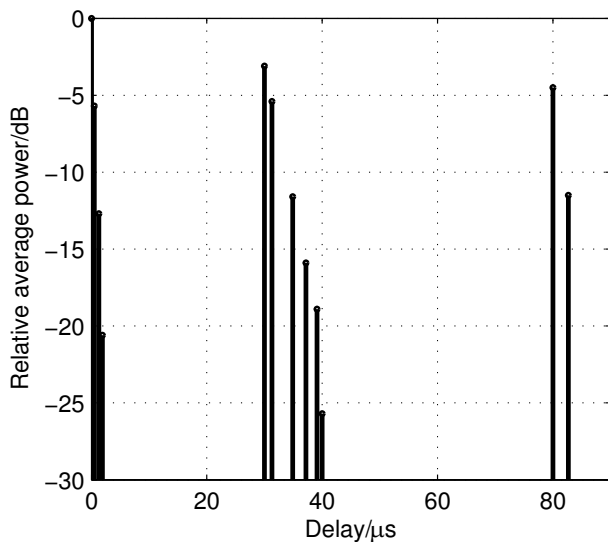
Delay Spread: 0,4  $\mu\text{s}$ , Coh. BW: 2,3 MHz





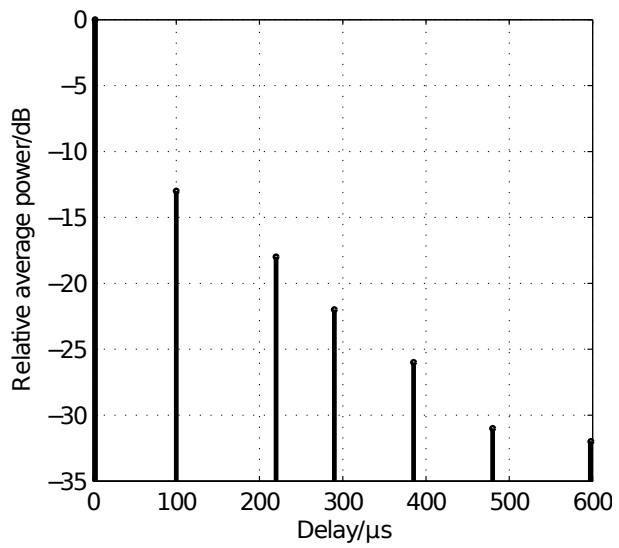
Channel profile 'Terrain Obstructed'			
Velocity: 60 km/h			
max. Doppler freq: 5,5 Hz			
Path Nr.	Delay in $\mu\text{s}$	Power level in dB	Doppler spectrum
1	0	-8	JAKES
2	0,3	-2	JAKES
3	0,5	0	JAKES
4	0,9	-1	JAKES
5	1,2	-2	JAKES
6	1,9	-3	JAKES
7	2,1	0	JAKES
8	2,5	-6	JAKES
9	3,0	-3	JAKES

Delay Spread: 5  $\mu\text{s}$ , Coh. BW: 0,2 MHz



Channel profile 'Hilly Terrain'			
Velocity: 100 km/h			
max. Doppler freq: 9,3 Hz			
Path Nr.	Delay in $\mu\text{s}$	Power level in dB	Doppler spectrum
1	0	0	JAKES
2	0,5	-5,7	JAKES
3	1,3	-12,7	JAKES
4	1,9	-20,6	JAKES
5	30	-3,1	GAUSS1
6	31,3	-5,4	GAUSS1
7	34,9	-11,6	GAUSS1
8	37,2	-15,9	GAUSS1
9	39,1	-18,9	GAUSS1
10	40	-25,7	GAUSS1
11	80	-4,5	GAUSS2
12	82,7	-11,5	GAUSS2

Delay Spread: 28,5  $\mu\text{s}$ , Coh. BW: 35 kHz



Channel profile 'SFN'			
Velocity: 150 km/h			
max. Doppler freq: 13,9 Hz			
Path Nr.	Delay in μs	Power level in dB	Doppler spectrum
1	0	0	JAKES
2	100	-13	GAUSS1
3	220	-18	GAUSS2
4	290	-22	GAUSS1
5	385	-26	GAUSS2
6	480	-31	GAUSS1
7	600	-32	GAUSS2

Delay Spread: 47 μs, Coh. BW: 20 kHz



# B Differential Operations

## The $\nabla$ operator

The  $\nabla$  operator is used in vector calculus, as a vector differential operator. It has been given the short and easy to pronounce monosyllable *del* [68]. When applied to a function defined on a one-dimensional domain, it denotes its standard derivative.

In the three-dimensional Cartesian coordinate system with coordinates  $(x, y, z)$ , *del* is defined in terms of partial derivative operators as:

$$\nabla = \mathbf{i} \frac{\partial}{\partial x} + \mathbf{j} \frac{\partial}{\partial y} + \mathbf{k} \frac{\partial}{\partial z} \quad (\text{B.1})$$

where  $\mathbf{i}$ ,  $\mathbf{j}$ ,  $\mathbf{k}$  are the standard unit vectors.

## Gradient

If the  $\nabla$  operator is applied to a scalar field  $f$ , the resulting vector  $\nabla f$  gives the direction of the most rapid increase of  $f$  [68]. This is called the gradient and is given as:

$$\nabla f = \frac{\partial f}{\partial x} \mathbf{i} + \frac{\partial f}{\partial y} \mathbf{j} + \frac{\partial f}{\partial z} \mathbf{k} \quad (\text{B.2})$$

$\mathbf{i}$ ,  $\mathbf{j}$ ,  $\mathbf{k}$  are the standard unit vectors.

## Divergence

The divergence of a three dimensional vector field is the extent to which the vector field flow behaves like a source or a sink at a given point. It is a local measure of the extent to which there is more exiting an infinitesimal region of space than entering it. If the divergence is nonzero at some point then there must be a source or sink at that position [69].

The divergence of a continuously differentiable vector field  $\mathbf{u}$  in Cartesian coordinates is given as:

$$\nabla \cdot \mathbf{u} = \text{div } \mathbf{u} = \frac{\partial u_x}{\partial x} + \frac{\partial u_y}{\partial y} + \frac{\partial u_z}{\partial z} \quad (\text{B.3})$$

## Curl

In the curl is a vector operator that describes the infinitesimal rotation of a 3-dimensional vector field. The curl of a vector function is itself a vector function of position in space. As the name indicates, it is closely connected with the angular velocity or spin of the flux at each point [68]. In Cartesian coordinates this is given by:

$$\nabla \times \mathbf{u} = \text{curl } \mathbf{u} = \left( \frac{\partial u_z}{\partial y} - \frac{\partial u_y}{\partial z} \right) \mathbf{i} + \left( \frac{\partial u_x}{\partial z} - \frac{\partial u_z}{\partial x} \right) \mathbf{j} + \left( \frac{\partial u_y}{\partial x} - \frac{\partial u_x}{\partial y} \right) \mathbf{k} \quad (\text{B.4})$$

### Laplace operator

The Laplace operator is a differential operator given by the divergence of the gradient of a scalar field  $f$  [69].

$$\Delta f = \nabla^2 f = \nabla \cdot \nabla f \quad (\text{B.5})$$

In Cartesian coordinates this leads to:

$$\Delta f = \frac{\partial^2 f}{\partial x^2} + \frac{\partial^2 f}{\partial y^2} + \frac{\partial^2 f}{\partial z^2}. \quad (\text{B.6})$$

### Vector Laplacian

The vector Laplacian of a vector field  $\mathbf{u}$  is defined as [69]:

$$\Delta \mathbf{u} = \nabla^2 \mathbf{u} = \nabla(\nabla \cdot \mathbf{u}) - \nabla \times (\nabla \times \mathbf{u}). \quad (\text{B.7})$$

In Cartesian coordinates, this reduces to

$$\Delta \mathbf{u} = (\Delta u_x)\mathbf{i} + (\Delta u_y)\mathbf{j} + (\Delta u_z)\mathbf{k} \quad (\text{B.8})$$

where  $u_x$ ,  $u_y$ , and  $u_z$  are the components of  $\mathbf{u}$ .

# List of Figures

2.1	Frequency bands overview, analogue radio compared to DRM and DAB . . .	5
2.2	The OFDM multiplex created in the DRM+ transmitter . . . . .	7
2.3	QAM mapping with corresponding bit pattern . . . . .	7
2.4	Received OFDM symbols with an echo produced by multipath propagation	9
2.5	Base band OFDM spektrum . . . . .	10
2.6	Receiver architecture . . . . .	11
3.1	Multipath propagation . . . . .	18
3.2	The Doppler effect with a moving receiver . . . . .	20
3.3	Jakes Doppler spectrum . . . . .	21
3.4	Tapped-delay-line model with variable delays . . . . .	23
3.5	Uniformly spaced TDL model . . . . .	24
3.6	COST 207 channel model 'Typical Urban' . . . . .	25
4.1	Field strength in urban environment (Raschplatz) (map source: Bundesamt für Kartographie und Geodäsie) . . . . .	29
4.2	Measurement of the audio data in the urban environment (Raschplatz), green: audio OK, red: one or more audio errors (map source: Bundesamt für Kartographie und Geodäsie) . . . . .	30
4.3	Measurement results in urban environment (Raschplatz) . . . . .	30
4.4	Field strength in 'Suedstadt' (map source: Bundesamt für Kartographie und Geodäsie) . . . . .	31
4.5	Measurement of the audio data in 'Suedstadt', green: audio OK, red: one or more audio errors (map source: Bundesamt für Kartographie und Geodäsie)	31
4.6	Measurement results in the Suedstadt . . . . .	32
4.7	Field strength measurement of the coverage limit, 4 QAM mode (code rate: 0.33), start of the measurement at the transmitter on the left side of the map, stop at right border (map source: Bundesamt für Kartographie und Geodäsie) . . . . .	33
4.8	Measurement of the coverage limit in 4 QAM mode (code rate: 0.33), green: audio frames ok, red: one or more audio frames corrupted (map source: Bundesamt für Kartographie und Geodäsie) . . . . .	33
4.9	Reception parameter on the B65 with 30 W ERP and 4 QAM mode (code rate: 0.33) . . . . .	34
4.10	Field strength measurement of the coverage limit, 16 QAM mode (code rate: 0.5) (map source: Bundesamt für Kartographie und Geodäsie) . . . . .	35



4.11	Measurement of the coverage limit, 16 QAM mode (code rate: 0.5), green: audio frames ok, red: one or more audio frames corrupted (map source: Bundesamt für Kartographie und Geodäsie) . . . . .	35
4.12	Reception parameter on the B65 with 30 W ERP and 16 QAM mode (code rate: 0.5) . . . . .	36
4.13	Evaluation of the necessary SNR and field strength in rural area . . . . .	37
4.14	Spectrum of a DRM+ and a FM transmitter with $\Delta f = 150$ kHz and $\Delta P = 23$ dB . . . . .	39
4.15	Signal setup for the evaluation of the protection ratios . . . . .	40
4.16	Protection ratios, FM interfered by DRM+ . . . . .	41
4.17	Community radio station Líder FM in Recanto dos Emas . . . . .	43
4.18	Measurement routes and points in Recanto dos Emas (mapdata (c) Vectordata from OpenStreetMap and contributors, CC-BY-SA) . . . . .	44
4.19	Mobile measurements in Recanto dos Emas with 4 QAM, green: audio frames ok, red: one or more audio frames corrupted (mapdata (c) Vectordata from OpenStreetMap and contributors, CC-BY-SA) . . . . .	46
4.20	Mobile measurements in Recanto dos Emas with 16 QAM, green: audio frames ok, red: one or more audio frames corrupted (mapdata (c) Vectordata from OpenStreetMap and contributors, CC-BY-SA) . . . . .	46
5.1	DRM+ performance in a 'rural' channel at different receiver velocities in the VHF Band III . . . . .	49
5.2	DRM+ performance in a 'rural' channel at different receiver velocities in the VHF Band II . . . . .	49
5.3	A 'Single Frequency Network' with two transmitters A and B in distance d. Each transmitter has its own coverage area which overlaps with the respective transmitter . . . . .	50
5.4	Performance in a 'Single Frequency Network' in Band III . . . . .	50
5.5	DRM + Pilot grid . . . . .	51
5.6	Coherence time over velocity at different frequencies . . . . .	52
5.7	Comparison of the performance in a slow and flat fading environment . . . . .	52
5.8	Field strength in urban environment (map source: Bundesamt für Kartographie und Geodäsie) . . . . .	54
5.9	Measurement of the audio data in the urban environment (green: Audio OK, red: one or more audio errors)(map source: Bundesamt für Kartographie und Geodäsie) . . . . .	55
5.10	Measurement results with 16-QAM in 'urban' environment in the VHF Band III . . . . .	55
5.11	Measurement results with 16-QAM in 'urban' environment in the VHF Band II . . . . .	56
5.12	Field strength measurement of the coverage limit 4 QAM mode (code rate: 0.5) in the VHF Band III (map source: Bundesamt für Kartographie und Geodäsie) . . . . .	57

5.13	Measurement of the coverage limit in 4 QAM mode (code rate: 0.5) in the VHF Band III (green: audio frames ok, red: one or more audio frames corrupted (map source: Bundesamt für Kartographie und Geodäsie) . . . .	57
5.14	Reception parameter on the B65 with 30 W ERP and 4 QAM mode (code rate: 0.5) in the VHF Band III, measurement while moving towards the transmitter (map source: Bundesamt für Kartographie und Geodäsie) . . . .	58
5.15	Field strength measurement of the coverage limit in 16 QAM mode (code rate: 0.5) in the VHF Band III (map source: Bundesamt für Kartographie und Geodäsie) . . . . .	59
5.16	Measurement of the coverage limit in 16 QAM mode (code rate: 0.5) in the VHF Band III (green: audio frames ok, red: one or more audio frames corrupted (map source: Bundesamt für Kartographie und Geodäsie) . . . .	59
5.17	Reception parameters on the B65 with 30 W ERP and 16 QAM mode (code rate: 0.5) in the VHF Band III (map source: Bundesamt für Kartographie und Geodäsie) . . . . .	60
6.1	Frontend of an OFDM transmitter with Delay Diversity . . . . .	62
6.2	Distribution of bit errors (blue dots) in an uncoded system with slow receiver velocity in an urban channel (left: without DD, right: with DD) . . . .	63
6.3	Simulation of the DD performance in an 'urban' channel with different correlation between the paths . . . . .	64
6.4	Frequency response of two correlated paths with different power ratios . . . .	65
6.5	Soft Delay Diversity BER simulation in an AWGN channel with different power ratios . . . . .	66
6.6	Soft Delay Diversity BER simulation in a mobile 'urban' channel with different power ratios . . . . .	66
6.7	Scattering model for calculating the correlation . . . . .	67
6.8	Correlation for horizontally spaced transmit antennas with a distance of 2 km between the transmitter and the receiver . . . . .	68
6.9	Mean correlation between the RX signals in urban environment from 2 vertically polarized TX antennas over distance between the TX antennas . . . .	69
6.10	Mean correlation between the RX signals in urban environment from 2 diagonal ( $\pm 45^\circ$ slanted) TX antennas over the distance between the TX antennas . . . . .	70
6.11	Block diagram of the Delay Diversity transmitter hardware setup . . . . .	71
6.12	The hardware setup of the DRM+ Delay Diversity transmitter . . . . .	71
6.13	Transmit antennas for delay diversity mounted on the roof of the university . . . .	72
6.14	Measurement locations (mapdata (c) OpenStreetMap and contributors, CC-BY-SA, <a href="http://www.openstreetmap.org">http://www.openstreetmap.org</a> ) . . . . .	73
6.15	Measurement results in 'urban' area (Suedstadt) without DD . . . . .	75
6.16	Measurement results in 'urban' area (Suedstadt) with DD . . . . .	75
7.1	A Single Frequency Network of two transmitters . . . . .	80

7.2	Sum power level in a perfectly synchronized SFN . . . . .	81
7.3	Sum power level in a SFN with different delays added to TX1 . . . . .	81
7.4	Sum power level in a 3 TX SFN, regions with an attenuation of more than 6 dB compared to the mean power level are marked dark blue . . . . .	82
7.5	Sum power level in a 3 TX SFN with a delay of 15 $\mu$ s added to TX1 and 30 $\mu$ s added to TX2 . . . . .	83
7.6	Block diagram of the Single Frequency Network transmitter setup . . . . .	84
7.7	Field strength prediction and measurement locations (Map data (c) OpenStreetMap and contributors, CC-BY-SA) . . . . .	85
7.8	Measurement of the coverage area (red: one or more audio errors, green, no audio error, Map data (c) OpenStreetMap and contributors, CC-BY-SA) .	86
7.9	High velocity measurement in the overlapping area of the SFN with a delay of 31 $\mu$ s added to TX1 . . . . .	87
7.10	High velocity measurement in the overlapping area of the SFN without delay	87
7.11	Culmulative distribution function in 'Bult' . . . . .	89
8.1	Impact of different SNR-thresholds on the performance of Switched Combining receiver diversity . . . . .	92
8.2	Simulation results for a very slow urban channel . . . . .	93
8.3	Simulation results for an urban channel . . . . .	93
8.4	Simulation results for a rural channel . . . . .	94
8.5	Correlation between two horizontally spaced antennas in a Rayleigh fading environment . . . . .	96
8.6	Antenna setup for the calculation of the antenna pattern . . . . .	97
8.7	3D far field antenna pattern with a one antenna setup . . . . .	97
8.8	Moving one antenna to the front of the van . . . . .	99
8.9	Moving one antenna to the back of the van . . . . .	99
8.10	Setup with two antennas and different distances in between . . . . .	100
8.11	Pattern of two antennas at distances from 140 cm to 170 cm . . . . .	100
8.12	Diversity DRM+ receiver prototype . . . . .	101
8.13	Measurement locations for the receiver diversity trial . . . . .	102
8.14	Measurement results at the location 'Linden Sued' with RX antenna A . .	103
8.15	Measurement results at the location 'Linden Sued' with RX antenna B . .	103
8.16	Measurement results at the location 'Linden Sued' with Selection Combining	104
8.17	Measurement results at the location 'Linden Sued' with Maximum Ratio Combining . . . . .	104

# List of Tables

2.1	DRM+ protection level and bit rates for 4-QAM modulation . . . . .	8
2.2	DRM+ system parameters . . . . .	10
4.1	Modulation settings used in the field trial . . . . .	27
4.2	Evaluation of the reception in different surroundings . . . . .	38
4.3	Protection ratios for FM disturbed with by DRM+ measured with different receivers at various frequency offsets . . . . .	41
4.4	Results of the stationary measurements in combined mode in Recanto dos Emas . . . . .	45
6.1	Measurement locations overview . . . . .	74
6.2	Measurement results of the transmitter Delay Diversity trial . . . . .	76
7.1	Measurement results of the SFN trial . . . . .	88
8.1	Evaluation of the antenna properties . . . . .	98
8.2	Details of the measurement locations for the receiver diversity trial . . . .	101
8.3	Measurement results of the receiver diversity trial . . . . .	105



# Bibliography

- [1] Digital Radio Mondiale Consortium. *DRM Introduction and Implementation Guide*. [online] <http://drm.org>, 2012. Last accessed on 2013-01-23.
- [2] Digital Radio Mondiale Website. [online] <http://www.drm.org/>.
- [3] S. Meltzer and G. Moser. *HE-AAC v2 - audio Coding for today's media world*. EBU Technical Review, January 2006.
- [4] European Telecommunications Standards Institute. *ETSI-ES 201 980, Digital Radio Mondiale (DRM) System Specification*. 2012.
- [5] Rhode & Schwarz. *COFDM Technology Basics*. The Association of Washington Executive Broadcast Engineers (WEBE), 2 GHz BAS Relocation Tech-Fair, 2007.
- [6] K.D. Kammeyer. *Nachrichtenübertragung*. Teubner Stuttgart, 2004.
- [7] H. Schulze and C. Lüders. *Theory and Applications of OFDM and CDMA Wideband Wireless Communications*. Wiley, 2005.
- [8] Digital Radio Mondiale Consortium. *Digital Radio Receiver Profiles*. [online] <http://drm.org>, 2009. Last accessed on 2013-01-23.
- [9] European Telecommunications Standards Institute. *ETSI-ES 102 349, Digital Radio Mondiale (DRM) Receiver Status and Control Interface (RSCI)*. 2009.
- [10] J. Clerk Maxwell. *A dynamical theory of the electromagnetic field*. Scientific Papers, 1865, reprinted by Dover, New York, 1952.
- [11] Meinke and Grundlach. *Taschenbuch der Hochfrequenztechnik*. Springer-Verlag, 1986.
- [12] S. R. Saunders and A. Aragón-Zavala. *Antennas and Propagation for Wireless Communication Systems*. Wiley, 2007.
- [13] M.F. Iskander and Z. Yun. *Propagation prediction models for wireless communication systems*, volume 50. IEEE Transactions on Microwave Theory and Techniques, 2002.
- [14] W. C. Jakes. *Microwave Mobile Communication*. IEEE Press, 1993. ISBN 0-7803-1069-1.
- [15] International Telecommunications Union – Radiocommunication Sector. *Recommendation ITU-R BS.1660-5: Technical basis for planning of terrestrial digital sound broadcasting in the VHF band*. December 2011.
- [16] International Telecommunications Union – Radiocommunication Sector. *Recommendation ITU-R P.1546-4, Method for point-to-area predictions for terrestrial services in the frequency range 30 MHz to 3000 MHz*. 2009.



- 
- [17] A. G. Longley and P. L. Rice. *Prediction of tropospheric radio transmission loss over irregular terrain. A computer method*. ESSA Tech. Rep. ERL 79-ITS 67, U.S. Government Printing Office, Washington, DC, 1968.
- [18] T.K. Sarkar, Z. Ji, K. Kim, A. Medouri, and M. Salazar-Palma. *A survey of various propagation models for mobile communication*, volume 45. IEEE Antennas and Propagation Magazine, 2003.
- [19] P. Bello. *Characterization of randomly time-variant linear channels*, volume 11. IEEE Transactions on Communications Systems, 1963.
- [20] E. Biglieri, J. Proakis, and S. Shamai. *Fading channels: Information-theoretic and communications aspects*, volume 44. IEEE Transactions on Information Theory, 1998.
- [21] T.S. Rappaport. *Wireless Communications*. Prentice Hall PTR, 2002.
- [22] COST207. *Digital land mobile communications, Final Report*. Commission of the European Union, 1989.
- [23] M. C. Jeruchim, P. Balaban, and K. S. Shanmugan. *Simulation of Communication Systems*. Kluwer Academic Publishers, 2000.
- [24] G. Zimmermann. *DRM+ Radio Channel Profiles for Use in Band II*. T-Systems, 2005.
- [25] F. Maier, A. Waal, and D. Pagel. *Abschlussbericht des Modellversuchs zur Erprobung der digitalen Hörfunkübertragung im lokalen Bereich mit dem System DRM*. Shaker, 2010.
- [26] International Telecommunications Union – Radiocommunication Study Groups F. Maier. *Preliminary report: DRM+ measurements in band II, ITU-R Document 6A/347-E*. October 2010.
- [27] International Telecommunications Union – Radiocommunication Study Groups F. Maier. *Results of the DRM Field Trial in Sri Lanka, ITU-R Document 6A/503-E*. May 2011.
- [28] K. Ramasubramanian and K. Baum. *An OFDM timing recovery scheme with inherent delay-spread estimation*. Proc. IEEE Global Telecommunications Conference, 2001.
- [29] International Telecommunications Union. *Final Acts of the Regional Administrative Conference for the Planning of VHF Sound Broadcasting (Region 1 and Part of Region 3)*. 1984.
- [30] A. Waal. *Konzeption und Realisierung eines digitalen Hörfunksystems mit Mehrwertdiensten zur lokalen Versorgung*. Shaker Verlag, Aachen, Hannoversche Beiträge zur Nachrichtentechnik, 2010.
- [31] A. Steil and J. Lehnert. *DRM+, a perfect complement to DAB/DAB+ in VHF band III - Technical results, planning aspects and regulatory work*. Proc. 11th Workshop Digital Broadcasting, Fraunhofer IIS, Erlangen, 2010.

- [32] International Telecommunications Union – Radiocommunication Sector. *Recommendation ITU-R BS.641 Determination of radio-frequency protection ratios for frequency-modulated sound broadcasting*. 1986.
- [33] BBC research. *DRM+ into FM Protection Ratios*. DRM Consortium, Coding and modulation group, internal document TC\_CM321, 2009.
- [34] T-Systems. *Protection Ratios measurements*. DRM Consortium, Coding and modulation group, internal document TC\_CM425, 2009.
- [35] A. Steil and F. Schad. *Abschlussbericht zum DRM+-Feldversuch Kaiserslautern, Versuchszeitraum: 1. März 2008 - 31. Mai 2008*. Fachhochschule Kaiserslautern, Landeszentrale für Medien und Kommunikation Rheinland-Pfalz, 2008.
- [36] T. Hasenpusch and F. Schad. *Compatibility Measurements DRM120, DRM+ and HD Radio interfering with FM Broadcast, Narrowband FM (BOS) and Aeronautical Radionavigation*. BNetzA Station München, Fachhochschule Kaiserslautern, 2007.
- [37] F. Maier, A. Tissen, and A. Waal. *Field Tests and Comparison of the Channel Properties for the DRM+ System in the VHF-Bands II (87.5 MHz-108.0 MHz) and III (174-230 MHz)*, volume 4. International Journal on Advances in Telecommunication, 2011.
- [38] F. Maier, A. Tissen, and A. Waal. *Evaluation of the Channel Properties for a DRM+ System and Field Tests in the VHF-Band III (174-230 MHz)*. Proc. Wireless and Mobile Communications (ICWMC), 2010 6th International Conference on, September 2010.
- [39] International Telecommunications Union – Radiocommunication Study Groups F. Maier, D. Pagel. *DRM+ for local radio broadcast - measurements in the 174 - 230 MHz band , ITU-R Document 6A/357-E*. October 2010.
- [40] Y. Li and L. Cimini. *Bound on the Interchannel Interference of OFDM in Time-Varying Impairments*. IEEE Transactions on Communications, 2001.
- [41] P. Robertson and S. Kaiser. *The effects of Doppler spreads in OFDM(A) mobile radio systems*. Proc. IEEE Vehicular Technology Conference, 1999.
- [42] M. Kühn. *Der digitale terrestrische Rundfunk*. ISBN 978-3-7785-4008-4. Hüthig, 2008.
- [43] F. Maier, A. Tissen, and A. Waal. *Evaluations and Measurements of a Transmitter Delay Diversity System for DRM+*. Proc. Wireless Communications and Networking Conference (WCNC), April 2012.
- [44] S. Kaiser. *Spatial transmit diversity techniques for broadband OFDM systems*. Proc. Global Telecommunications Conference, GLOBECOM'00. IEEE, 2000.
- [45] F. Hofmann. *Narrowband digital broadcasting with DRM+ in band I and II*. Proc. 7th Workshop Digital Broadcasting in Erlangen, Sept. 2006.
- [46] S. M Alamouti. *A simple transmit diversity technique for wireless communications*,

- volume 16. IEEE Journal on selected areas in communications, 1998.
- [47] H. Schulze. *A comparison between Alamouti transmit diversity and (cyclic) delay diversity for a DRM+ system*. Proc. International OFDM Workshop, 2006.
- [48] A. Dammann and S. Plass. *Cyclic delay diversity: Effective channel properties and applications*. Proceedings IEEE International Conference on Communications (ICC 2007), Glasgow, Scotland, 2007.
- [49] A. Dammann. *On Antenne Diversity Techniques for OFDM Systems*. VDI Verlag, 2006.
- [50] A. Dammann, R. Raulefs, and S. Plass. *Soft Cyclic Delay Diversity and its Performance for DVB-T in Ricean Channels*. Proc. Global Telecommunications Conference, GLOBECOM'07. IEEE, 2007.
- [51] F. Maier, A. Tissen, and A. Waal. *Evaluation of Soft Delay Diversity for the Digital Broadcast-System DRM+*. 11th International Conference on Digital Signal Processing and its Applications, 2009.
- [52] J. J. A. Lempiainen, J. K. Laiho-Steffens, and A. F. Wacker. *Experimental results of cross polarization discrimination and signal correlation values for a polarization diversity scheme*. Proc. Vehicular Technology Conference, IEEE 47th, 1997.
- [53] Y. C. Huang and B. Senadji. *Orientation invariant diversity gain using transmit polarization diversity*. Proc. ICSPCS 2nd International Conference on Signal Processing and Communication Systems, 2008.
- [54] F. Maier, A. Tissen, and A. Waal. *Evaluations and Measurements of a Single Frequency Network with DRM+*. European Wireless 2012 (EW2012), Poznan, Poland, April 2012.
- [55] J. Lehnert. *First results on compatibility and coverage analyses of DRM+ single frequency networks (SFN) in the VHF band II*. Proc. 10th Workshop on Digital Broadcasting, 2010.
- [56] A. Ligeti and J. Zander. *Minimal cost coverage planning for single frequency networks*, volume 45. IEEE Transactions on Broadcasting, 1999.
- [57] R. Brugger and K. Mayer. *RRC-06 – Technical Basis and Planning Configurations for T-DAB and DVB-T*. EBU Technical Review, April 2005.
- [58] J. R. Perez, J. Basterrechea, J. Morgade, A. Arrinda, and P. Angueira. *Optimization of the coverage area for DVB-T single frequency networks using a particle swarm based method*. Proc. IEEE 69th Vehicular Technology Conference, VTC Spring, 2009.
- [59] Hong Jiang, Paul A. Wilford, and Stephen A. Wilkus. *Providing Local Content in a Hybrid Single Frequency Network Using Hierarchical Modulation*, volume 56. IEEE Transactions on Broadcasting, 2010.
- [60] B. Müller and J. Philipp. *Flat Fading in Mittelwellen-DRM-Gleichwellennetzen*. Advances in Radio Science Vol. 5, 2007.

- 
- [61] International Telecommunications Union – Radiocommunication Study Groups F. Maier. *DRM Single Frequency Network Field Test Results, ITU-R Document 6A/504-E*. May 2011.
- [62] A. Dammann and S. Kaiser. *Transmit/Receive-antenna diversity techniques for OFDM systems*, volume 13. European Transactions on Telecommunications, 2002.
- [63] F. Hofmann, H. Schulze, and T. Lauterbach. *Diversity Reception for Digital Audio Broadcasting*. Proc. IEEE International Symposium on Broadband Multimedia Systems and Broadcasting (BMSB), 2011.
- [64] F. Maier, J. Peissig, A. Waal, and S. Galler. *Simulations and Measurements of a Receiver Diversity System for DRM+*. Proc. 12th Workshop on Digital Broadcasting Ilmenau, September 2012.
- [65] Sugbong Kang and J.S. Lehnert. *Receiver diversity scheme for OFDM systems*, volume 39. Electronics Letters, sept. 2003.
- [66] T.W.C. Brown, S.R. Saunders, and B.G. Evans. *Analysis of mobile terminal diversity antennas*, volume 152. IEE Proceedings - Microwaves, Antennas and Propagation, 2005.
- [67] Numerical Electromagnetics Code (NEC2). [online] <http://www.nec2.org/>, Last accessed 2013-01-23.
- [68] J. Willard Gibbs. *Vector analysis: a text-book for the use of students of mathematics and physics, founded upon the lectures of J. Willard Gibbs*. New York: C. Scribner's Sons, 1901.
- [69] I.N. Bronstein and K.A. Semendjajew. *Taschenbuch der Mathematik*. Harri Deutsch, 1991.



